Simulation of oxygen dynamics in the Baltic Sea deep water.

Dissertation

zur

Erlangung des akademischen Grades

doctor rerum naturalium (Dr. rer. nat.)

der Mathematisch-Naturwissenschaftlichen Fakultät

der Universität Rostock

vorgelegt von

Ivan Kuznetsov, geb. am 31.03.1981 in Moskau

aus Rostock

Rostock, November 2008

urn:nbn:de:gbv:28-diss2009-0102-1

Reviewers :

Prof. Dr. Hans Burchard

The Leibniz Institute for Baltic Sea Research, Physical Oceanography and Instrumentation

Prof. Dr. Wolfgang Fennel

The Leibniz Institute for Baltic Sea Research, Physical Oceanography and Instrumentation

Associate Prof. Ph. D. Oleg Savchuk

State Oceanographic Institute, St. Petersburg branch;

Baltic Nest Institute, Stockholm University

Day of defence: 06. May 2009

Abstract

Anoxic conditions are a natural feature of numerous areas in coastal and marginal seas. These conditions arise, when transport rates of organic matter and oxygen in to deeper layers of the coastal seas do not balance and oxygen is used up leaving an excess of organic material to be decomposed. The decomposition processes are continued by bacterial activity employing other electron acceptors than oxygen and usually end up with sulphate (a major constituent in seawater) reduction. This process leads to the production of hydrogen sulfide as one of end product, which is toxic to higher life forms. Its appearance in water is a threat for the functioning of healthy coastal ecosystems and thereby a direct danger to human health and economic welfare of coastal societies (Richardson and Jorgenson, 1996).

The Baltic Sea is a small sea on the global scale and at the same time one of the largest brackish water area in the world. The narrow and shallow Danish straits connect the Baltic Sea with the North Sea and limit the water exchange of the Baltic Sea with the world's oceans. Due to strong limited water exchange with the North Sea the residence time of the Baltic waters lasts up to 30 years. The ecological state of the Baltic Sea is determined *inter alia* by the dynamics of its anoxic zone. Development of the oxygen depletion in the Baltic Sea in the future depends on natural and anthropogenic factors (i.e. eutrophication, climate change). The main aim of this dissertation is the investigation of biogeochemical factors influencing the oxygen dynamics of the Baltic Sea, by means of mathematical modeling tools.

In this work coupled physical-biogeochemical models were used. Several modifications of the ERGOM model (The Baltic Sea Research Institutes Ecosystem Model) were elaborated. These modified biogeochemical models were coupled to the physical models: 1D model GOTM (General Ocean Turbulence Model) and 3D model MOM (Modular Ocean Model).

One of the most important processes in the ecosystem of the Baltic Sea is the nitrogen-fixation, which plays a significant role in balancing of the marine nutrient budget. It is known from observations that the composition of cyanobacteria changes drastically over the growth season. Variations in the elemental composition of cyanobacteria on the sea surface can lead to changes of C flux into the deep layers. It is not clear how the contents of organic matter affects our ability to quantify future changes. One of the goals of this work (Chapters 3 and 6) was to estimate the effect of changes in the elemental composition of cyanobacteria on the development of the Baltic Seas ecological state.

It was found that the increase of C:N:P ratios in cyanobacteria increase N-fixing rates significantly. At the same time no significant changes in the dynamics of nutrients near the sea

surface occur. Also, dynamics of nutrients and oxygen near the bottom do not change in shallow waters. However, the increase of C:N:P ratios in cyanobacteria affects the concentrations of oxygen and dissolved inorganic nitrogen in the bottom layer of the deep regions. The total anoxic area increased after 8 years of simulation. Oxygen consumption rates near the bottom increased during the stagnation periods increase in the simulation by approximately 10 - 15%, when a variable C:N:P ratio in cyanobacteria was used instead of the Redfield ratio. On a short-time perspective of some years the effect of a non-Redfield ratio in cyanobacteria is negligible for nutrients and oxygen dynamics. Such effects can become signicant for prognostic long-term simulations of the Baltic Sea.

Most biogeochemical models that study large scale processes of oxygen depletion in the Baltic Sea (Fennel and Neumann, 1996; Savchuk and Wulff, 1999) do not consider the additional oxygen consumption due to the oxidation of reduced forms of sulfur, Mn and Fe in the suboxic layer. The aim of chapter 4 was to estimate the effect of this additional oxygen consumption on the oxygen dynamic in the Baltic Sea. It has been found that the parametrization of this effect increase the rate of oxygen depletion and raise the redoxcline depth. Changing the depth of the redoxcline causes changes of the anoxic area in the basin, which affects the flux conditions at the sediment - water interface. However, the effects mostly play a role during the first years of a stagnation period.

Extending a biogeochemical model with a carbon cycle can contribute to the verification of these models. One more goal of this study was to simulate seasonal changes of the carbon dioxide flux and to verify the modeling results with observational data. This allows to improve the ability of the model to estimate the nitrogen fixation rates in the Central Baltic and to study its impact on the development of the ecological state of the Baltic Sea (Chapter 5). In chapter 5 the possibility to verify biogeochemical models with the observed pCO_2 data was shown. However, it was found that for correct simulation of the sea surface pCO_2 with 1D model it is necessary to add an additional phytoplankton group in the model that is able to fix and utilize atmospheric nitrogen and that reaches its highest abundance in late spring. Resulting nitrogen fixation rates for the year 2005 were 259 - 278 $mmol\ N\ m^{-2}\ year^{-1}$.

Contents

Chapter 1

Introduction

1.1 Anoxic conditions

Permanent or temporary zones with anaerobic conditions where hydrogen sulfide toxic for higher life forms occurs significantly affect the ecological balance of water bodies. Anoxic events vary on a time scale: in the Black Sea stable hydrogen - sulfide region exists, in the Gotland Basin of the Baltic Sea anoxic conditions last up to years, but are occasionally eliminated by the oxygen-rich water intrusions from the North Sea. In the Elefsis Bay of the Aegean Sea hydrogen-sulfide conditions annually appear in deep horizons, however its intensity changes every year. In the Sea of Azov the anoxic conditions in the near-bottom layers appear once within few years. The occurrence of those conditions can be related to changes in anthropogenic load as well as to climatic variations.

1.2 Oxygen conditions in the Baltic sea

The Baltic Sea (see Fig. 1.1) is a brackish marine water body with features of an estuary especially sensitive to changes of environmental conditions. In summer waters of the Baltic Sea are always strongly stratified. Region of a sharp temperature gradient - thermocline - is allocated to a depth of 10 – 20 m. In the Gulf of Finland it sinks below the 30 m horizon. The thermocline is a barrier for mixing of two water masses: the upper mixed layer, which warms up during summer, and the cold bottom layer or winter water, which is not affected by mixing. During the fall water cooling the thermocline disappears and water masses are mixed up, resulting in homogeneous temperature. In the northern part of the Gulf of Bothnia the water column mixes up completely, however, in the main Baltic Sea mixing is restricted by the halocline. In the Baltic Sea a permanent halocline is assigned to the depth of 60 – 90 m, some times dropping to 100–120 m. Below this jump the water is more dense and even the

fall mixing does not disrupt this stratification, leaving the bottom layers excluded from mixing with surface waters. Therefore the deep layers are prevented from oxygen inflow. Such state of water masses can be defined as "stagnation" (HELCOM, 2003).

Large amounts of material deposit in deep layers, including those of organic origin. Decomposing microorganisms consume oxygen. When in layers of 120 – 150 m waters are stagnant, and no oxygen enrichment takes place, the concentration of dissolved oxygen decreases, and finally reaches zero. From this point on anaerobe bacteria are responsible for the process of decomposition of organic matter. Their activity results in the formation of toxic hydrogen sulfide in the near-bottom layers. The absence of oxygen and the appearance of hydrogen sulfide forces all fish to abandon the region and kills the benthic organisms: the bottom becomes lifeless (Richardson and Jorgenson, 1996). The lack of oxygen also gives rise to other processes, like nutrients release from bottom sediments entering into the water column. This has the effect that their concentrations in near-bottom layers increase (Balzer et al., 1987). This process is called as "internal loading". The Sea pollutes itself from the side of the sea floor where the sources of loading - organic material - have accumulated before. The stagnation can only be broken by sufficiently large inflows of saline oxygen-rich water, which enter into the Baltic Sea from the North Sea through the Danish passages. Small inflows do not affect significantly the deep basins of the Baltic Sea. More intense inflows of saline waters supersede water masses of the Bornholm basin, but do not reach the Gotland basin.

Only during some rare years the magnitude of saline water inflows into the Baltic Sea is large enough to enter the Gotland basin. Thus, new, oxygen - rich, dense water masses replace the waters from the stagnation zone, in which absence of oxygen is accompanied by high nutrient concentrations. The latter water masses shift towards shallower areas, into the Archipelago Sea to coastal regions. This causes bottom waters to be lifted towards the sea surface. After large saline intrusions the salinity temporarily increases almost all over the Baltic Sea. In the northern part of the Gulf of Bothnia halocline does not form a strong pycnocline, salinity changes only slightly with depth. In the Gulf of Finland a halocline is occasionally formed around 60 m depth. The reason of its formation is the penetration of more saline waters from the Baltic Sea into the gulf.

The halocline at 70 m is also the upper limit for the occurrence of hydrogen sulfide during extended periods of stagnation; during most years hydrogen sulfide does not occur above 120 - 150 m depth.

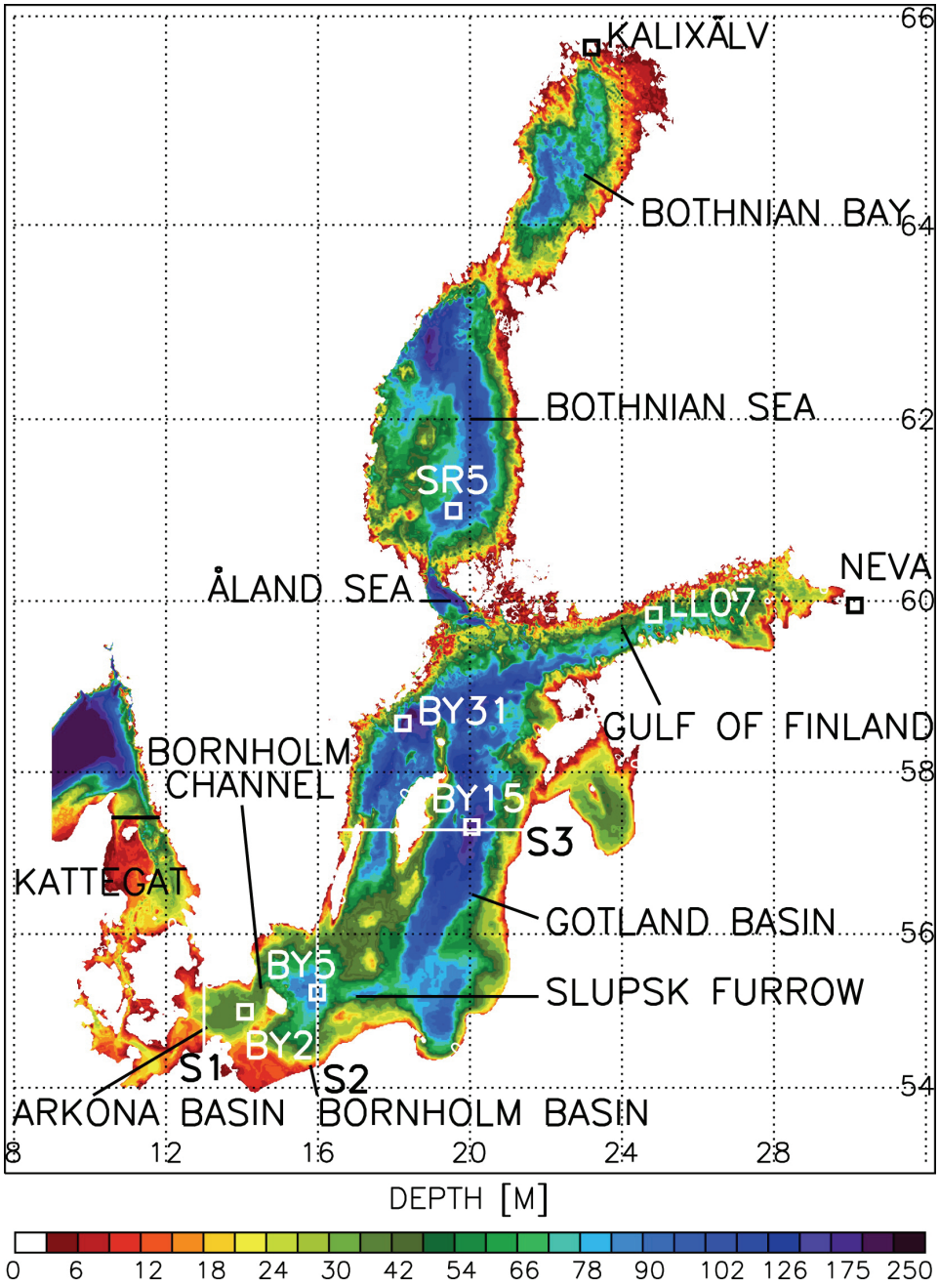

Figure 1.1: Bottom topography of the Baltic Sea. The domain of the Rossby Centre Ocean model (RCO) is limited with open boundaries in the northern Kattegat (black line). In addition, the monitoring stations at Arkona Deep (BY2), Bornholm Deep (BY5), Gotland Deep (BY15), Landsort Deep (BY31), in the Gulf of Finland (LL07), and in the Bothnian Sea (SR5), cross-sections (S1-S3, white lines), and the mouths of the rivers Neva and Kalixälv are depicted.(taken from Markus Meier (2007)).

1.3 Water renewal in the Baltic sea

Dissolved oxygen concentrations below the halocline are very low. This has two reasons. Deep waters penetrate in the Baltic Sea from the North Sea through the Danish passages flowing below the less saline surface waters. These waters are not affected by mixing and, therefore, oxygen does not enter them. The renewal of steady stagnation zones in the deep Baltic Sea below 120 - 150 m happens on the average only once in 7 - 10 years (Matthäus and Franck, 1992). In northern part of the Gulf of Bothnia oxygen concentrations decrease only slightly from the surface to the bottom and remain at rather high level even in the near-bottom horizons. Here no halocline is formed, mixing involves the whole water column annually and oxygen reserves of benthic layers are renewed. In the Gulf of Finland the absence of oxygen is also detected occasionally, similar to those observed in the largest Baltic basin and in the Archipelago Sea.

The lack of oxygen in the sea is caused by the formation of halocline in the near-bottom horizons. For the Archipelago Sea waters the main reason is hidden in the formation of abrupt summer thermocline, which hinders waters from mixing. Moreover, eutrophication leads to the high ingress of organic matter into deep layers. However, here the thermocline vanishes in fall and the fall mixing brings fresh oxygen into these layers. When nutrients, available for plants and algae growth, enter the water body in concentrations so large that growth and specific composition change significantly, the notion of eutrophication is used (HELCOM, 2006). In the Baltic Sea such nutrients are phosphorus, nitrogen and their various forms. This process is mainly anthropogenic, caused by human activity. Eutrophication also occurs when saline waters are passing through the Danish straits into the Baltic Sea, reaching the deep hollows and supersede the bottom waters, enriched by nutrients. This phenomenon is, called lifting of deep waters or internal loading of the Baltic Sea. Though, this is a natural process, human activity contributes to the increase of nutrients concentration in the bottom layers. Eutrophication has both positive and negative consequences. The gain in the biomass and productivity of zooplankton, benthos and fish species can be considered as positive. This results in an increase of fish catch volumes. However, if eutrophication proceeds, negative consequences start to prevail and the ecosystem becomes unbalanced. The penetration of light decreases, the abundance of brown alga focus, which forms the habitats of small fishes and crustaceans, diminishes.

Some algae and bacteria species evolve dramatically. Large amounts of biomass of trichomonosis seaweed is a food source for microorganisms, which also eat focuses. The latter vanishes, and together with them the large number of species inhabiting focuses vanishes. Phy-

toplankton growth raises water turbidity and limits the distribution of macrophytes. Both dead and alive algae form extensive floor-mats, which fall to the sea floor. Under those "floor-mats" the oxygen regime worsens and the benthos perishes. Sedimentation accelerates as a result of the increase of primary production and the organic matter accumulates rapidly in the depressions of the sea floor. The activity of decomposing organisms becomes more intense and the oxygen consumption speeds up. The oxygen regime in the basins deteriorates. When under the halocline in deep layers bacterial activity results in oxygen disappears, highly toxic hydrogen sulfide forms. The dwelling conditions of fish and benthic life forms eventually become absolutely unacceptable, the bottom becomes lifeless. Sediment deposits record the history of the Baltic Sea. Their analysis show that the stagnation conditions, accompanied by the disappearance of dissolved oxygen and hydrogen sulfide formation, are a characteristic natural phenomenon of the Baltic Sea. The size of the areas, where it is observed varies depending on it's hydrographic features. In spite of the fact that natural physical factors "have the basic responsibility" for the disappearance of dissolved oxygen, human activity promotes and accelerates the natural eutrophication, together with the sedimentation of organic matter. Sedimentation speed in the Baltic Sea has augmented of about 60 % during the 20th century.

During the last decades, when the processes described above were most intense, approximately one third of the total deep-water areas of the Baltic Sea (or 100,000 km^2) experienced the complete lack of oxygen. In 1993 this area became two times smaller, due to the arrival of a large inflow of oxygen-rich waters from the North Sea. However, afterwards waters were stratified again, and the anoxic area again increased to its greatest values. In 2000 it reached it's highest level within the whole history of observations, with high concentrations of hydrogen sulfide. The year 2001 became, once again within the whole observational history, the most negative year for the Gulf of Finland. Both in the regions around the islands and in the open anoxia was observed, which destroyed benthic life within a huge territory.

Saline water intrusions from the North Sea, which renewed the waters of benthonic horizons of deep-water Baltic hollows, also both have negative and positive influences. Oxygen disappearance in waters causes a transition of nutrients from the sediment into the near-bottom water layers.

When those layers that accumulated nutrients for years, lift towards the surface, as a result of the inflow of saline waters, primary production processes become more rapid and also accelerates eutrophication. On the other hand, the same intrusions bring oxygen-rich waters resulting in a decrease of lifeless areas in the deep water decrease; and slowing down the process

of the transition of nutrients into the water column. These improved oxygen conditions attract benthic organisms into the deep-water areas. Phosphorus entering the Baltic waters now is eight times higher than those observed in the beginning of the last century, volumes of nitrogen is four times higher. The sharpest increase of these volumes began after the Second World War, with its peak in 1960th and 1970th. The growth on nitrogen loads of some Baltic states has slowed down and the dumps of phosphorus within last decade were even reduced. Biological consequences of acceleration of eutrophication do not always come to light, as in nature there is an existential variability of various parameters that complicate monitoring design and the analysis of measurements results.

Nevertheless, some changes connected with eutrophication can be defined with confidence. E.g., increase in the biomass of trichomonosis, frequent occurrence of "floor-mats", composed of seaweeds, at the bottom, specific changes in plant and animal species composition. For example, the proportion of dinoflagellates in spring bloom prevails more and more. The intensity and scale of summer development of cyanobacteria, which fixate nitrogen, increase. In comparison with the beginning of the 20 century, biomass of phytoplankton has enhanced by 30 - 70 %. The amount of zooplankton, only during the period between 1951 and 1969, has increased by 50 %. The number of macroscopic benthic species of shallow waters increased between 1920 and 1976 3 - 5 times, while their number in the deep-water regions, on the contrary, has decreased. As a result of oxygen deficiency large territories of the deep sea floor of the Baltic Sea have turned into lifeless deserts. The oxygen conditions in the Gulf of Finland experienced the most dramatic negative changes in the 90s. The quantity of fish has repeatedly increased, comparing with 19 century. Since the species richness and biomass of fish are influenced by various factors it is incorrect to consider the phenomenon of eutrophication has been the only reason of this growth.

It is known that periodic inflows of North Sea waters play a significant role in the ecosystem of the Baltic Sea. In fact, because of the presence of a thin layer with high vertical gradients of density, the Baltic Sea is split vertically into two layers: the homogeneous surface layer, subject to the wave mixing processes, significantly influenced by fresh water river runoff, and the bottom layer, saline, formed under the influence of Atlantic waters. As a result the Baltic Sea has appeared to be the subject of stagnation phenomenon when the oxygen concentration in deep waters decreases up to the formation of near-bottom hydrogen-sulfide reach horizons and benthic deserts. However, from time to time the considerable intrusions occur. Within the period between 1880 and 1994 there were 111 intrusion events recorded. Ventilation of bottom

layers occurs, this is considered to be due to the formation of extensive near-bottom gravity currents only during the saline intrusions of a great volume (up to 20 % of the North Sea waters entering in to the Baltic Sea, which occur, on average, once every ten years). Smaller or regular inflows arise repeatedly every year, however their negative buoyancy is not sufficient for them to immerse down to the bottom of the deep basins and for the replacement of embedded water masses. So, the waters of the North Sea get into Baltic in the form of benthic gravity flows which extend along the horizontal bottom or its slope, overcome a layer of rapid vertical growth of the water density, the pycnocline, and pass through the submarine barriers.

In the work Gritsenko (2001) the numerical model of benthic currents was employed to investigate the main stages of the process of water distribution from the North Sea into the Baltic Sea. For the purposes of verification, a task considering the distribution of an anterior part or a front of the benthic gravity current on the horizontal bottom has been chosen. The calculations executed by the model have shown the vertical nature of penetration of waters of bottom currents in to the non-perturbed fluid. Simulations confirmed the ability of bottom current (in case of presence of sufficient negative buoyancy) to penetrate through the pycnocline down to the bottom of the geometrical space of the model. This corresponds to the situations arising during the large intrusions of the North Sea waters into Baltic. In cases, when the inflowing water masses are more light than the bottom layer, the current separates from the bottom slope. The received results testify that the current structure in the vicinity of the separation point, more precisely its topology, is completely defined by features of the pressure field distribution.

In the work Zhurbas et al. (2002) the numerical model of ocean circulation of Blumberg and Mellor (POM) is applied for the description of distribution of saline waters into the East Gotland basin after an extensive North Sea water intrusion. Calculations have shown that two processes participate in this water transport: the near-bottom intrusion and deepwater cyclonic vortex. Both processes are responsible for the ventilation of deep layers of the Baltic Sea.

One of the first attempt of a simulation with a full three-dimensional Baltic Sea ecosystem model over a period of 10 years was done by Neumann (2000). This is an important step beyond one-dimensional water column models or box models, which filter out mesoscale processes and which are basically unable to describe realistic transport of nutrients near the river outlets. The model consists of a circulation model, which is an implementation of the Modular Ocean Model (MOM 2) for the Baltic Sea and an embedded ecosystem model based on a nine-component model ERGOM Neumann (2000). The model was driven with realistic atmospheric forcing,

river loads, and atmospheric deposition of nutrients. A simulation with the realistic forcing was carried out as a control run in order to study in a further experimental simulation the response of the model ecosystem to a 50% reduction of riverine nutrient loads. It was found that the model food web reacts on the load reduction in a complex manner. The changes in dissolved nutrients and in phytoplankton display a spatial variability and different species-specific reactions. While the total biomass and nutrient inventories are reduced, there are significant regional differences.

1.4 Modelling of biogeochemical processes in anoxic conditions

Modelling of biogeochemical processes in anoxic conditions is not yet developed as well as the modelling in aerobic conditions. The intensive development of this field only began at the end of 20th century. In early models interactions of chemical compounds were described considering the chemical kinetics. For example, in Skopincev (1964), for the parametrization of process of hydrogen sulfide oxidation by oxygen, the reaction speed was accepted as directly proportional to concentration of ions of hydrogen sulfide:

$$\frac{d[HS^-]}{dt} = -k_1[HS^-] \tag{1.1}$$

where k_1 is a constant. In the more complicated model of Cline and Richards (Cline and Richards (1969)) the dependencies on both concentrations of hydrogen sulfide, and oxygen were taken into account, applying the second order equation (the first order for oxygen and the first order for hydrogen sulfide were used):

$$\frac{d[HS^-]}{dt} = -k_{11}[HS^-][O_2] \tag{1.2}$$

where k_{11} is a constant of the second order equation. Such approaches have been applied in works of Skopintsev B.A., Ajzatullin T.A., Leonov A.V. models Ayzatulllin and Leonov (1975); Ayzatulllin and Skopincev (1974); Leonov and Ajzatillin (1987), devoted to the description of experiments. In those studies intermediate products of hydrogen sulfide oxidation were considered and sets of equations were based on relationships of the first and second order.

For the description of formation of anoxic conditions in terms of nitrogen model, based on literature data covering the experiments of processes speeds definition, Yakushev (1992) offered the simple semi-empirical functions, which were "merged together" describing the relationships of reaction speed on oxygen concentration, providing "a switching" from the first order reaction, similar to eq. 1.1, to the reaction, similar to eq. 1.1.

For similar purposes Boudreau Boudreau (1996) used the hyperbolic functions, common to the functions of Michaelis-Menten-Mono, for modelling of anoxic conditions in marine deposits. In addition, the same author parametrized the dependencies accounting for effect of inhibition. As a result, the relationships were rather complicated; for example, to parametrize the speed of sulphate reduction the following equation was used:

$$R_{SO_4} = \frac{SO_4}{K_{SO_4} + SO_4} \frac{K'_{O_2}}{K'_{O_2} + O_2} \frac{K'_{NO_3}}{K'_{NO_3} + NO_3} \frac{1}{1 + \frac{K_{MnO_2} MnO_2}{(MnO_2)_0}} \frac{1}{1 + \frac{K_{Fe(III)} Fe(III)}{(Fe(III))_0}} \tag{1.3}$$

where is K_{SO_4} the Michaelis-Menten-Mono constant for sulphates and K'_{O_2}, K'_{NO_3}, K_{MnO_2}, $K_{Fe(III)}$ - are the inhibition constants for oxygen, nitrates, tetravalent manganese and trivalent iron, accordingly. Besides, problems occur due to the definition of numerical values for extremely large number of constants.

In the model of Savchuk and Wulff (1996), authors employed an assumption of stick-slip occurrence of denitrification, after the drop of oxygen concentrations to some fixed level. The speed of denitrification W_{denit} was linked to nitrate concentrations:

$$W_{denit} = \frac{1}{1 + \left(\frac{O_2}{O_{2d}}\right)^{dencr}} \frac{NO_3}{h_{sd} + NO_3} \tag{1.4}$$

where $dencr = 6.0$, $h_{sd} = 14\ \mu g/l$, $O_{2d} = 0.72\ mg\ _2/l$- are constants. In models, which describe the ecosystems of a redox zone (e.g. Belyaev et al. (1997); Lyubartseva and Lyubartsev (1997, 1998), the equations for the description of biomass of bacteria ammonifiers, nitrifiers, denitrifiers, sulfate-reducing and Thiobacillus - were involved, that generated the need to deal with a huge number of constants, undefinable by experiments. Until 90th the oxidation of H_2S in deep layers was usually explained by the inflow of oxygen from the overlying layers, in accordance with the hypothesis about the presence of a layer where O_2 and H_2S coexist. After the data was collected, confirming the absence of such a layer Murray et al. (1995); Lukashev and Yakushev (1999) there was a necessity for working out an alternative hypothesis about the oxidation and disappearance of H_2S in deep layers.

As it has been shown in the work of Yakushev and Debolskaya (2000), covering the Black Sea, the key role for H_2S oxidation in the boundary of its disappearance can belong to Mn_{susp} (suspended manganese). Authors concluded, that the formation of Mn_{susp} takes place under the reaction of Mn_{diss} (dissolved manganese), incoming from the deeper layers, and O_2, along with the reaction with NO_3 (Luther et al., 1997), and also owning to its inflow with coastal drain. Thus, the formation and consumption of Mn_{susp} in various sea regions should differ.

On a broader scale the question of the formation of Mn_{susp} in proper quantities is still open. The cycle of Fe is similar to the cycle of Mn, but this element is available in smaller

concentrations. Fe can also be an additional, but not dominating, factor of H_2S oxidation at the horizon of its thinning.

1.5 Aims of the thesis

The ecological state of the Baltic Sea is determined *inter alia* by the dynamics of its anoxic zone. Future development of the oxygen depletion in the Baltic Sea depends on natural and anthropogenic factors (i.e. eutrophication, climate change). The main aim of this dissertation is the investigation of biogeochemical factors influencing the oxygen dynamics of the Baltic Sea, by means of mathematical modeling tools. Realization of the set of problem assumes the accomplishment of following primary goals:

The effect of changes in the elemental composition of cyanobacteria on the Baltic Seas ecological state

The Baltic Sea is one of the few brackish water areas in the world where diazotrophic cyanobacteria, some of which are toxic, are an important component of the phytoplankton (Howarth et al., 1988). It is known from observations that the elemental composition of cyanobacteria changes drastically over the growth season. The C:P ratio of the peak population may reach values of up to 420, almost fourfold the Redeld value (106), while the C:N ratio, 6.5, is near Redeld (Larsson et al., 2001).

Changes in the elemental composition of cyanobacteria on the sea surface can lead to changes of C flux into the deep layers. This in turn can increase (in case of increased C deposition) the oxygen depletion in those layers.

One of the goals of this work (Chapters 3 and 6) was to estimate the effect of changes in the elemental composition of cyanobacteria on the development of the Baltic Seas ecological state, especially on oxygen depletion in the deep layers.

The pCO_2 dynamics in the Baltic Sea surface waters

Estimates of N_2 fixation rates in the Baltic Sea area were obtained by different methods. Model studies of N_2 fixation rates were performed by Savchuk and Wulff (1999) and Neumann et al. (2002). Different measurement-based methods, founded on nitrogen,phosphate and CO_2 budgets (Larsson et al. (2001), Rahm et al. (2000), Schneider et al. (2003),Schneider et al. (2009)), N^{15} isotope tracer techniques (Wasmund et al. (2001)) and ocean color satellite data

(Kahru et al. (2007)) were used to evaluate nitrogen fixation rates. These different estimates give N_2 fixation rates varying from 10 to 318 $mmol\ N\ m^{-2}\ year^{-1}$.

Mathematical modelling of marine ecosystems is one of the effective ways for improving our understanding of biogeochemical processes and the estimation of the marine ecological state. An important step in such modeling work is the verification of ecosystem models. The carbon cycle combines the most part of biogeochemical processes in a marine ecosystem, and at the same time carbon is not the limiting factor for such processes as primary production. Most ecological models are not calibrated against CO_2. Extending a biogeochemical model with a carbon cycle can contribute to the verification of these models.

One more goal of this study was to simulate seasonal changes of the carbon dioxide flux and to verify modeling results with the data from observations. That will allow to improve the ability of the model to estimate the nitrogen fixation rates in the Central Baltic and to study its impact on the development of the ecological state of the Baltic Sea (Chapter 5).

The consumption of dissolved oxygen in the water column with anoxic conditions

The origin and maintenance of the suboxic layer and the redox reactions taking place across the anoxic interface are not fully understood and deserve further observational and modeling studies. Based on available data from the Black Sea and other similar basins, several mechanisms have been hypothesized to contribute to the interface structure between the suboxic and anoxic layers (Murray et al., 1995, 1999). The first involves anaerobic sulfide oxidation and nitrogen transformations coupled to the manganese and iron cycles. It was proposed that the upward fluxes of sulfide and ammonium may be oxidized by Mn(III, IV) and Fe(III) species, whereas the downward flux of nitrate may be reduced by dissolved manganese and ammonium. Mn(II) and Fe(II) oxidation and Mn(IV) and Fe(III) reduction are both microbially catalyzed, but dissolved chemical reduction may also play a role in Mn(IV) reduction (Oguz et al., 2001).

Most of the biogeochemical models that study the large scale processes of oxygen depletion in the Baltic Sea (Fennel and Neumann, 1996; Savchuk and Wulff, 1999) does not consider the additional oxygen consumption due to the oxidation of reduced forms of sulfur, Mn and Fe in the suboxic layer.

The aim of the chapter 4 was to estimate the effect of additional oxygen consumption due to oxidation of reduced forms of sulfur, Mn and Fe, on the oxygen dynamic in the Baltic Sea.

Chapter 2

Methodology

2.1 The physical model GOTM

GOTM is the abbreviation for General Ocean Turbulence Model. It is a one-dimensional water column model for the most important hydrodynamic and thermodynamic processes related to vertical mixing in natural waters. In addition, it has been designed such that it can easily be coupled to 3-D circulation models, and used as a module for the computation of vertical turbulent mixing. The core of the model computes solutions for the one-dimensional versions of the transport equations of momentum, salt and heat. The key component in solving these equations is the model for the turbulent uxes of these quantities. The strength of GOTM is the vast number of well-tested turbulence models that have been implemented in the code. These models span the range from simple prescribed expressions for the turbulent diffusivities up to complex Reynolds-stress models with several differential transport equations to solve. Even though, evidently, not all turbulence models published in oceanography could be implemented, at least one member of every relevant model family can be found in GOTM (empirical models, energy models, two-equation models, Algebraic Stress Models, K-profie parametrization, etc) (Umlauf et al., 2007).

Due to the one-dimensional character of GOTM, the state-variables listed above are assumed to be horizontally homogeneous, depending only on the vertical z-coordinate. As a consequence, all horizontal gradients have to be taken from observations, or they have to be estimated, parametrized or neglected.

With the Boussinesq approximation, the NavierStokes equations reduce to two one-dimensional equations describing the vertical distribution of momentum according to:

$$\partial_t u - \nu \partial_{zz} u + \partial_z \langle u'w' \rangle - fv = -g \frac{\rho(\zeta)}{\rho_0} \partial_x \zeta \tag{2.1}$$

$$\partial_t v - \nu \partial_{zz} v + \partial_z \langle v'w' \rangle + fu = -g \frac{\rho(\zeta)}{\rho_0} \partial_y \zeta \tag{2.2}$$

where u and v denote the mean velocities in the spatial directions $x_1 = x$ (eastward) and $x_2 = y$ (northward), respectively. The coordinate $x_3 = z$ is taken to point upwards with the origin $z = 0$ at the mean sea surface elevation. ζ is the elevation of the free surface, the gradient of which has to be supplied from an independent source in a one-dimensional model. If the surface slope is known, it can be related to the barotropic pressure gradient with the help of the acceleration of gravity, g, the mean density, ρ, and a constant reference density, ρ_0, resulting from the Boussinesq approximation. The Coriolis parameter is denoted by f and the molecular diffusivity of momentum by ν. Angular brackets indicate the ensemble average of fluctuating quantities.

With the assumptions mentioned above, the temperature and salinity equations reduces to

$$\partial_t T - \nu\prime\partial_{zz} T + \partial_z \langle w'T' \rangle = \frac{\partial_z I}{c_p \rho_0} \tag{2.3}$$

$$\partial_t S - \nu\prime\prime\partial_{zz} S + \partial_z \langle w'S' \rangle = \tau_R^{-1}(S_R - S) \tag{2.4}$$

where $\nu\prime$ and $\nu\prime\prime$ denotes the molecular diffusivity of heat and salt, respectively.c_p is the heat capacity. The only source term in temperature equation results from the vertical divergence of short wave radiation, I. The term on the right hand side of salinity equation describes a relaxation of S towards the observed salinity distribution S_R with the relaxation time scale τ_R.

The mean vertical turbulent fluxes of momentum and heat appearing in Eqs. (2.1)-(2.4) are computed according to

$$\begin{aligned}
\langle u'w' \rangle &= -A_V \partial_z \nu \\
\langle v'w' \rangle &= -A_V \partial_z \nu \\
A_V &= c_\mu k^{\frac{1}{2}} l \\
\langle w'T' \rangle &= -K_V \partial_z T \\
\langle w'S' \rangle &= -K_V \partial_z S \\
-K_V &= c'_\mu k^{\frac{1}{2}} l
\end{aligned} \tag{2.5}$$

where A_V,K_V denote the vertical turbulent diffusivities of momentum and heat, respectively. k is the turbulent kinetic energy, $l \propto k^{\frac{3}{2}} \varepsilon^{-1}$ is the integral length scale, computed from dissipation rate, ε. The turbulent kinetic energy, k, and the dissipation rate, ε, are computed prognostically from parametrized transport equations, corresponding to the k model (Burchard et al., 2006).

2.2 The physical model MOM

MOM (Modular Ocean Model) is a finite difference version of the ocean primitive equations, which govern much of the large scale ocean circulation. As described by Bryan (1969), the equations consist of the Navier-Stokes equations subject to the Boussinesq and hydrostatic approximations. The equation of state relating density to temperature, salinity, and pressure can generally be nonlinear, thus representing important aspects of the oceans thermodynamics. Prognostic variables are the two active tracers potential temperature and salinity, the two horizontal velocity components, any number of passive tracer elds, and optionally the height of the free ocean surface. The discretization consists of spatial coordinates xed in time (fully Eulerian), with surfaces of constant depth determining the vertical discretization and a spherical (latitude/longitude) grid for the horizontal (Pacanowski and Griffies (2000)).

The continuous equations solved by MOM, the horizontal momentum equations:

$$\partial_t u = -\nabla \cdot (u\mathbf{u}) + v\left(f + \frac{u\,\tan\phi}{a}\right) - \left(\frac{1}{a\rho_o \cos\phi}\right)\partial_\lambda p + \partial_z(k_m \partial_u) + F^u \tag{2.6}$$

$$\partial_t v = -\nabla \cdot (v\mathbf{u}) - u\left(f + \frac{u\,\tan\phi}{a}\right) - \left(\frac{1}{a\rho_o}\right)\partial_\phi p + \partial_z(k_m \partial_z v) + F^v \tag{2.7}$$

where, the velocity field

$$\mathbf{u} = (u, v, w) = (\mathbf{u}_h, w) \tag{2.8}$$

is written in terms of the zonal, meridional and vertical components, respectively. The coordinate ϕ is latitude, which increases northward and is zero at the equator. λ is longitude, which increases eastward with zero dened at an arbitrary longitude (e.g., Greenwich, England). z is the vertical coordinate, which is positive upwards and zero at the surface of a resting ocean. Boldface characters represent vector quantities. $\rho_o = 1.035\,g\,cm^{-3}$ is the Boussinesq density. The mean acceleration from gravity is given by $g = 980.6\,cm\,s^{-2}$. $a = 6371 \times 10^5\,cm$ is the mean radius of the Earth. The Coriolis parameter is given by $f = 2\Omega \sin\phi$, with the earth's angular velocity $\Omega = 7.292 \times 10^{-5}\,s^{-1}$.

The vertical velocity is diagnosed through the continuity equation:

$$\partial_z w = -\nabla_h \cdot \mathbf{u}_h \tag{2.9}$$

The pressure p is diagnosed through the hydrostatic equation:

$$\partial_z p = -\rho g \tag{2.10}$$

here, the in situ density ρ is employed, where $\rho = \rho(\theta, s, p)$ is a diagnostic expression for the equation of state.

Equations for the active tracers potential temperature θ and salinity s:

$$\partial_t \theta = -\nabla \cdot [\mathbf{u}\theta + \mathbf{F}(\theta)] \tag{2.11}$$

$$\partial_t s = -\nabla \cdot [\mathbf{u}s + \mathbf{F}(s)] \tag{2.12}$$

where, the flux vector F takes on one of a variety of forms depending on the choice of subgrid scale parametrization.

The system of model equations (2.6)-(2.12) is completed by a set of boundary conditions. The kinematic boundary conditions dene the ocean domain and describe its volume budget. The sea oor is dened by specifying a surface with no normal ow. The sea surface is dened by means of an equation of motion of the sea surface height.

The dynamic boundary conditions prescribe the ux of various quantities such as momentum, heat, and passive tracers through the ocean boundaries. The sea oor employs insulation conditions for heat, salt, and passive tracers; i.e., no-normal tracer ux through the sea oor. Geothermal heating can be set through the models tracer source eld. At the ocean surface, boundary conditions are supplied for heat, passive tracers, and momentum. If fresh water ux is not considered in the volume budget, an additional virtual salinity ux is needed.

MOM assumes the volume of a uid parcel is conserved, unless the parcel is affected by external sources such as surface fresh water uxes. This assumption is part of the standard Boussinesq approximation. Mass conservation is more fundamental than volume conservation. One place where the limitations of volume conservation are most apparent is when formulating the equations for the free surface(Pacanowski and Griffies (2000)). Fig. 2.1 shows the model topography (Neumann and Schernewski, 2008).

2.3 The biogeochemical model ROLM

ROLM (RedOx Layer Model) is the biogeochemical 25-components O-N-S-P-Mn-Fe model allowed to simulate basic features of biogeochemical structure changes in oxic, anoxic and changeable conditions (Yakushev et al., 2007). The processes of OM formation, decay, reduction and oxidation of species of N, S, Mn, Fe and P species changes were parametrized in the model. ROLM can be easily coupled with 1D or 3D models. It is available on website of GOTM (see below). The model was applied for the description of the oxic/anoxic interface structure and estimating of the processes rates in the Black and Baltic Seas (Yakushev et al., 2007)) and to study the consequences of the oxygenated intrusions into the anoxic layers.

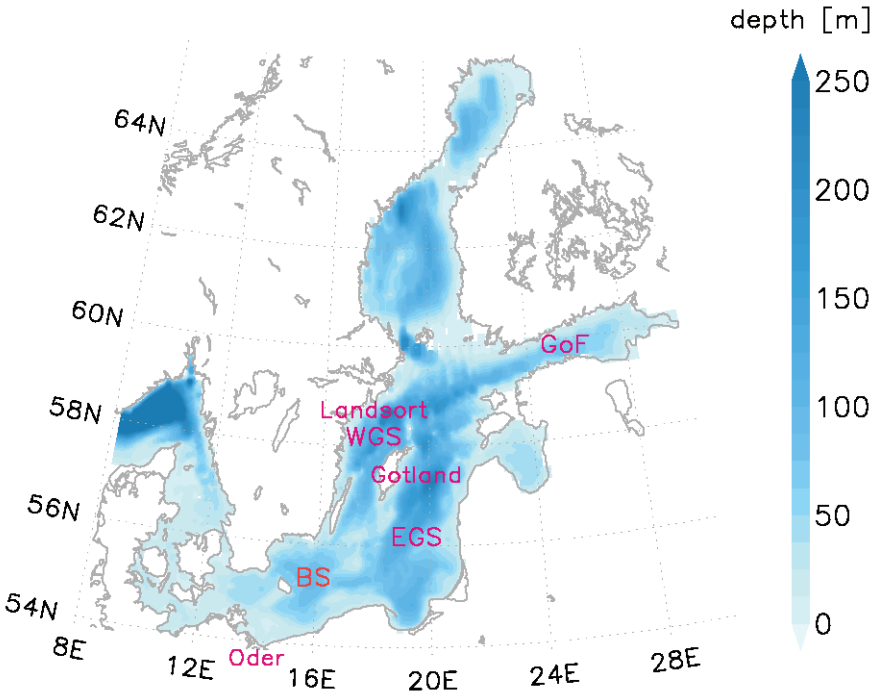

Figure 2.1: Model topography with some geographic annotations. BS, Bornholm Sea; EGS, Eastern Gotland Sea; WGS, Western Gotland Sea; GoF, Gulf of Finland. Oder refers to the River Oder, Gotland to the Island Gotland, and Landsort to the location of the Landsort sea level gauge. (taken from Neumann and Schernewski (2008))

ROLM is the abbreviation for "RedOx Layer Model" – one-dimensional biogeochemical 25-components O-N-S-P-Mn-Fe-water column model. It was developed to study the cycling of the main elements in the pelagic redox layer in seas with anoxic conditions. The formation and decay of organic matter; the reduction and oxidation of nitrogen, sulfur, manganese, and iron species; and the transformation of phosphorus species were parametrized. Temporal and spatial developments of the model's variables are described by a system of horizontally integrated vertical diffusion equations for non-conservative substances. The following biogeochemical variables are considered: dissolved oxygen, (O2), hydrogen sulfide (H2S), total elemental sulfur (S0), thiosulfate (S2O3), sulfate (SO4), ammonia(NH4), nitrite (NO2), nitrate (NO3), particulate organic nitrogen (PON), dissolved organic nitrogen (DON), phosphate (PO4), particulate organic phosphorus (POP), dissolved organic phosphorus (DOP), bivalent manganese (Mn(II)), trivalent manganese (Mn(III)), quadrivalent manganese (Mn(IV)), bivalent iron (Fe(II)), trivalent iron (Fe(III)), phytoplankton (Phy), zooplankton (Zoo), aerobic heterotrophic bacteria (Bhe), aerobic autotrophic bacteria (Bae), anaerobic heterotrophic bacteria (Bha), and anaer-

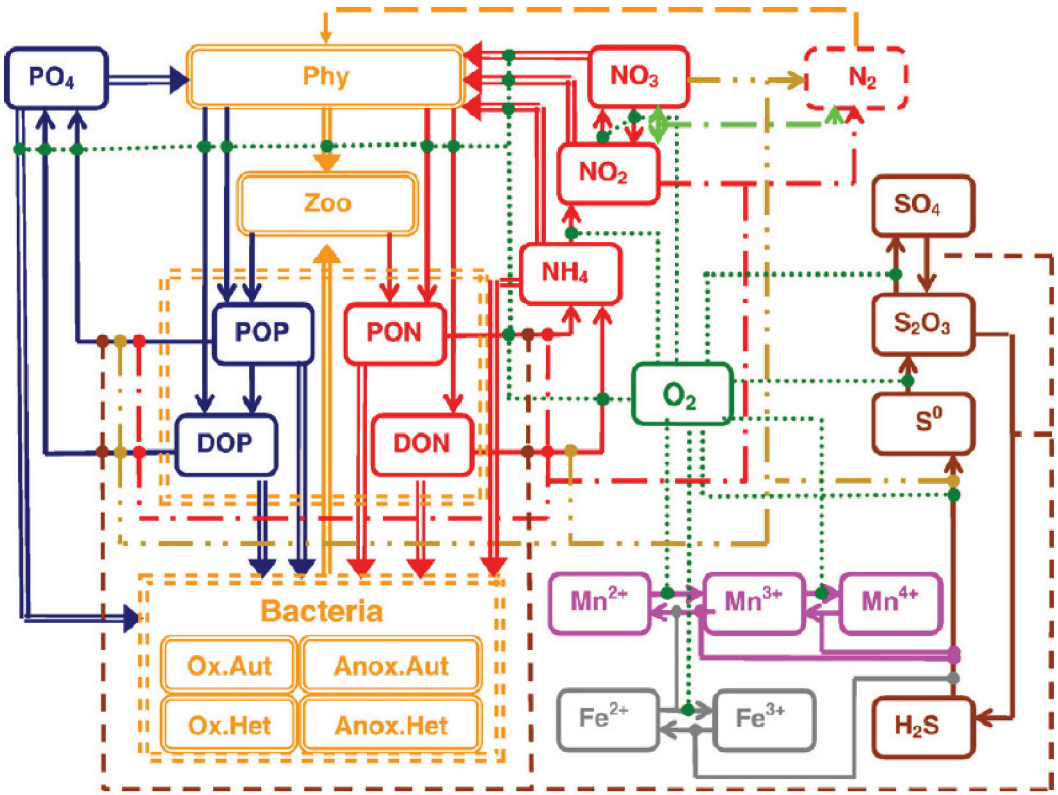

Figure 2.2: Structure of the biogeochemical model ROLM.

obic autotrophic bacteria (Baa). The time-space evolution of the model variables is described by a system of horizontally integrated vertical diffusion equations for non-conservative substances:

$$\partial_t C_i = \partial_z \left(K_z \partial_z C_i \right) - \partial_z ((W_c + W_{Mn}) C_i) + R_{Ci} \tag{2.13}$$

where C_i - concentration of a model variable; K_z - vertical turbulent diffusion coefficient; W_C is the sinking rate of particulate matter; W_{Mn}, - accelerated rate of sinking of particles with settling Mn hydroxides; $R_{Ci} = \sum_j Rate_{BjCi}$ - sources and sinks of a substance (rates of transformation) which is an algebraic sum if local fluxes are caused by biogeochemical interaction ($Rate_{BjCi}$) (Yakushev et al. (2006)). ROLM can be easily coupled with 1D or 3D models. The model was applied for the description of the oxic/anoxic interface structure and estimating of the processes rates in the Black and Baltic Seas and to study the consequences of the oxygenated intrusions into the anoxic layers. A detailed description of this model is presented in chapter 4 and Yakushev et al. (2006). The code of ROLM is available along with the GOTM code at http://www.gotm.net.

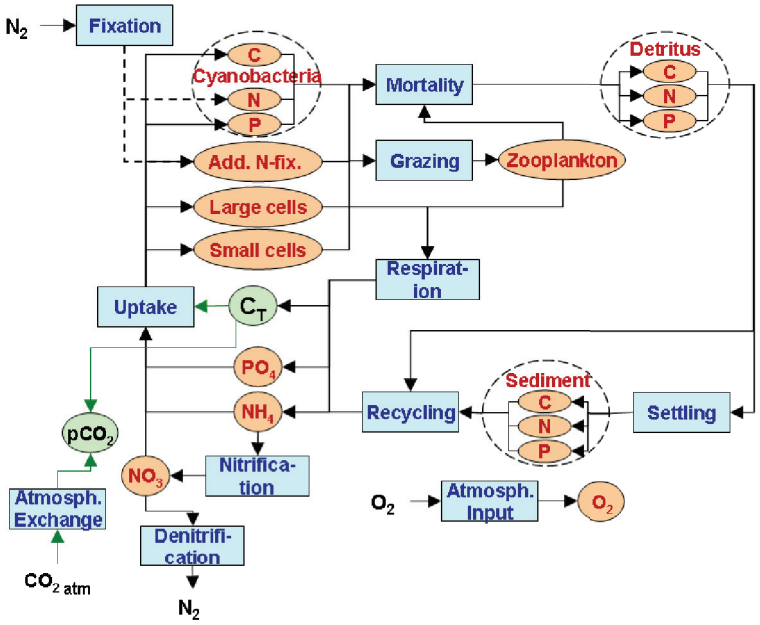

Figure 2.3: Structure of the biogeochemical model with C, N and P in cyanobacteria, large cells, small cells, additional nitrogen fixation phytoplankton group (Add.N-Fix.), zooplankton, C,N and P in detritus, C, N and P in sediment detritus, ammonium (NH_4), nitrate (NO_3), phosphorus (PO_4), carbon (C_T) and oxygen (O_2). The concentrations are in $mmol\ C\ m^{-3}$, $mmol\ C\ m^{-2}$, $mmol\ N\ m^{-3}$, $mmol\ N\ m^{-2}$, $mmol\ P\ m^{-3}$, $mmol\ P\ m^{-2}$ and $mmol\ O_2\ m^{-3}$. Orange and green ovals are models state variables. Blue rectangles are models processes.

2.4 The biogeochemical model ERGOM with modifications

One of the biogeochemical model described in this study is based on the Baltic Sea ecosystem model ERGOM (Neumann et al. (2002)). The biogeochemical model ERGOM is coupled to the physical model as an Eulerian-type model in which all state variables, dissolved (O_2, NH_4, PO_4, ...) and particulated (zooplankton, phytoplankton,...) are expressed as concentrations. The biogeochemical model consists of 18 state variables. The basic structure of the model is explained in Fig. 2.3.

The nutrient state variables are dissolved ammonium, nitrate, phosphate and total CO_2. Primary production is provided by four functional phytoplankton groups: diatoms, flagellates and two groups of cyanobacteria. Diatoms represent larger cells that grow fast in nutrient-rich conditions. Flagellates represent smaller cells with an advantage at lower nutrient concentra-

tions during summer conditions. The cyanobacteria are able to fix and utilize atmospheric nitrogen and, therefore, the model assumes that phosphate is the only limiting nutrient for cyanobacteria. Owing to their ability to fix nitrogen, cyanobacteria are a nitrogen source for the ecosystem. A dynamically developing bulk zooplankton variable provides grazing pressure on the phytoplankton. Dead particles are accumulated in a detritus state variable. The detritus is mineralized into dissolved ammonium,phosphate and total CO_2 during the sedimentation process. A certain amount of the detritus reaches the bottom, where it accumulates in the sedimentary detritus. Detritus is buried in the sediment, mineralized, or resuspended into the water column. The development of oxygen in the model is coupled to the biogeochemical processes via stoichiometric ratios. The oxygen concentration controls processes such as denitrification and nitrification Neumann et al. (2002); Neumann and Schernewski (2005). The ecosystem model ERGOM has been successfully applied for several studies in the Baltic Sea (Neumann et al. (2002); Fennel and Neumann (1996); Janssen et al. (2004); Schernewski and Neumann (2005); Neumann and Schernewski (2005)). A detailed description of this model and modification of it made by author is presented in chapters 3 and 5.

Chapter 3

Model study on the ecosystem impact of a variable C:N:P ratio for cyanobacteria in the Baltic Proper

This chapter has been published as :

Kuznetsov, I., Neumann, T., Burchard, H. 2008. Model study on the ecosystem impact of a variable C:N:P ratio for cyanobacteria in the Baltic proper. Ecological Modelling 219 (1-2), 107-114.

Statement on my contribution to this publication :

The model modification, model setup and analysis of the results were done by me. The paper was written by myself. T. Neumann and H. Burchard contributed in editing the writing, expertise and scientific advice.

Abstract

The goal of this work is to estimate the significance of changes in the elemental composition of cyanobacteria on the ecosystem of the Baltic Sea, especially on oxygen depletion in the deep layers of the Baltic Proper, by means of mathematical modeling tools. In solving this problem a coupled physical-biogeochemical model is used. The physical basis for this model approach is the water column model GOTM (General Ocean Turbulence Model, see www.gotm.net). The biogeochemical basis for this model study is the ERGOM model (The Baltic Sea Research Institutes Ecosystem Model) with some modifications. The ERGOM model was modified to allow the dynamics of N:P and C:P ratios in cyanobacteria. These ratios are controlled by phosphate concentrations in ambient water. Variable C:N:P ratios are used for cyanobacteria, detritus and sediment detritus.

It has been found that the changes in the elemental composition of cyanobacteria from constant C:N:P=106:16:1 ratio to variable C:N:P=(106-400):(16-60):1 ratio lead to larger consumption of oxygen in the deep layers of the Baltic Proper at the long time scale (50 M after 15 years, that amount to approximately 10 %)). This may be a considerable value in multidecadal prognostic model calculations.

3.1 Introduction

Anoxic conditions are a natural feature of numerous areas in coastal and marginal seas. These conditions arise, when transport rates of organic matter (OM) and oxygen into deeper layers of the coastal seas do not balance and oxygen is used up, leaving an excess of organic material to be decomposed. The decomposition processes continue by bacterial activity employing electron acceptors other than oxygen and usually ends up with the reduction of sulphate (a major constituent in seawater). This process leads to the production of hydrogen sulfide, noxious and toxic to higher life forms (Yakushev et al., 2007). Its appearance in water is a threat for the functioning of healthy coastal ecosystems and thereby a direct danger to human health and economic welfare of coastal societies (Richardson and Jorgenson, 1996).

The Baltic Sea region is one of the largest brackish water areas in the world with a salinity of about 10 PSU in the southern Baltic Proper, declining through the Bothnian Sea to 2 PSU in the northern Bothnian Bay (see Fig. 3.1). It is surrounded by 14 densely populated and industrialized countries, where 90 million people live within the drainage area. The narrow and shallow Danish straits limit the water exchange and result in a residence time of the water of 25 - 30 years. The north-south salinity gradient restricts the northward penetration of marine organisms, and the few which do occur in the north often show dwarfism. A permanent halocline at about 60 - 80 m depth suppressed vertical mixing, and oxygenation of the deep water is limited to a few events of salt-water inflow from the North Sea (Reissmann et al., 2007). In average, about one third of the bottom area of the Baltic Proper is devoid of higher life due to low oxygen. Furthermore, tides in the Baltic Sea are very weak and do not contribute to vertical mixing (Kautsky and Kautsky, 2000).

The ecological state of the Baltic Proper is determined *inter alia* by the dynamics of its anoxic zone. Future development of the oxygen depletion in the Baltic Sea depends on natural and anthropogenic factors (i.e. eutrophication, climate change).

Redeld (1934) estimated that C, N and P in oceanic phytoplankton have the average ratio of 106:16:1. Employment of this relationship is convenient to reveal the element that limits the

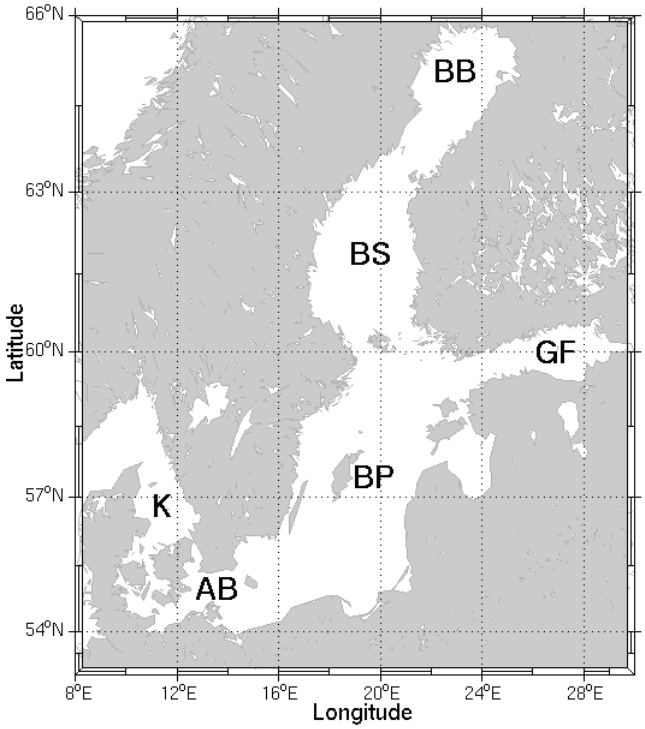

Figure 3.1: Map of the Baltic Sea, indicated regions are the Kattegat (K), the Arkona Basin (AB), the Baltic Proper (BP), the Gulf of Finland (GF), the Bothnian Sea (BS) and the Bothnian Bay (BB).

photosynthesis process, and to describe the peculiarities of OM decay. However, variations in the C:N:P composition of phytoplankton differ greatly, being subject to its life strategy.

The Baltic Sea is one of the few brackish water areas in the world where diazotrophic cyanobacteria, some of which are toxic, are an important component of the phytoplankton (Howarth et al., 1988). It is known from observations that the elemental composition of cyanobacteria changes drastically over the growth season. The C:P ratio of the peak population may reach values of up to 420, almost fourfold the Redfield value, while the C:N ratio, 6.5, is near Redfield (Larsson et al., 2001).

Changes in the elemental composition of cyanobacteria on the sea surface can lead to changes of C flux into the deep layers. This in turn can increase (in case of increased C deposition) the oxygen depletion in those layers. A number of numerical models have been developed for describing elemental changes in phytoplankton (cell quota models), such as models of Moore et al. (2002) and Touratier et al. (2001).

The goal of this work was to estimate the effect of changes in the elemental composition of cyanobacteria on the numerical estimates of the development of the Baltic Seas ecological state, especially on oxygen depletion in the deep layers of the Baltic Proper, by means of mathematical modeling tools.

3.2 Methodology

The model used in this work is a coupled physical-biogeochemical model described by Burchard et al. (2006). The physical part of the model is the water column model GOTM (General Ocean Turbulence Model, see www.gotm.net, and Umlauf et al. (2005)). The model is based on the Reynolds-averaged Navier-Stokes equations in a rotating reference frame, as well as on Reynolds-averaged versions of the transport equations of temperature and salinity. A detailed description of the model can be found in Burchard et al. (2006).

The biogeochemical part of the model described in this study is the Baltic Sea ecosystem model ERGOM (Neumann et al., 2002) with some modifications. The biogeochemical module now consists of 16 state variables. The basic structure of the model is explained in Fig. 3.2. The nutrient state variables are dissolved ammonium, nitrate and phosphate. Primary production is provided by three functional phytoplankton groups: diatoms, flagellates, and cyanobacteria. Diatoms represent larger cells that grow fast in nutrient-rich conditions. Flagellates represent smaller cells with an advantage at lower nutrient concentrations during summer conditions. The cyanobacteria are able to fix and utilize atmospheric nitrogen and, therefore, the model

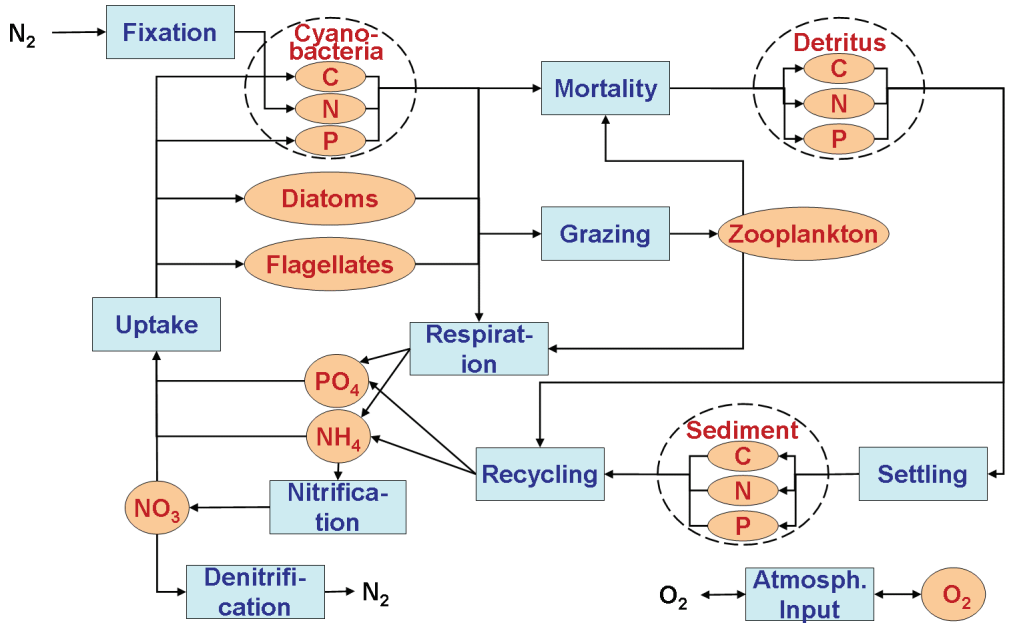

Figure 3.2: Structure of the biogeochemical model with C, N and P in cyanobacteria, diatoms, flagellates, zooplankton, C, N and P in detritus, C, N and P in detritus sediment, ammonium (NH_4), nitrate (NO_3), phosphorus (PO_4) and oxygen (O_2). The concentrations are in $mmol\ C\ m^{-3}$, $mmol\ C\ m^{-2}$, $mmol\ N\ m^{-3}$, $mmol\ N\ m^{-2}$, $mmol\ P\ m^{-3}$, $mmol\ P\ m^{-2}$ and $mmol\ O_2\ m^{-3}$. Orange ovals are models state variables. Blue rectangles are models processes.

assumes that phosphate is the only limiting nutrient for cyanobacteria. Owing to their ability to fix nitrogen, cyanobacteria are a nitrogen source for the ecosystem. A dynamically developing bulk zooplankton variable provides grazing pressure on the phytoplankton. Dead particles are accumulated in a detritus state variable. The detritus is mineralized into dissolved ammonium and phosphate during the sedimentation process. A certain amount of the detritus reaches the bottom, where it accumulates in the sedimentary detritus. Detritus in the sediment is buried in the sediment, mineralized, or resuspended into the water column. The development of oxygen in the model is coupled to the biogeochemical processes via stoichiometric ratios. The oxygen concentration controls processes such as denitrification and nitrification. All variables of the model are presented in table 1. A detailed description of the model can be found in Neumann (2000); Neumann et al. (2002). The ecosystem model has been successfully applied for several studies in the Baltic Sea (Neumann et al., 2002; Fennel and Neumann, 2003; Janssen et al., 2004; Neumann and Schernewski, 2005; Schernewski and Neumann, 2005).

The classical Redfield ratio for N-fixing as implemented in the standard model is relaxed for the present study and a variable C:N:P ratio is now used instead. It includes a variable C:N:P

ratio for cyanobacteria, detritus and sediment detritus, and hence, the number of variables in the model has increased from 10 (standard model) to 16.

Empirical model parameters for such processes as mineralization of detritus and sediment detritus, sedimentation of detritus and cyanobacteria as well as mortality of cyanobacteria, have been taken the same as in the standard version of the model. Exception is the uptake of nutrients N and C by cyanobacteria, which became related to the concentration of phosphate in the water column.

The dependence of the biogeochemistry on the physics is established via vertical mixing, temperature and salinity dependence of process rates, light availability and many other mechanisms. The feedback from the biogeochemistry to the water column physics is mainly due to modified turbidity changing the light absorption in the water (Burchard et al., 2006).

In this paper, we will discus only modifications which were made in the basic model, to describe a variable C:N:P ratio. The equations for cyanobacteria, detritus and sediment detritus of the "basic" model have been replaced each with 3 equations for the description of its C, N and P components. The derived equations are similar to the equations in the "basic" model and we stick to the notation used in Neumann et al. (2002). Newly defined variables are introduced in Table 3.1.

In the cyanobacteria equations the growth term (nitrogen fixation term) was modified. A function was added to increase C:P and N:P ratios in cyanobacteria:

$$Nit.fix. = \begin{cases} f_C(PO_4)R_3Cya_P \\ f_N(PO_4)R_3Cya_P \\ R_3Cya_P \end{cases} \tag{3.1}$$

with the growth rate for cyanobacteria,

$$R_3 = r_3^{max}\frac{1}{1+exp(\beta_{bg}(T_{bg}-T))}min\left[Y\left(s_{NP}\alpha_3, PO_4\right), PPI\right] \tag{3.2}$$

(Neumann et al., 2002) PPI - is the light limitation and

$$Y\left(s_R\alpha_3, PO_4\right) = \frac{PO_4^2}{s_R^2\alpha_3^2 + PO_4^2} \tag{3.3}$$

the phosphorous limitation from Neumann et al. (2002). The modified model includes a dynamic C:N:P = (106-400):(16-60):1 ratio in cyanobacteria with the relation:

$$f_C(PO4) = 106 + 147\left(1 + tanh\left(\frac{\gamma_{P0} - PO_4}{\gamma_{P1}}\right)\right) \tag{3.4}$$

$$f_N(PO4) = 16 + 22\left(1 + tanh\left(\frac{\gamma_{P0} - PO_4}{\gamma_{P1}}\right)\right) \tag{3.5}$$

Table 3.1: State variables of the model.

Variable	Meaning
O_2	Dissolved oxygen
	N
NH_4	Ammonium
NO_3	Nitrate
Det_N	Nitrogen in detritus
Sed_N	Nitrogen in sediments
	P
PO_4	Phosphorus
Det_P	Phosphorus in detritus
Sed_P	Phosphorus in sediments
	C
Det_C	Carbon in detritus
Sed_C	Carbon in sediments
	Biological parameters
Dia	Diatoms
Fla	Flagellates
Cya_C	Carbon in cyanobacteria
Cya_N	Nitrogen in cyanobacteria
Cya_P	Phosphorus in cyanobacteria
Zoo	Zooplankton

$\gamma_{P0} = 0.1$ [mmol P m^{-3}] is a constant which defines a phosphorus concentration, where changes of the cyanobacteria C:P and N:P ratios double, $\gamma_{P1} = 0.03$ [mmol P m^{-3}] is a constant which determines the rate of changes of C:P and N:P ratios. $f_C(PO_4)$ ranges from 106 to 400 and $f_N(PO_4)$ ranges from 16 to 60. In Fig. 3.3 these functions are shown. These functions control the uptake dynamics and realize increased C:P and N:P ratios in the case of a low PO4 concentration. The functions were taken in such a way that modeled C:P and N:P ratios in cyanobacteria match data from Larsson et al. (2001).

For grazing of the bulk zooplankton on phytoplankton we assumed:

$$Graz. = \frac{G_1 Dia + G_2 Fla + G_3 Cya_N}{P_{sum}} Zoo \tag{3.6}$$

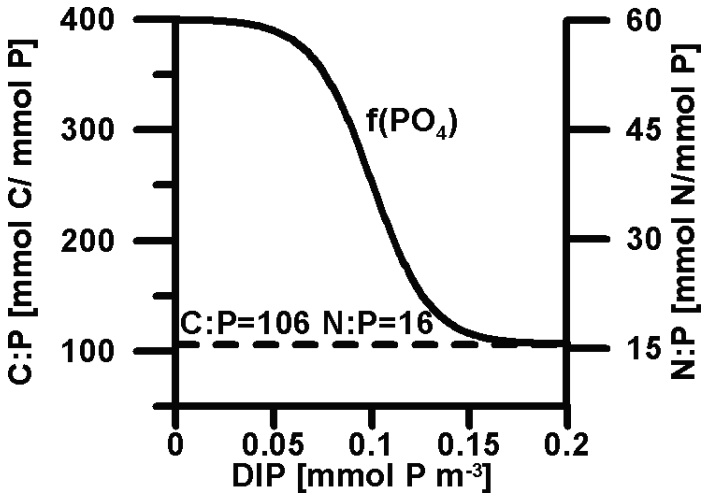

Figure 3.3: Function which controls the nutrients N and C uptake dynamics and realizes increased N:P and C:P ratios in the cyanobacteria in the case of low PO_4 concentration.

where , $P_{sum} = Dia + Fla + Cya_N$, G_n is the zooplankton grazing on phytoplankton ($n = Dia, Fla, Cya$), see Neumann et al. (2002).

In the cyanobacteria equations we assumed the zooplankton grazing terms as : $-G_3 \frac{Cya_C}{P_{sum}} Zoo$ in the equation for C in cyanobacteria, $-G_3 \frac{Cya_N}{P_{sum}} Zoo$ in the equation for N in cyanobacteria and $-G_3 \frac{Cya_P}{P_{sum}} Zoo$ in the equation for P in cyanobacteria. Ratios between these terms are not in the Redfield ratio. However, the model zooplankton remains in the Redfield ratio, but grazing on phytoplankton is in non Redfield ratio. For solving this problems with the additional sources for C and N we assume additional sink terms in the detritus equations, and thus the system is completed as follows: $+G_3 \frac{Cya_C - 106 Cya_P}{P_{sum}} Zoo$ in the equation for Det_C and $+G_3 \frac{Cya_N - 16 Cya_P}{P_{sum}} Zoo$ in the equation for Det_N. This means that parts of N and C component are transferred to detritus immediately.

This one-dimensional model was applied to the Central Eastern Gotland Sea at 250 m water depth ($20°E$, $57.3°N$). Initial conditions for variables: NO_3, NO_4, PO_4, O_2, temperature and salinity were derived from measurements by interpolations of the observed data for the first time step. For other variables constant vertical distributions were taken. Meteorological forcing was available from the ERA40 reanalysis data set (Uppala et al., 2005). The surface fluxes of nutrients have been calibrated in such way that a compromise was found between too low winter nutrient concentrations and too high spring and summer chlorophyll concentrations in the surface mixed layer (see Burchard et al. (2006)). By doing so, the effect of lateral nutrient transport is parameterized. Salinity concentrations are nudged to observations with a time

scale of $\tau_R = 2$ days. Model results and observations will be compared for the years 1978-1993, the period of the longest and most serious stagnation in the Central Baltic deep water during the 20th century. The water column has been divided into 240 vertical layers with a resolution of 1m. The time step for the simulations was $\Delta t = 60min$.

3.3 Results

In this section we discuss the results of two simulations, one with a standard Redfield C:N:P ratio and a simulation with a variable C:N:P ratio, and compare the findings with observations from the Baltic Monitoring Program of the Baltic Sea Research Institute Warnemuende (IOW) at a station in the central Gotland Sea. We assumed $f_C(PO_4) = 106$, $f_N(PO_4) = 16$ (see eq. 3.4) in simulations with the standard Redfield C:N:P ratio.

3.3.1 Physical Parameters

First we compare the simulated temperature with observed data. For both simulations (variable and Redfield ratios of C:N:P) the physical scenarios were near the same. The difference between physical scenarios was owing to feedback from the biogeochemistry to the water column physics. In Fig. 3.4 the temperature and salinity evolution in the upper 80m is shown. In summer a thermocline in about 20 m water depth develops. During winter the vertical stratification vanishes and deep mixing down to the halocline occurs.

A comparison of the modeled and observed sea surface temperature in the Eastern Gotland See is shown in Fig. 3.5(a). Taking into account that comparisons of point measurements of a patchy distribution are subject to observational undersampling, the model reproduces the observed data reasonably well. The interannual trends of the minimum and maximum temperatures are also seen in the model. However, in some instances the summer temperature is slightly overestimated.

3.3.2 Biological and Biogeochemical Variables at constant C:N:P=106:16:1

In Fig. 3.6 the simulated and observed oxygen dynamics (negative oxygen is an equivalent for hydrogen sulfide i.e. 0.5 μM H_2S equals 1 μM of negative oxygen) are shown. In the model we have only one inflow event in 1978 as an initial condition, and no inflows during the calculations, while in nature moderate inflows have been observed in November 1982 and January 1983 (Francke and Nehring, 1986) and weak inflows were present during the whole simulation period.

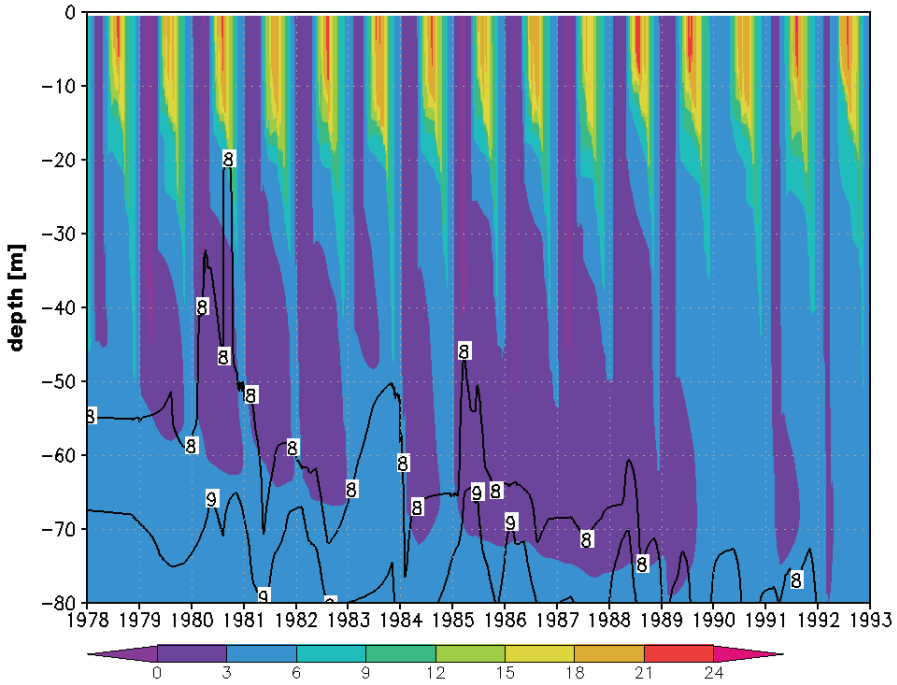

Figure 3.4: Temperature (shaded, $[C^{\circ}]$) and salinity evolution in the upper 80m of the Gotland Sea. The 8 and 9 isohalines are indicated as black lines.

Near the sea surface the model oxygen followed well the observed annual cycle (see Fig. 3.6). In the intermediate and bottom waters the simulated oxygen was depleted slower after the 1978 inflow than in the observations. However, after 5 years of modeling the simulated concentration of oxygen in 110 - 130 meters depth was smaller. That can be explained by the impact of small inflows, which were not parameterized in the model. Taking into account the small inflows in 1982 and 1983, the near-bottom oxygen is reproduced within the range of the observations (see Fig. 3.5(g)).

Next, we compared the dynamics of the model phytoplankton with observations. We plotted the sum of the model phytoplankton groups (as chlorophyll concentration estimated with a constant N: chlorophyll ratio) together with observations in Fig. 3.5(b). The simulated chlorophyll is generally higher in the short periods of the blooms. However, the conversion factors of nitrogen or carbon units to chlorophyll units are highly variable. Moreover, the observed data are sparse. Probably there were no observations when the chlorophyll reached its maximum, because sometimes (1988, 1991) the observed data correspond well to the simulation results.

In Fig. 3.5(c) the simulated and observed concentrations of dissolved inorganic nitrogen, DIN, (sum of nitrate and ammonium) are shown. The model DIN near the sea surface follows

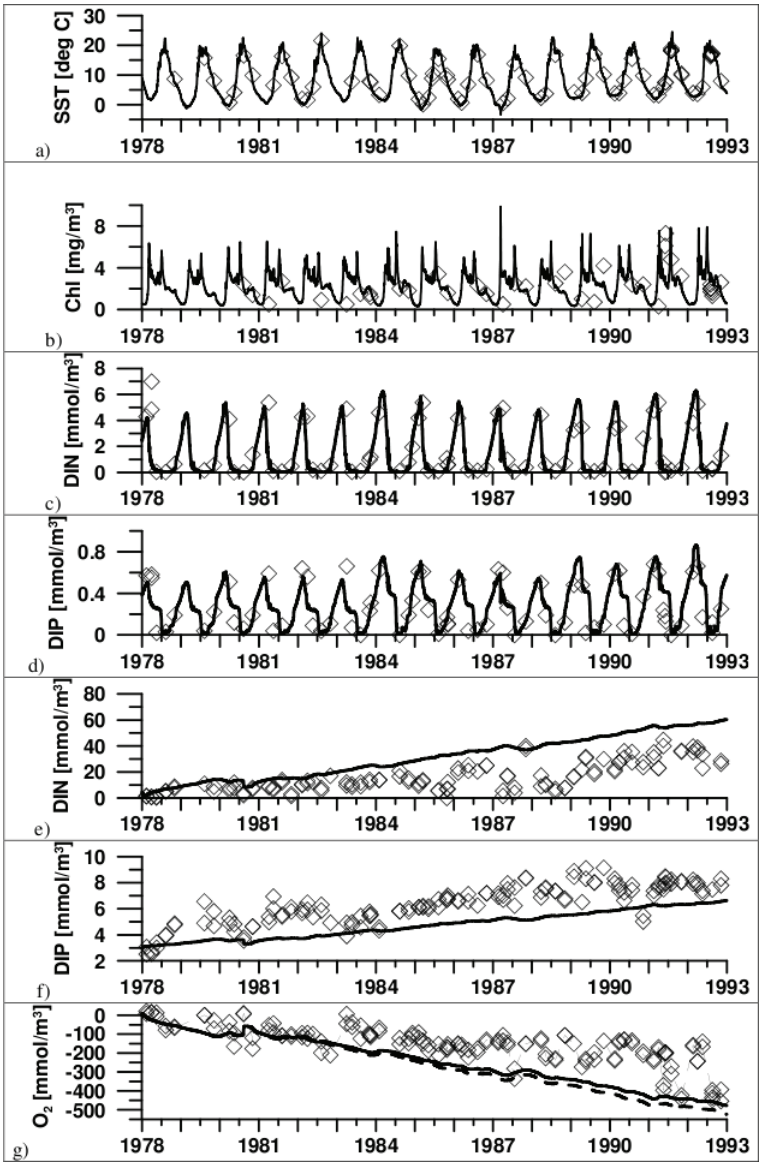

Figure 3.5: Modeled (solid line), simulation with Redfield ratios C:N:P and observed (squares): (a) sea surface temperature, (b) concentrations of chlorophyll near the sea surface, (c) surface dissolved inorganic nitrogen (DIN), (d) surface dissolved inorganic phosphate (DIP), (e) near-bottom dissolved inorganic nitrogen (DIN), (f) near-bottom dissolved inorganic phosphate (DIP), (g) near-bottom oxygen, dashed lines refer to simulation with non-Redfield ratios C:N:P. Negative oxygen is a equivalent for hydrogen sulfate with molar ratio 1/2.

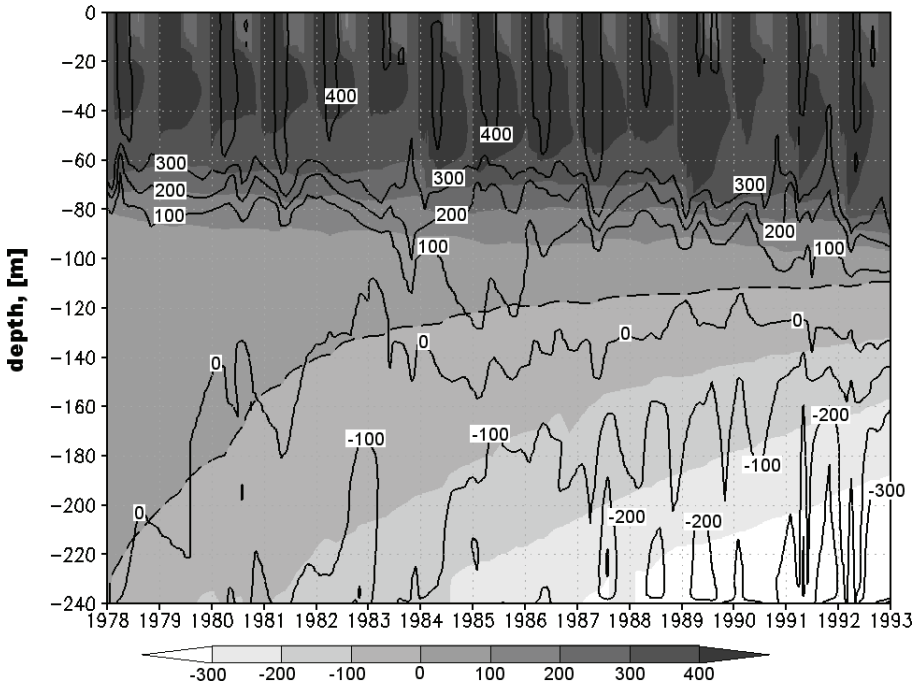

Figure 3.6: Oxygen dynamics in the Central Gotland Sea, solid contour: observation, shaded: modeling results, simulation with Redfield ratios C:N:P (negative oxygen is a equivalent for hydrogen sulfate with molar ratio 1/2), dashed line modeled oxygen 0 level, units are $mmol\ m^{-3}$.

the annual cycle. The summer minimum and the recovering of DIN during the winter are reproduced within the range of the observations.

The near-bottom values of observed DIN are not well reproduced by the simulation (see Fig. 3.5(e)). During the first five years the model DIN is in the range of the observations, but after the year 1983 the modeled values are too high. This can be explained again by inflow events in the Baltic See (see Fig. 3.5(g)), which are missed in this one-dimensional model.

A comparison of modeled and observed near-surface phosphate is shown in Fig. 3.5(d). The model phosphate follows the annual cycle, but in contrast to DIN in some years the concentrations were underestimated. This can be related to underestimated concentrations of phosphate in deep layers, which implies a too small release of phosphate from the sediments during the first years of the simulation (see Fig. 3.5(f)). A too small release of phosphate from the sediments in the model is probable due to that the model does not consider the change in the P-flux rate connected with the changing oxygen condition, when additional amounts of P bounded by Fe and Mn compounds might appear (Balzer et al., 1987).

Summarizing, the model reasonably simulates the annual cycles of the state variables in the upper part of the Baltic Sea. Surface temperature is well simulated by the model. This applies

also to the variations of the winter minimum, which are important for the timing of the spring bloom. Annual cycling of dissolved nutrients in the surface waters reflects the observations and the expected behavior.

Small and moderate lateral intrusions which affect the observed oxygen dynamics are not included in the model. Therefore, the rate of near-bottom oxygen depletion reproduced in the simulation is smaller than in the observations. However, the model reflects well the interannual tendency of increase of the H_2S concentration. Varying river runoff, transports from coastal areas to open sea, inflow events and different upwelling intensities were not taken into account. These processes are known to be important for interannual variations.

3.3.3 Variable C:N:P =(106-400):(16-60):1

Here we compare the control run (with Redfield ratios in cyanobacteria) and the run with the variable C:N:P ratios. After the increase of C:N:P ratios in cyanobacteria, we get significant changes in the dynamics of two types of phytoplankton (cyanobacteria and flagellates) and in the concentrations of oxygen and DIN in the bottom layer. DIN and DIP near the sea surface, as well as DIP in the bottom layer have remained close to the control run, except for a not significant maximum of surface DIN concentrations reached right after the cyanobacteria bloom. The difference in winter concentration of nutrients in both cases did not exceed 3%.

In Fig. 3.7(a) changes of chlorophyll at the sea surface are shown. A difference between the two simulations for chlorophyll can be seen only in the second half of a year. The increase of chlorophyll during the fall bloom is provided mostly by an increase in concentrations of C and N in cyanobacteria due to N-fixation.

The spring peak of chlorophyll have not changed. It is determined by diatoms, that have a fixed C:N:P ratio and depend on winter concentrations of nutrients which are at the same level as noted above.

The elemental composition of cyanobacteria in the model changed drastically over the growth season (see Fig. 3.7(b)). During the spring bloom C:P and N:P ratios were in Redfield values. From June, when the concentration of cyanobacteria started to increase and DIP became depleted, C:P and N:P ratios started to rise. The C:P ratio of the peak population reached 300-400, N:P ratio reached 50-60 (the values fluctuated from year to year).

Owing to the increased C:P ratio in cyanobacteria the OM flux towards deep layers has increased too. This affects the deep water oxygen dynamics and led to an increase of H_2S. After 15 years of modeling the difference between concentration of H_2S in the bottom layer

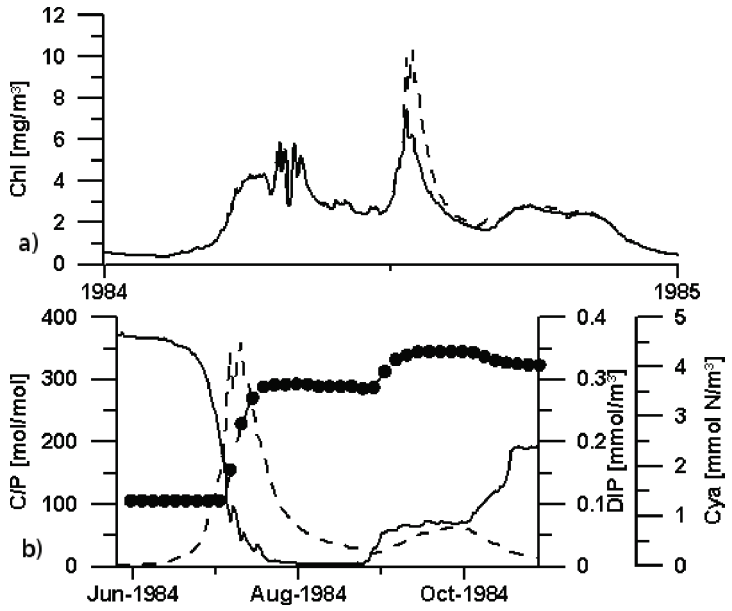

Figure 3.7: (a) Modeled chlorophyll near the sea surface. Solid line refers to the simulation with Redfield ratios C:N:P, dashed line refers to the simulation with variable ratios C:N:P. (b) Modeled stoichiometric composition C:P (mol/mol) of cyanobacteria at the surface (black points), surface dissolved inorganic phosphate (DIP) (solid line) and cyanobacteria in nitrogen units (dashed line).

has reached 25 mmol (equivalent for 50 mmol negative oxygen) (see Fig. 3.5(g)), which is approximately 10 % more compared to the control run.

3.4 Conclusions

To study the influence of non-Redfield stoichiometry on the ecosystem of the Baltic Sea we elaborated a modification of the ERGOM model, where we considered C, N and P concentrations in cyanobacteria and detritus in separate model variables. We proposed a dependence on PO_4 for the parameterization of seasonal dynamics of the C:N:P ratio in cyanobacteria. We also modified the parameterization of zooplankton grazing in conditions of a variable C:N:P ratio.

After the increase of C:N:P ratios in cyanobacteria, we get significant changes in the dynamics of two types of phytoplankton (cyanobacteria and flagellates). A maximum of surface DIN concentrations reached right after the cyanobacteria bloom. A difference between the simulations with variable and constant C:N:P for chlorophyll can be seen only in the second half of a year. Owing to the increased C:P ratio in cyanobacteria the OM flux towards deep

layers has increased too. This affects the concentrations of oxygen and DIN in the bottom layer.

On the basis of this model we found that the changes in the elemental composition of cyanobacteria from C:N:P=106:16:1 to C:N:P=(106-400):(16-60):1 yield a larger consumption of O_2 in the deep layers of the Baltic Proper at the long time scale (50 μM after 15 years (in units of negative oxygen), or approximately 10 %). This effect can become significant for prognostic long-term simulations of the Baltic Proper development. On a short-time perspective of several years the effect is negligible.

Acknowledgments

We thank Evgeniy Yakushev, Falk Pollehne and Bernd Schneider for constructive comments. We also thank three anonymous referees for their constructive comments. The German part of the Baltic Monitoring Program (COMBINE) in the Baltic Sea are conducted by IOW on behalf of the Bundesamt für Seeschifffahrt and Hydrographie (BSH), financed by the Bundesministerium für Verkehr, Bau- und Wohnungswesen (BMCBW). Funding for this work was received from the DFG-grant: NE G17/3-1.

Chapter 4

Analysis of the water column oxic/anoxic interface in the Black and Baltic seas with a numerical model

This chapter has been published as :

Yakushev, E., Pollehne, F., Jost, G., Kuznetsov, I., Schneider, B., Umlauf, L., 2007. Analysis of the water column oxic/anoxic interface in the Black and Baltic seas with a numerical model. Marine Chemistry 107 (3), 388410.

Statement on my contribution to this publication :

In this work I took part in the model setup, data processing and preparation/analysis of the results and text. Results for consumption of O_2 in the suboxic layer were received by me. On a basis of the results of this paper modification of the ERGOM model was performed, that is discussed in section 4.5.

Abstract

A 1D hydrophysical-biogeochemical model was developed to study the cycling of the main elements in the pelagic redox layer in seas with anoxic conditions. The formation and decay of organic matter; the reduction and oxidation of nitrogen, sulfur, manganese, and iron species; and the transformation of phosphorus species were parametrized. Temporal and spatial developments of the models variables were described by a system of horizontally integrated vertical diffusion equations for non-conservative substances. The calculated spatial and temporal distributions of the above-mentioned parameters were in good agreement with observed vertical distribution patterns of these processes.

To study the influence of seasonal variability on the chemical structure of the pelagic redox

layer, specific and distinct hydrophysical scenarios for the Black Sea and for the Baltic Sea were used. The results clearly showed that organic matter, formed during the bloom periods by phytoplankton, exerts a major and direct influence on the structure of the remote redox interface in both seas as well as on the processes occurring in them. This is due to competition for dissolved oxygen between its consumption for oxidation of organic matter originating in the euphotic layer and the consumption for oxidation of reductants supplied from the anoxic deep water. As a result, ammonification, nitrification, denitrification and sulfate reduction dominate in the spring and summer, while the oxidation of reduced forms of metals and of hydrogen sulfide dominates in the winter.

4.1 Introduction

Anoxic conditions are a natural feature of water columns in many of the worlds seas. They arise from an imbalance in the transport rates of organic matter (OM) and oxygen into deeper layers, such that oxygen is depleted and an excess of organic material is left to be decomposed. Nonetheless, decomposition processes continue due to bacterial activities employing electron acceptors other than oxygen. In some cases, this results in the reduction of sulfate, a major constituent of seawater, and in the production of hydrogen sulfide, which is toxic to most higher life forms.

The energy derived from the oxidation of reduced inorganic compounds in the anoxic zone fuels microbial communities that produce OM via chemosynthesis (Nealson and Stahl, 1997; Fenchel et al., 1998; Sorokin, 2002; Canfield et al., 2005). This process together with the oxic, anoxic, and suboxic mineralization of OM as well as chemical reactions between reduced and oxidized compounds accounts for the complexity of the redox layer.

The above-mentioned imbalance between OM transport and oxygen occurs when a hydrophysical structure with a pronounced pycnocline is created. The existence of such structures can be temporary or permanent, and they create corresponding zones of temporary or permanent anoxia. Permanent anoxic conditions are observed in numerous lakes, fjords, and some regions of the World Ocean (Black Sea, Baltic Sea Deeps, Cariaco Basin). The processes that affect the formation of each systems hydrophysical structure vary in scale, ranging from molecular diffusion to climatic variability.

The redox interfaces of marine basins have many features in common. The hydrochemical structures of the oxic/anoxic interfaces found in the Black and Baltic Seas are shown in Fig. 4.1. In both of these interfaces, the nitrate maximum is located at a depth where the vertical gradient

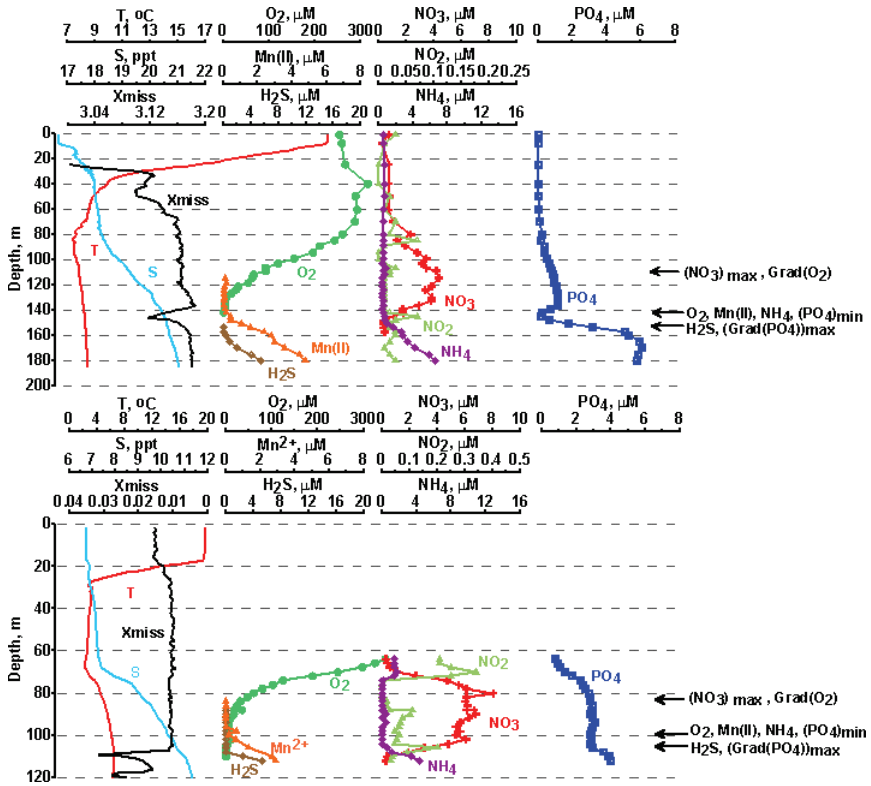

Figure 4.1: Vertical distributions of hydrochemical parameters in the Black (upper panel) and Baltic (lower panel) Seas. Xmiss corresponds to Dr Haardt, turbidity (A) and to Chelsea transmissometer (B) data. The arrows shows the depths of: (1) NO_3 maximum and the lower portion of the oxycline; (2) O_2 depletion, the onsets of Mn(II) and NH_4, and the PO_4 minimum; and (3) the onset of H_2S and the maximum PO_4 gradient.

of oxygen decreases (lower part of the oxycline). The depths of the onset of ammonia and dissolved manganese correspond to the position of the most pronounced phosphate minimum in the Black Sea. This depth is identical to the one at which oxygen depletion occurs, whereas the hydrogen sulfide onset is 5-10 m deeper. The vertical distribution of transmission (Xmiss, Fig. 4.1) is characterized by the presence of a turbidity layer in the vicinity of sulfide onset.

In the present study, a model designed to analyze the various systems that are active in the water column is described. This 1D, hydrophysical-biogeochemical, O-N-S-P-Mn-Fe model simulates the main distribution patterns of the biogeochemical variables and processes at the redox interface. Accordingly, the water column between the surface and a depth of about 100 m below the oxic/anoxic interface was considered. In contrast to previous versions of this model (Yakushev, 1992, 1999; Yakushev and Neretin, 1997) and to other models devoted to analyzing oxic/anoxic interface processes in the water column (Oguz et al., 1998; Konovalov et al., 2006),

we parametrized OM formation during photosynthesis and chemosynthesis. Hence, our current model includes feedbacks between the upward fluxes of nutrients and OM production.

This model was used to analyze key processes driving the formation of the redox-layer structure, i.e., sulfide oxidation, oxygen consumption, and phosphate distribution. The structure and seasonality of a redox interface were simulated based on two hydrophysical scenariosa simplified one for the Black Sea and a more complicated one for the Baltic Sea that was calculated using the General Ocean Turbulent Model (GOTM;Burchard et al. (1999)).

4.2 The model

The following biogeochemical parameters (C_i) were considered (Fig. 2.2): dissolved oxygen, (O_2), hydrogen sulfide (H_2S), total elemental sulfur (S^0), thiosulfate (S_2O_3), sulfate (SO_4), ammonia (NH_4), nitrite (NO_2), nitrate (NO_3), particulate organic nitrogen (PON), dissolved organic nitrogen (DON), phosphate (PO_4), particulate organic phosphorus (POP), dissolved organic phosphorus (DOP), bivalent manganese (Mn(II)), trivalent manganese (Mn(III)), quadrivalent manganese (Mn(IV)), bivalent iron (Fe(II)), trivalent iron (Fe(III)), phytoplankton (Phy), zooplankton (Zoo), aerobic heterotrophic bacteria (Bhe), aerobic autotrophic bacteria (Bae), anaerobic heterotrophic bacteria (Bha), and anaerobic autotrophic bacteria (Baa).

The time-space evolution of the models variables is described by a system of horizontally integrated vertical-diffusion equations for non-conservative substances:

$$\partial_t C_i = \partial_z \left(K_z \partial_z C_i\right) - \partial_z((W_c + W_{Mn})C_i) + R_{Ci} \tag{4.1}$$

where C_i is the concentration of a model variable, K_z the vertical turbulent diffusion coefficient, W_C the sinking rate of particulate matter; W_{Me} the acceleration of the sinking rate due to the settling of Mn hydroxides, and $R_{Ci} = \sum_j Rate_{RateBjCi}$ the rate of biogeochemical production/consumption of C_i, which is an algebraic sum of local fluxes (sources and sinks) caused by biogeochemical interaction ($RateBjCi$). A table with R_{Ci} is presented in the Appendix (Table 4.4). A detailed description of this model is given in Yakushev et al. (2006).

4.2.1 Hydrophysical Scenarios

For the Black Sea K_z in the redox layer was determined based on the vertical density structure and calculated according to Gargett (1984):

$$K_z = a_0 N^{-q}, \text{ where } N = \sqrt{-\frac{g}{\rho}\frac{\partial \rho}{\partial z}} \tag{4.2}$$

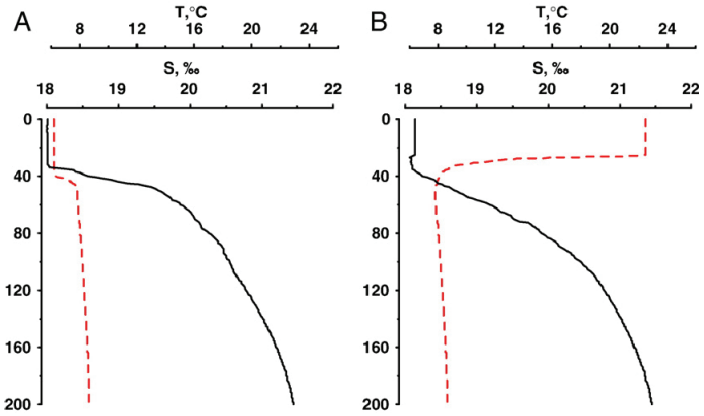

Figure 4.2: Typical temperature (dotted) and salinity (solid) distributions for the central Black Sea in winter (A) and summer (B). Data from RVKnorr and RV Akvanavt cruises.

where N is the buoyancy frequency, g is the acceleration of gravity, ρ is the mean density, and a_0 and q are empirical coefficients. Estimates for the Black Sea redox layer obtained with $K_z = 1.62 \cdot 10^{-3} \cdot \left(\frac{g}{\rho}\frac{\partial \rho}{\partial z}\right)^{-0.5}$ yielded values of about $1 \cdot 10^{-5}\ m^2\ s^{-1}$ (Samodurov and Ivanov, 1998).

The estimates of K_z obtained by Stokozov (2004), who analyzed the spreading of ^{137}Cs after the Chernobyl accident, were $1-3 \cdot 10^{-5}$ in the Black Sea Central Basin and $3-11 \cdot 10^{-5}\ m^2/s$ in the region of the rim current. These larger estimates are more realistic because they were calibrated using the flux of a passive tracer and may therefore reflect processes not considered in the Gargett (1984) approach. In order to match this higher Kz, the coefficients were revised accordingly and used to re-calculate Kz:

$$K_z = 1.94 \cdot 10^{-2} \cdot \left(\frac{g}{\rho}\frac{\partial \rho}{\partial z}\right)^{-0.5} \tag{4.3}$$

Seasonal variabilities in light and hydrophysical structure were considered as external parameters. To describe the variability between the surface and the cold intermediate layer, the changes between two typical distributions observed in the central Black Sea in winter and summer were considered (Fig. 4.2). It was assumed that the changes between typical summer and typical winter structures occur according to a sinusoidal function. Daily calculated density values were used for estimations of Kz according to Eq. (4.3).

For the Baltic Sea, temperature, Kz, and irradiance were determined based on the results of the GOTM (Burchard et al., 1999) for 1992, when the vertical distribution in the Gotland Basin was stable and anoxia had developed. The calculated arrays reflecting the daily changes in these variables were directly applied in the models equations.

4.2.2 Particle sinking

Constant W_{Ci} values were assumed for phytoplankton, zooplankton, bacteria, and detritus (Table 4.4). However, the effect of increased sinking rates due to the formation of Mn(IV) and Fe(III) oxides and their association with particulate organic matter (POM) was parametrized. Yakushev and Debolskaya (2000) found that the precipitation of particulate Mn oxide significantly increases the flux of sinking particles, which, in turn, affects the overall distribution of particles. This effect was parametrized in Eq. (4.1) as an additional term reflecting this effect:

$$W_{Me} = W_{Me}^{max} \frac{Mn(IV)}{Mn(IV) + K_{Me}} \tag{4.4}$$

Coefficients W_{Me}^{max} and K_{Me} are given in Table 4.2.

4.2.3 Boundary conditions

A 1D water column that ranged between the sea surface (upper boundary) and a water depth of 200 m (lower boundary) was considered.

At the upper boundary except for O_2, PO_4, and inorganic nitrogen compounds, the surface fluxes of the chemical constituents considered in the model were assumed to be zero. O_2 exchange is given by the flux equation:

$$Q_{O_2} = k_{660}(Sc/660)^{-0.5}(Oxsat - O_2) \tag{4.5}$$

where Oxsat is the oxygen saturation concentration as a function of temperature and salinity, according to UNESCO (1986); Sc is the Schmidt number; and $k660$ is the reference (Sc = 660, CO_2 at 20°C) gas-exchange transfer velocity. To describe k660 as a function of wind speed, the following equation (Schneider et al., 2002) was used:

$$k_{660} = 0.365u^2 + 0.46u \tag{4.6}$$

Simulations were carried out based on a mean wind speed of 5 $m\ s^{-1}$ for both the Black Sea and the Baltic Sea.

The input of phosphorus (Q_P) and total inorganic nitrogen (Q_N) from rivers and atmospheric precipitates was taken into account. Q_P and Q_N for the Black Sea were calculated with data from Fonselius (1974) and amounted to $Q_P = 0.13\ mmol\ m^{-2}\ d^{-1}$ and $Q_N = 1.5\ mmol\ m^{-2}\ d^{-1}$. For the Baltic Sea, $Q_P = 0.0085\ mmol\ m^{-2}\ d^{-1}$ and $Q_{NO_3} = 0.46\ mmol\ m^{-2}\ d^{-1}$ were determined on the basis of estimates for total-N (990000 t/year) and total-P (40000 t/year) input (HELCOM, 2002) and an area of 415,266 km^2.

At the lower boundary since this model does not consider the nutrient dynamics below 200 m, the concentrations of the main reductants at the lower boundary were assumed to be constant. According to observations, the values for the Black Sea are: $NH_4 = 20\mu M$, $H_2S = 60\mu M$, $Mn(II) = 8\mu M$, $Fe(II) = 0.4\mu M$, $PO_4 = 4.5\mu M$. Those for the Baltic Sea were: $NH_4 = 10\mu M$, $H_2S = 40\mu M$, $Mn(II) = 10\mu M$, $Fe(II) = 0.4\mu M$, $PO_4 = 4.5\mu M$. For the other parameters, an absence of flux was assumed.

4.2.4 Parametrization of biogeochemical processes

The chemical and biological pathways (shown in Fig. 2.2) were formally described by using our previously reported parametrizations (Yakushev, 1992, 1999; Yakushev and Neretin, 1997) as well as those of others (Fasham et al., 1990; Fennel and Neumann, 2004; Ayzatulllin and Leonov, 1975; Savchuk and Wulff, 1996; Boudreau, 1996; Oguz et al., 1998; Gregoire et al., 1997; Konovalov et al., 2006). The values for the coefficients in the rate equations were obtained either from the literature or from fitting the model to measured concentration profiles. A detailed description of the model is given in (Yakushev et al., 2006). Here, the biogeochemical processes considered, their chemical equations, and formulas and coefficients for the parametrization are given in the Appendix list (Table 4.4,Table 4.2).

The mineralization of OM is a key process in the modeling of oxygen-deficient and anoxic conditions, because the electron acceptors for this reaction change from oxygen to nitrate, metal oxides, and finally sulfate. In addition, the rates of mineralization vary between the different electron acceptors. Microbial degradation of the various types of OM, with different stabilities, covers time scales from hours to millions of years. Detailed kinetics of these decompositions are needed for modeling long-term processes in sediments, and they can be described with multi-G models, in which OM is divided into several classes according to its degradability (Westrich and Berner, 1984; Boudreau, 1996).

In this model, a simplified approach was used in that OM was divided into dissolved organic matter (DOM) and POM, with different rates of mineralization. POM was considered as a detrital labile OM that can be mineralized directly. This approach was widely used in previous models (e.g., Fasham et al. (1990); Gregoire et al. (1997); Fennel and Neumann (2004). Here, the stoichiometry of mineralization reactions proposed by Richards (1965) was used in modeling oxic and anoxic conditions.

The main goal of this model was to explain component processes in the redox layer. This was achieved with a model of living organisms that is much simpler than other models for the

Black (Gregoire et al., 1997; Oguz et al., 1998) and Baltic (Savchuk and Wulff, 1996; Fennel and Neumann, 2004) Seas. Since the main role of the Phy and Zoo parameters was to describe the seasonality of OM production, they were not further subdivided. It was also assumed that the uptake rate of inorganic nutrients by phytoplankton equals the growth rate of the phytoplankton. The role of bacteria at the redox interface is very important; hence, based on the results of a series of experiments, bacteria were divided into four groups according to their relation to a particular energy source and to OM transformation (Table 4.4,Table 4.2).

The formulation for the biogeochemical production/consumption rates, R_{Ci}, as an algebraic sum of reactions affecting the concentrations of certain compartments, is presented in Table 4.3.

4.2.5 Computational aspects

The initial calculations employed a uniform distribution of the considered variables. Numerical integration was conducted with the Eurelian scheme and by process splitting. The time steps were 0.00125 d^{-1} for diffusion and 0.0025 d^{-1} for biogeochemical processes and sedimentation. The vertical resolution was 2 m. A quasi-stationary solution with seasonal forced oscillations was reached. There were no changes in the year-averaged concentrations of the variables for at least 100 model years.

4.3 Results and discussion

Redox-layer development in response to seasonal changes and, for the Black Sea, according to the above-described hydrophysical scenario was simulated by the model (Fig. 4.3). The similarities in the basic chemical structures of the redox interfaces of the Black Sea and the Baltic Sea allowed a comparison of the results.

4.3.1 Distributions of biogeochemical parameters

In the model, the dissolved oxygen structure was characterized by a uniform distribution in the upper mixed layer (270 μM), the presence of a pronounced oxycline with a vertical gradient of 7 μM m^{-1}, and a decreased vertical gradient in the deeper layers.

The vertical profiles of nitrogen compounds (NH_4, NO_2, NO_3), as calculated by the model, reflected the main features of the distributions of these compounds as observed in nature. Nitrate concentrations in the maximum layer reached 4.5 μM in the model, as is the case in nature. The NO_2 maximum peak was situated at approximately the same depth, where the concentrations of NH_4 and NO_3 were equal.

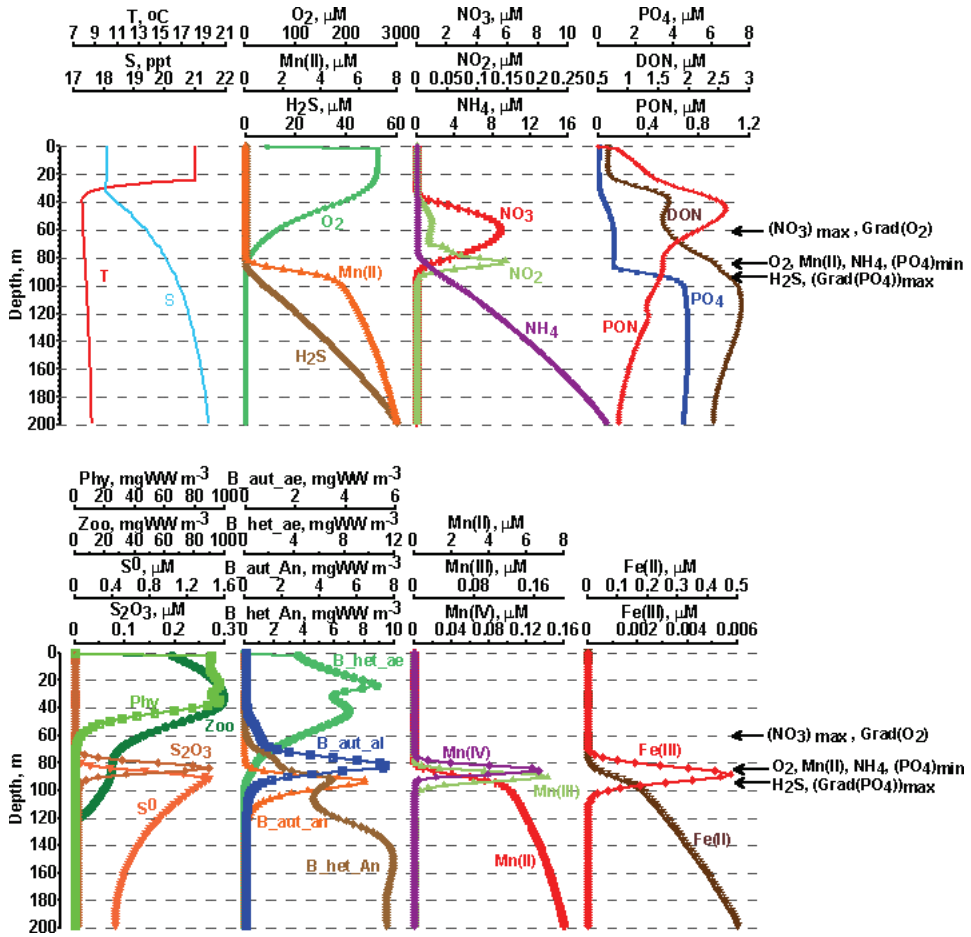

Figure 4.3: The vertical distribution of the parameters in summer (Black Sea) as calculated by the model.

According to the model, H_2S was present about 5-10 m below the onset of the increase in NH_4, while maximum absolute values (1.5 μM) for S_0 occurred at the depth at which H_2S appeared. The S_2O_3 concentrations were uniform, with a small maximum of 0.2 μM at a depth slightly above the H_2S onset. The Mn(II) onset occurred at the same depth as the NH_4 onset. The maxima of Mn(III) and Mn(IV) also formed there. The vertical distribution of Fe was similar to that of Mn.

The P distribution was characterized by a slight minimum at the depth of the Mn(II) onset and an intensive concentration increase that extended down to the depth of the H_2S appearance.

In general, the vertical structure calculated by the model reflected the basic structural features that characterize the redox interfaces of the natural water column, in particular: (i) the correspondence between the depth of the nitrate maximum and the changing O_2 concentrations, (ii) the similarity of the depth of onsets of Mn(II) and NH_4, and (iii) the positions of both the H_2S onset and a layer with maximum gradients of phosphate, located several meters below. Therefore, the model confirmed that the sequences of the disappearance of electron acceptors from the vertical profile (O_2 $\rightarrow$$NO_3$ $\rightarrow$Mn(IV) $\rightarrow$Fe(III)) and of the appearance of electron donors (Mn(II) $\rightarrow$$NH_4$ $\rightarrow$Fe(II)$\rightarrow$$H_2S$) correspond to the sequences of the theoretical electron tower (Nealson and Stahl, 1997; Fenchel et al., 1998; Canfield et al., 2005).

Estimations of the maxima of the various parameters and of the vertical gradients were comparable with observed values. The vertical gradient of H_2S in the model ranged from 0.66 to 0.5 μM m-1, with a maximum several meters below the onset (compared to 0.63 μM m^{-1} in the Black Sea, according to Volkov et al. (1992)). The modeled vertical gradient, in which dissolved Mn(II) was located more shallowly than the H_2S onset, was about 0.6 μM m-1, whereas the values obtained from the field measurements (0.3-0.5 μM m^{-1}) were smaller (Yakushev et al., 2006; Pakhomova, 2005). In the model, Mn(IV) concentrations reached 0.1-0.2 μM in the zone between the onset of oxygen and the onset of hydrogen sulfide. These values are in agreement with data for the Black (Erdogan et al., 2003) and the Baltic (Neretin et al., 2003) Seas. The model-calculated Mn(III) concentrations correspond to those measured by Trouwborst et al. (2006). The maximum concentrations of Fe(III) (0.01 μM) corresponded to previous observations (Pakhomova, 2005) and were located deeper than the Mn(IV) maximum. Therefore, the modeled iron interface was slightly deeper than the manganese interface, as is observed in nature (Lewis and Landing, 1991).

The biological characteristics, defined in terms of the biomasses of phytoplankton and zoo-

plankton, ranged from 50 to 250 mg m^{-3} depending on the season, in agreement with the observations for the Black Sea (Sorokin, 2002). The calculated bacterial biomass in the redox zone (5-10 mg m^{-3}) as a whole also corresponded to the observed values (Pimenov and Neretin, 2006). The model parameters PON and DON (0.3-2.0 μM and 2-5 μM, respectively) were lower than the reported observed values from the Black Sea (Konovalov et al., 2006; Yakushev et al., 2006) and the Baltic Sea (2.9 μM and 14.6 μM, Nagel, personal communication, 2006). The difference can be explained by the fact that our model computes only autochthonous OM and does not consider allochtonous material derived from rivers (and during North Sea water inflow events in the Baltic Sea).

4.3.2 Processes

The similarities of the basic structural features of the redox interface in the Black and Baltic Seas were related to the comparable rates of the respective biogeochemical processes (Table 4.1).

The model results for primary production and dark CO_2 fixation were close to the observed values. The model calculated a maximum rate of chemosynthesis of 0.3-0.7 μM C l^{-1}, which corresponded well to the results of actual measurements. As determined from the observed values, the rate of chemosynthesis is 0.8-1.0 μM C l^{-1} in the Baltic Sea and 0.2-2 μM C l^{-1} in the Balck Sea (Table 4.1).

The models ratio of the annually integrated rate of photosynthesis and the rate of chemosynthesis was about 4-5. This corresponded to estimates that the rate of chemoautotrophic production in the central Black Sea is 10-32% of that of surface photoautotrophic production (Yilmaz et al., 2006). A similar ratio was reported for the Baltic Sea (Detmer et al., 1993).

The processes of sulfide oxidation and sulfate reduction described by the model corresponded well to observations from the Black Sea (Table 4.1).

The modeled rate of ammonification was similar to the value obtained for the Black Sea by Sorokin (2002), but much higher than the estimates by Kuypers et al. (2003). The models nitrification rate was close to the rates of the Baltic and Black Seas. Denitrification was larger than observed, while thiodenitrification was at the limit of possible values for the Baltic Sea. Modeled values of anammox corresponded well to the observed results, whereas the rate of nitrogen fixation was twice as large as that measured in the Black Sea. The rates of manganese oxidation (1.0 μM Mn d^{-1}) and manganese reduction (0.9 μM Mn d^{-1}) were in accordance with observations (Table 4.1).

Table 4.1: Comparison of the rates of biogeochemical processes in model, Black Sea and Baltic Sea.

Process(units)	Model	Black Sea	Baltic Sea
Primary Production (g C m^{-2} yr^{-1})	90	40-240 (Sorokin, 2002) (Yilmaz et al., 2006)	150 (Wasmund et al., 2005)
Dark CO_2 fixation (μM C d^{-1})	0.3-0.7	0.2 (Pimenov and Neretin, 2006), 0.4-2 (Yilmaz et al., 2006), 0.2- 0.6 (Morgan et al., 2006)	0.8-1.0 (Jost, p.c. 2006)
Sulfide oxidation (μM S d^{-1})	1.9	0.3 -4.5 (Jorgensen et al., 1991) (Sorokin, 2002)	
S^0 oxidation (μM S d^{-1})	0.3	0.6-0.9 (Sorokin, 2002)	
S_2O_3 oxidation (μM S d^{-1})	0.2	0.2-0.6 (Sorokin, 2002)	
Sulfate reduction (μM S d^{-1})	0.02	0.003-0.036 (Jorgensen et al., 1991) 0.2-0.6 (Pimenov and Neretin, 2006)	
Ammonification in oxic zone (μM N d^{-1})	0.1-0.5	0.1-0.5 (Sorokin et al., 1991) 0.005-0.05 (Kuypers et al., 2003)	
Nitrification (μM N d^{-1})	0.2 - 0.75 (deep NO_2 max)	NH_4 oxidation - 0.005-0.05 (Ward and Kilpatrick, 1991) 0.02-0.05 (Sorokin, 2002) NO_2 oxidation - 0.05-0.24 (Ward and Kilpatrick, 1991)	0.001-0.28 (Enoksson, 1986) 0.017-0.48 (Bauer, 2003)
Denitrification (μM N d^{-1})	0.2	0.002 (Ward and Kilpatrick, 1991)	0.044-0.11 (Brettar and Rheinheimer, 1991)
Nitrogen fixation (μM N d^{-1})	0.1-0.5	0.02-0.04 (Sorokin, 2002)	0.08-2.3 $mmol\,N\,m^{-2}\,d^{-1}$ (Wasmund et al., 2005) 0.68-0.74 $mmol\,N\,m^{-2}\,d^{-1}$ (Stal and Walsby, 2000)
Thiodenitrification (μM N d^{-1})	0.2	Is possible (Sorokin, 2002)	0- 2.7 (Hannig et al., 2006)
Anammox (μM N d^{-1})	0-0.03	0.007 (Kuypers et al., 2003)	0-0.05 (Hannig et al., 2006)
Mn oxidation (μM Mn d^{-1})	1.0	0.18-1.9 (Tebo, 1991)	
Mn reduction	0.9	0.96-3.6 (Nealson et al., 1991)	

Generally, the models estimates agreed well with the observed values for the same processes, but there were also a few differences. These may have been due to the fact that the model represents an averaged balanced picture, while observational data frequently reflect a transient situation, due to intrusions or temporal variability.

4.3.3 Model experiments

Models are developed in order to analyze data obtained through observations. It was shown in the previous section that the calculated spatial and temporal distributions of the parameters of interest agreed reasonably well with those data. The extent of this agreement supports application of the model to the analysis of results from other studies. In this section, examples of applications to specific questions concerning the function of the redox layer are provided.

Oxidation of H_2S

In the 1990s, it became evident that the potential sink of H_2S is not balanced solely by the O_2 supply (Murray et al., 1995). This discrepancy continues to challenge current thinking regarding the biogeochemistry of marine redox interfaces. It has been generally assumed that the oxidation of H_2S is connected with the activity of chemolithotrophic bacteria (Zopfi et al., 2001).

While experiments with labeled S have demonstrated that the maximum rate of H_2S oxidation is 0-20 m below the sulfide onset, the electron acceptor of this reaction below the sulfide interface has not been identified experimentally. Maximum dark CO_2 fixation is also observed in the 10 to 20-m layer below the sulfide interface (Pimenov and Neretin, 2006).

The model was therefore used to analyze the roles of different electron acceptors. H_2S oxidation was represented by the following reactions:

$$2H_2S + O_2 \rightarrow 2S^0 + 2H_2O \tag{4.7}$$

$$3H_2S + 4NO_3^- + 6OH^- \rightarrow 3SO_4^{2-} + 2N_2 + 6H_2O \tag{4.8}$$

$$H_2S + MnO_2 \rightarrow S^0 + Mn^{2+} + 2OH^- \tag{4.9}$$

$$H_2S + 2FeOOH \rightarrow 2Fe^{2+} + S^0 + 2OH^- \tag{4.10}$$

The modeled vertical profiles of these processes rates are presented in Fig. 4.4(A).

Estimates obtained with the model showed that H_2S oxidation with O_2 is very slow (less than 0.01 μM d^{-1}, or 0.02 μM S d^{-1}). The maximum rates of Mn reduction were 0.8 μM d^{-1},

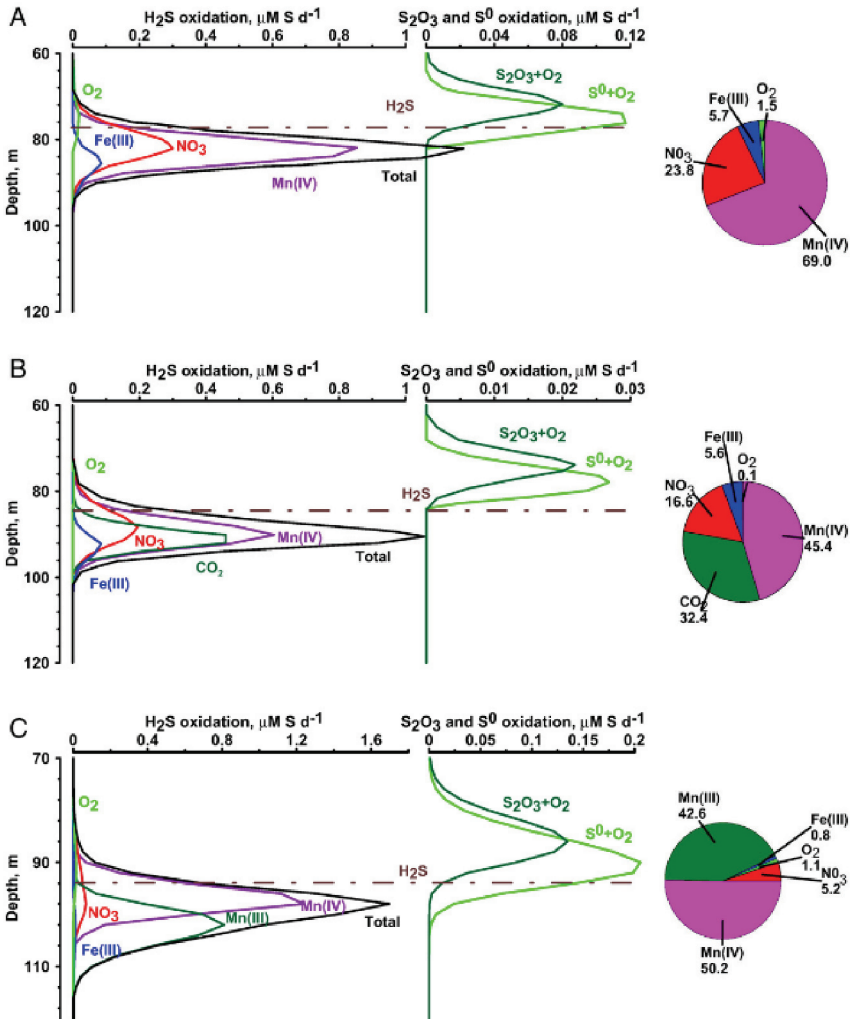

Figure 4.4: Left column: rates of oxidation of hydrogen sulfide with O_2, NO_3, Mn(IV), Fe(III) (A), O_2, NO_3, Mn(IV), Fe(III), CO_2 (B) and O_2, NO_3, Mn(IV), Mn(III), Fe(III) (C). Middle column: corresponding rates of oxidation of S^0 and S_2O_3 with O_2. Right column: potential electron acceptors and their extent of involvement in sulfide oxidation.

Fe reduction 0.10 μM d^{-}1, and NO_3 reduction about 0.30 μM d^{-1}. Therefore, H_2S oxidation was due primarily to the reduction of Mn(IV) - 69%, NO_3 - 24%, Fe(III) - 6%, and O_2 - 1% Fig. 4.4(A). The oxidation of elemental sulfur and thiosulfate to sulfate with dissolved oxygen occurred at depths that were several meters shallower (Fig. 4.4(A), central column).

In addition to the above-mentioned reactions, H_2S can be oxidized through anoxygenic photosynthesis (Canfield et al., 2005; Overmann and Manske, 2005):

$$2H_2S + CO_2 \rightarrow CH_2O + 2S^0 + H_2O \tag{4.11}$$

Simulations that parametrized all dark CO_2 fixation occurring in connection with the above-mentioned processes were carried out using the model. The results are presented in Fig. 4.4(B). In this case, CO_2 consumption would have resulted in an oxidation rate of 0.1-0.5 μM S d^{-1}. This was a significant share of the total sulfide oxidation (32%) but, the highest share of sulfide was still oxidized with Mn(IV).

Recently, the production of dissolved oxidized Mn, in the form of Mn(III), by Mn(II)-oxidizing bacteria and by incubations with Black Sea suboxic zone water was described (Webb et al., 2005). Dissolved Mn(III) has also been directly detected in the suboxic zone (Trouwborst et al., 2006). Mn(III), in dissolved or solid form, is an important intermediate product of the Mn cycle (Kostka et al., 1995). Therefore, the model was employed to take into account Mn reduction through the intermediate Mn(III):

$$2Mn_4 + +HS^- + OH^- \rightarrow 2Mn_3 + +S^0 + H_2O \tag{4.12}$$

$$2Mn_3 + HS^- \rightarrow 2Mn_2 + +S^0 + H^+ \tag{4.13}$$

In this case, sulfide oxidation was due to a decrease in Mn(IV) -50%, Mn(III) -43%, NO_3 -5%, Fe(III) -1%, and O_2 -1% (Fig. 4.4(C)).

These numerical experiments likely reflected specific situations that occur in natural water, under stable conditions or following intrusions. The role of anoxygenic photosynthesis should be subject to change depending on the depth of the redox interface. In any case, a dominant role in the oxidation of sulfide seems to be played by oxidized Mn species, which are formed several meters higher than the sulfide onset via the reaction of dissolved Mn(II) with O_2. The precipitation of Mn(IV) leads to an increase in the particles density and thus an accelerated rate of sinking (Yakushev and Debolskaya, 2000). Consequently, the depths of sulfide and Mn(II) onset differ. Our model demonstrated that an acceleration of the sinking rate significantly affects one of the key features of the oxic/anoxic interface, i.e., the 5 to 10-m difference between

the depths of the Mn(II) and sulfide onsets (Fig. 4.5(A)). In the absence of an accelerated sinking of Mn hydroxide (W_{Mn}=0), the oxic/anoxic interface became shallower, such that the H_2S onset was located at the same depth as the Mn(II) onset, and a layer appeared in which both O_2 and H_2S were present (Fig. 4.5(B)).

The intense vertical transport of detrital particles and heavy Mn components explains why there is a zone where oxygen and sulfide are absent. This, in turn, facilitates processes such as anammox (Dalsgaard et al., 2003; Kuypers et al., 2003) and the oxidation of Fe with Mn, and allows the presence of Mn in the form of Mn(III), which otherwise is quickly oxidized by O_2 or reduced by H_2S (Webb et al., 2005).

Consumption of O_2 in the suboxic layer

We used our model to analyze the roles of different processes in O_2 consumption. The vertical distributions of these processes from the surface to 200 m are presented in Fig. 4.6(A). Both OM mineralization (49%) and the respiration of living organisms (29%) were found to play dominant roles in O_2 consumption. These were the main processes that compensated for the production of O_2 by photosynthesis. Nitrification consumed 11% of the O_2 available in the lower part of the oxic zone, while the oxidation of reduced compounds in the water column of a sea with anoxic conditions was estimated at less than 10%.

Under oxygen-deficient conditions, i.e., from O_2 concentrations ¡40 μM to the sulfidic boundary Fig. 4.6(B), less O_2 was consumed in connection with the mineralization of OM and respiration (about 30%), because in this layer OM decomposition was mainly associated with denitrification. The largest amount of O_2 was consumed by nitrification (mainly ammonia oxidation to nitrate - 13%, and nitrite oxidation to nitrate - 8%). Consumption by the oxidation of reductants was about 50%, with a dominant share for Mn(III) (20.1%) and Mn(II) (17.9%) and less for reduced sulfur species. The amount of O_2 consumed by the oxidation of Fe(II) was negligible. These estimates are important for the modification of ecological models (Fennel and Neumann, 2004; Savchuk and Wulff, 1996) that describe oxygen processes but do not consider S, Mn, and Fe cycles.

Phosphate dipole

The vertical distribution of phosphate in the Black Sea is characterized by increased concentrations in the oxycline, a well-defined shallow minimum about 5-10 m shallower than the sulfide onset, a maximum below the sulfide onset, and a second deep minimum about 30-50 m deeper

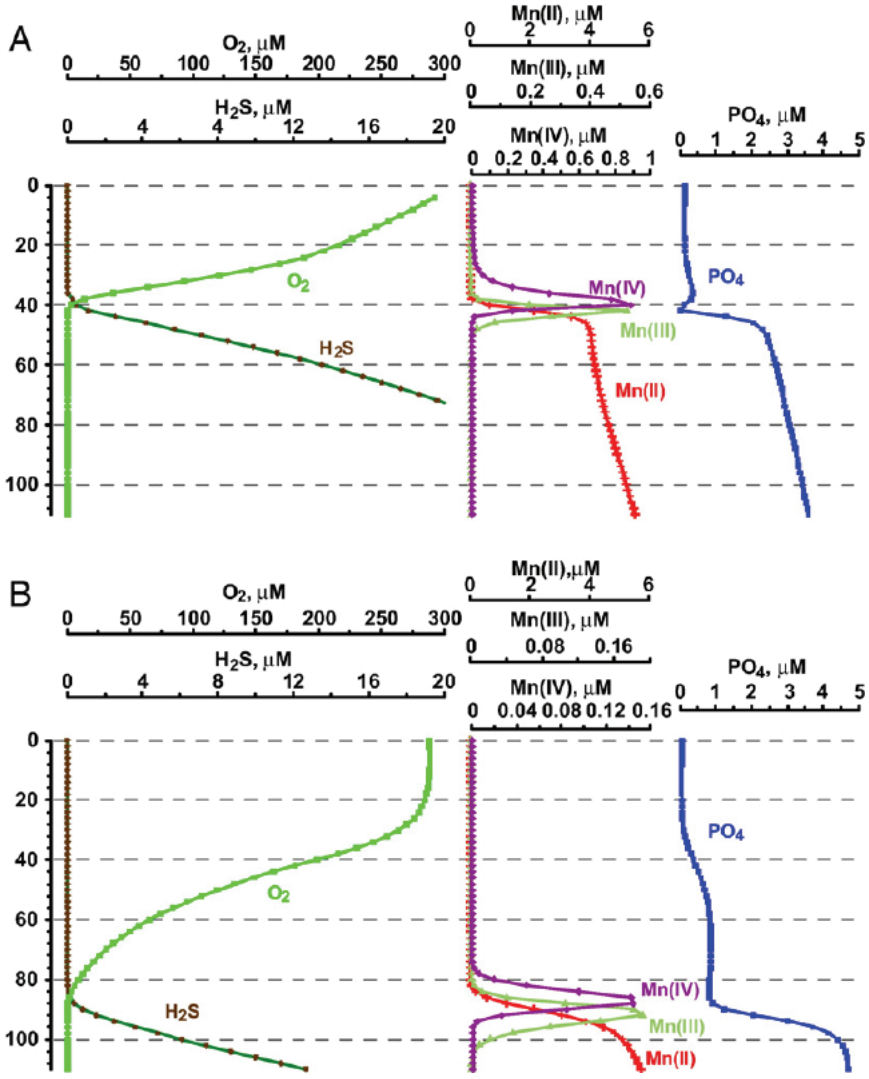

Figure 4.5: Vertical distribution of O_2, H_2S, Mn(II), Mn(III), Mn(IV), and PO_4 due to the accelerated sinking of particles with Mn hydroxides; $W_{Mn} = 18\,m\,d^{-1}$ (A) and $W_{Mn} = 0\,m\,d^{-1}$ (B).

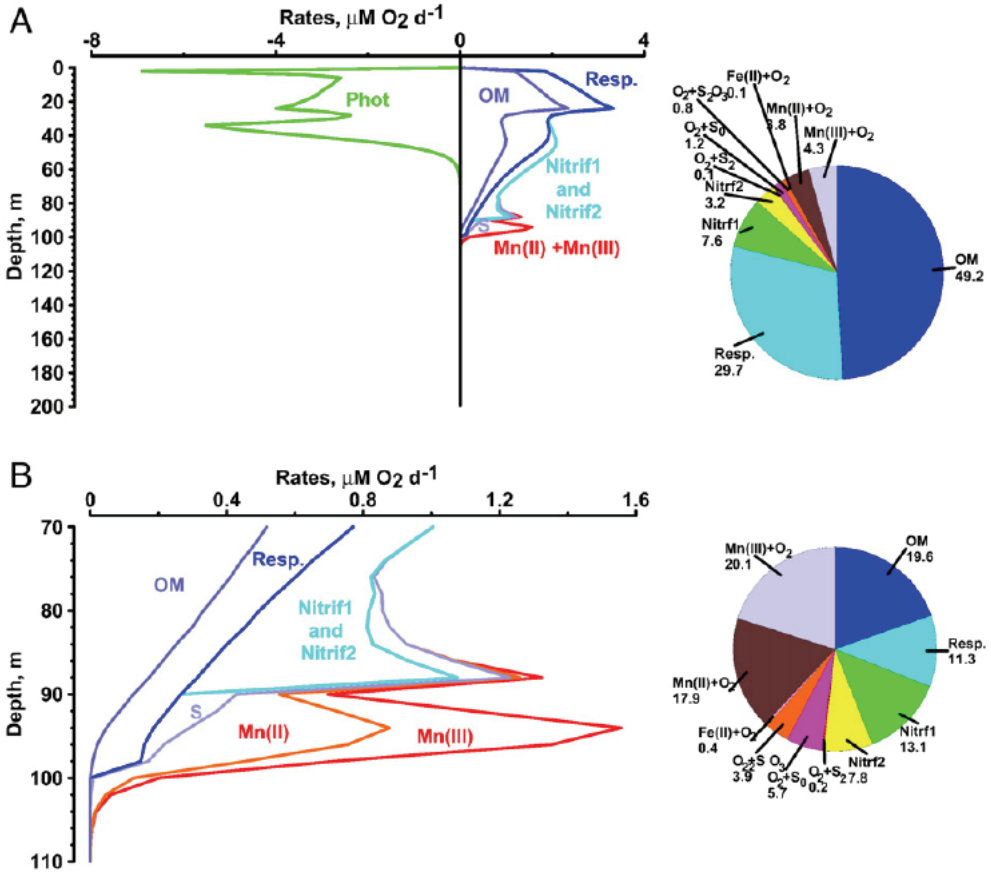

Figure 4.6: Dissolved oxygen consumption in a water column of 0 - 200 m (A) and in the layer below 70 m (O_2 <40 μM) (B).

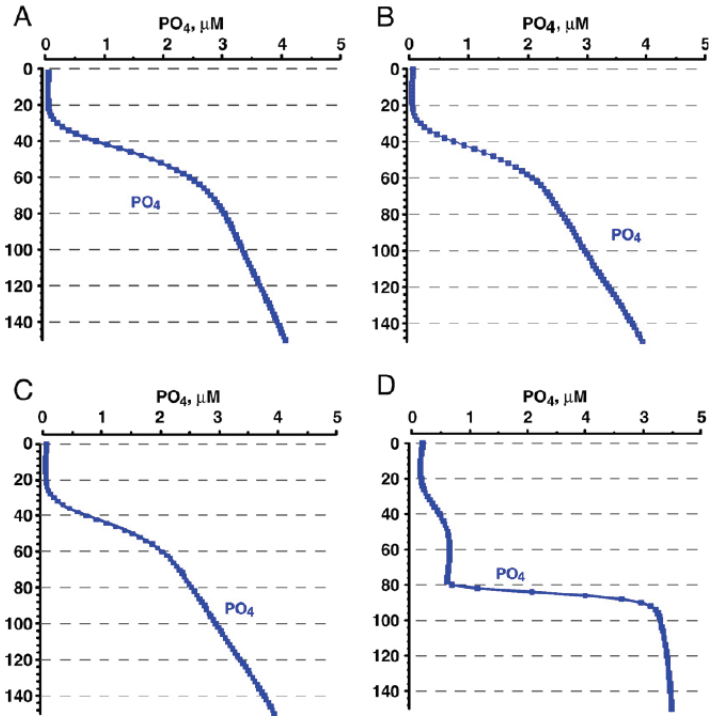

Figure 4.7: Influence of chemosynthesis and co-precipitation with iron or manganese on the formation of the phosphate dipole. See text for a more detailed explanation.

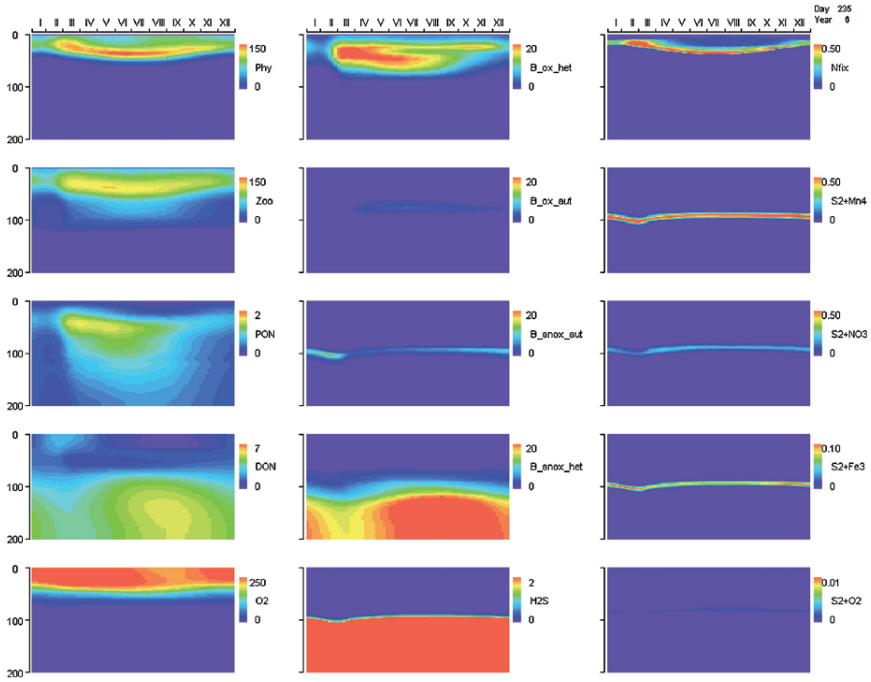

Figure 4.8: Seasonal changes in vertical structure (Black Sea).

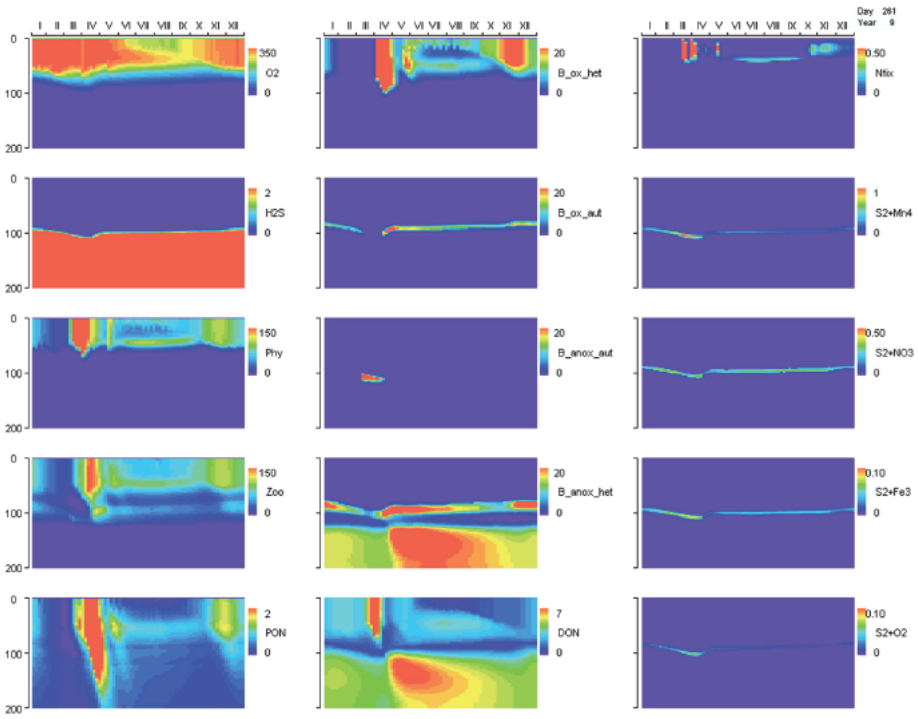

Figure 4.9: Seasonal changes in vertical structure (Baltic Sea).

Fig. 4.1(a). This structure is called the phosphate dipole (Shaffer, 1986). A similar phosphate distribution is observed in the Baltic Sea Fig. 4.1(b). The reason for the formation of this dipolar structure is unclear. Previously, it was thought to be connected with chemosynthesis (Sorokin, 2002) and/or the co-precipitation of phosphate with metal hydroxides (Shaffer, 1986). However, both theories are probably incorrect because the maximum values of chemosynthesis occur below the sulfide onset, where the phosphate content is also maximal, and the co-precipitation of phosphate with iron hydroxides is not large enough to account for its consumption. The Fe:P ratio during co-precipitation with iron hydroxides has been reported to be 4 (Savenko, 1995) or 2.7 (T. Leipe, personal communication, 2006). Laboratory experiments showed very high ratios of Mn:P = 1000 in the co-precipitation of Mn hydroxides (Savenko and Baturin, 1996). Therefore, phosphorous removal by precipitation of Mn hydroxides can be ignored.

It is possible, however, that Mn(III), an intermediate product between Mn(IV) and Mn(II), plays a key role in precipitation of phosphate. Known Mn(III) ligands that bind with enough strength to stabilize Mn(III) in solution include inorganic ligands, such as pyrophosphate (Webb et al., 2005). Mn(III) present in the Black Sea suboxic zone (Trouwborst et al., 2006) might easily form complexes with pyrophosphate. The phosphorus minimum is located at the same depth where Mn(II) is depleted due to possible oxidation with oxygen, and its maximum is

located about 5 m below the sulfide interface. Pyrophosphate particles were observed (T. Leipe, personal communication, 2006) at the redox interface of the Baltic Sea, and we observed a maximum of polyphosphate in the same layer in the Northeastern Black Sea in 2006. These depths coincide with the likely limits of the Mn(III) maximum.

The influence of PO_4 distribution on its consumption by (1) chemosynthesis, (2) co-precipitation with Fe(III), and (3) the formation of complexes with Mn(III) was therefore studied in a series of numerical experiments employing our model. The results are presented in Fig. 4.7.

In the absence of these three factors, there were no anomalies in phosphate distribution in the vicinity of the oxic/anoxic interface (Fig. 4.7(A)). Chemosynthesis resulted in negligible changes (Fig. 4.7(B)), and co-precipitation with Fe(III) at Fe:P=2.7 led to a minor decrease in the phosphate concentration (Fig. 4.7(C)). Inclusion of the formation of complexes with Mn(III) yielded a vertical distribution very similar to the observed one (Fig. 4.7(D)). According to Davies (1969), the ratios of Mn(III) pyrophosphate complexes may be Mn:P=0.25 for $Mn(HP_2O_7)_2^{3-}$ or Mn:P =0.17 for $Mn(H_2P_2O_7)_3^{3-}$. In our model, Mn:P was set at 0.66, about 2.5-4 times higher than those values. At this ratio, only about 25% of the Mn(III) was predicted to form complexes with polyphosphate, while the rest would complex with other ligands. The Mn(III) concentration calculated by the model was 0.2 μM (Fig. 4.7(E)), i.e., smaller than the observed concentration range (0.5-1.5 μM, Trouwborst et al. (2006)). This concentration could explain the phosphate dipole, even if only a fraction of the Mn(III) formed complexes with P. Further study of the relationships between Mn(III), pyrophosphate, and polyphosphate are important for a better understanding of the ecology of the Black Sea and the Baltic Sea, since the upward flux of phosphate limits the amount of photosynthesis during certain periods.

Seasonal changes in the redox-layer

The model was also employed to study the effects of seasonal variability on structural differences in the redox layer in the Black Sea and the Baltic Sea with respect to two different scenarios.

In the simplified scenario applied to the study of the Black Sea, the seasonality of phytoplankton development led to a summer-time increase in the flux of POM into the anoxic zone. The oxygen content in the suboxic zone changed seasonally depending on the amount of OM degradation (Fig. 4.8). Calculations for the Baltic Sea were based on the results of GOTM model (Burchard et al., 1999). In this more realistic scenario, the details regarding seasonal variability differed from those of the Black Sea: the spring bloom was more intense and shorter, and in fall a second phytoplankton bloom occurred (Fig. 4.9). As was the case for numerical

experiments involving the Black Sea, the model reproduced the seasonal changes in the depths of the redox layer.

For both scenarios, the calculations clearly showed that OM formed in the euphotic layer significantly influences the structure of the redox interface and the processes that take place in it. The redox zone is most likely marked by a competition for consumption of dissolved oxygen between OM supplied from the upper layers and reduced species of S, Mn, Fe and N supplied from the anoxic zone. The increase in OM flux in the summer causes more intense activity of heterotrophic (Fig. 4.8,Fig. 4.9) (both in oxic and anoxic zones) and aerobic autotrophic (nitrifiers) bacteria, whereas the activity of anaerobic chemolithotrophic organisms is reduced (Fig. 4.8,Fig. 4.9). In the winter months, the oxidation of reduced species of S, Mn, Fe and the upward flux of ammonia from the deep water intensifies. As a result, larger amounts of oxidized Mn species are formed, and sulfide oxidation reactions as well as the growth of chemolithotrophic bacteria play more important roles. Therefore, according to the models estimates, processes such as ammonification, denitrification, sulfate reduction, and nitrification predominate in the spring and summer, while the oxidation of reduced forms of metals and of hydrogen sulfide (with all possible electron acceptors) predominates in the winter.

The model demonstrated that in seas with anoxic conditions N_2 fixation should occur. The large NO_3 losses due to denitrification must be compensated for in order to maintain the system at steady state with regard to dissolved inorganic nitrogen. According to the model, N2 fixation should occur during the summer in the low boundary of the photic layer (Fig. 4.8,Fig. 4.9). The role of N_2 fixation in the nitrogen balance of the Baltic Sea is very large, (Schneider et al., 2002; Wasmund et al., 2005) testify that this process can contribute up to 60 % of the annual nitrogen consumption in the central Baltic Sea surface water. In the Black Sea there are no direct observations on N_2 fixation in the last decades, while in the 1950s-1960s N2 fixation in the Black Sea was intensive (Pshenin, 1963). Its possible that the absence of N_2 fixation in 1990s is connected with the intensive eutrophication of the Black Sea in 1970s-1980s, and favorable conditions for the N_2-fixation have now re-appeared. Yilmaz et al. (2006) reported that the concentrations of nitrate decreased considerably at the beginning of 2000s and nitrogen became a limiting element. The 15Nof suspended PON was around 0 ‰in the surface watersof the NE Black Sea during the late June 2005 which could indicate the presence of N fixing organisms (C.Fuschman, persomal communication).

4.3.4 Summary and conclusions

On the basis of this model it was possible to demonstrate the relationships between biogeochemical transformation processes and the distribution of biogeochemical parameters. In addition, three layers within the boundaries of the redox zone were distinguished:

Depth of the NO3 maximum

In the upper part of the redox zone, the concentrations of O_2 decreased to 15-20 μM; the O_2 vertical gradient decreased and became equal to that of nitrate. At lower depths, nitrate, instead of oxygen, was the main electron acceptor in OM degradation. The reason for the decrease in the O_2 gradient may have been the decrease in O_2 consumption during OM mineralization in conditions of low O_2 concentrations (Naqvi, 2006).

Depth of O_2 depletion

In the middle of the redox zone, the concentrations of oxidized chemical compounds diffusing downwards from the upper layer (O_2 and NO_3) decreased to zero. This occurred simultaneously with the depletion of reductants (deep NH_4, Mn (II)) diffusing upwards from the anoxic zone. A minimum of PO_4 was also found in this middle region. According to the model, the redox reactions that depleted the remaining O_2 also resulted in the disappearance or a decrease of the above-mentioned reductants and the formation of alternative electron acceptors, dissolved Mn(III) and particulate Mn(IV) and Fe(III). In addition to their transport by diffusion, these latter compounds have a sinking rate that accelerates their downward transport. Thus, a PO_4 minimum could be established, depending on the extent of its complexation with Mn(III). Our experiments showed that other factors, such as co-precipitation with Fe and Mn hydroxides and chemosynthesis, are less important.

Depth of the H2S onset

The peaks of oxidized Mn and Fe are located at this depth. There is an intense reduction of Mn(III) and Mn(IV) by sulfide in reactions that are balanced by the H_2S flux from below. Either a decrease in the PO_4 vertical gradient or the formation of the deep phosphate maximum occurs as a result of the degradation of phosphate complexes with reducing Mn(III).

The ability of this 1D model to reproduce the main features of the chemical structures of the central Black Sea and the Gotland Deep of the Baltic Sea suggests that the observed

structures are formed by biogeochemical transformations as well as the processes included in the model, specifically, biogeochemical interactions, vertical turbulence, and sinking.

Our numerical experiments showed that the seasonality of OM production results in: (1) competition for dissolved oxygen by consumption for OM mineralization and for oxidation of reduced compounds (H_2S, NH_4, Mn(II)), and (2) the seasonal activity of the functional groups of bacteria involved in these processes. Heterotrophic processes were shown to likely be more intense during the summer, and the development of heterotrophic aerobic and anaerobic bacteria as well as nitrifiers more pronounced. Chemolithotrophic bacteria, responsible for the intensity of redox processes, should be especially abundant in winter.

The nitrogen balance of seas with anoxic conditions includes compensation for the high level of denitrification by N fixation, the intensity of which is, in turn, influenced by the development of anoxic zones.

The scenarios included in the model offer an explanation for phosphate-dipole formation, as the results indicated that Mn(III) accounts for a large fraction of the dissolved Mn at that depth.

The model also suggested that the redox zone contains a layer in which O_2 and H_2S are absent, which allows the presence of Mn, in the form of Mn(III) and the anammox reaction. A dominant role in the oxidation of H_2S at its onset level was ascribed to oxidized Mn compounds. H_2S oxidation occurs through the reduction of several compounds in varying amounts: Mn(IV) -50%, Mn(III) -43%, NO_3 -5%, Fe(III) -1%, and O_2 -1%. By contrast, iron cycling in the formation of the redox layer structure was determined to be insignificant.

The results of this study allow us to conclude that mathematical modeling of the redox system is a useful tool for filling in the gaps in our knowledge and for determining the direction of further studies, including analysis of redox-system reactions and the effects of natural and anthropogenic forces upon them.

Acknowledgments

We appreciate the continuous support and critical and useful discussions with our colleagues from the Baltic Sea Research Institute Warnemuende and the Shirshov Institute of Oceanology, RAS. This research was supported by the Baltic Sea Research Institute Warnemuende, the Shirshov Institute of Oceanology, Russian Foundation for Basic Reasearch grants 06-05-96676 yug, 07-05-01024 and CRDF grant RUG1-2828-KS06.

4.4 Appendix

Table 4.2: Parameters names, notations, values and units of the coefficients used in the model.

Parameter	Notation	Units	Value
Specific rate of decomposition of POM to DOM	K_{PD}	d^{-1}	0.1
Mineralization in oxic conditions			
Specific rate of decomposition of DON and DOP	K_{ND4}	d^{-1}	0.1
Specific rate of decomposition of PON and POP	K_{NP4}	d^{-1}	0.04
Temperature parameter for oxic mineralization	$Ktox$	$^{\circ}C^{-1}$	0.15
Oxigen parameter for oxic mineralization	O_2ox	μM	0
Half saturation constant for oxic mineralization	Kox	μM	15
Denitrification			
Specific rate of 1st stage of denitrification	K_{N32}	d^{-1}	0.12
Specific rate of 2d stage of denitrification	K_{N24}	d^{-1}	0.2
Oxigen parameter for denitrification	O_2dn	μM	25
NO_3 parameter for denitrification	NO_3mi	μM	0.001
NO_2 parameter for denitrification	NO_2mi	μM	0.0001
Sulfate reductiuon			
Specific rate of sulfate reduction with sulfate	$K_{\_s4\_rd}$	d^{-1}	$2.5*10^{-7}$
Specific rate of sulfate reduction with thiosulfate	$K_{\_s23\_rd}$	d^{-1}	1.2
Oxygen parameter for sulfate reduction	O_2sr	μM	25
NO_3 and NO_2 parameter for sulfate reduction	$NOsr$	μM	0.5
Nitrification			
Specific rate of the 1st stage of nitrification	K_{N42}	d^{-1}	0.9
Specific rate of 2d stage of nitrification	K_{N23}	d^{-1}	2.5
Oxygen parameter for nitrification	O_2nf	μM	1
Nitrogen fixation			
Specific rate of nitrogen fixation	K_{Nfix}^{max}	d^{-1}	20
Anammox			
Anammox constant	$K_{anammox}$	d^{-1}	0.03
Oxidation of the hydrogen sulfide			
Specific rate of oxidation of H_2S with O_2	$K_{\_hs\_ox}$	d^{-1}	0.2
Specific rate of oxidation of S^0 with O_2	$K_{\_s0\_ox}$	d^{-1}	4
Specific rate of oxidation of S_2O_3 with O_2	$K_{\_s23\_ox}$	d^{-1}	1.5
S^0 disproportionation			
Specific rate of S^0 disproportionation	$Kdisp$	d^{-1}	0.01
Thiodenitrification			
Thiodenitrification constant	K_T	$\mu M^{-1}d^{-1}$	0.8
Oxidation and reduction of Mn and Fe			
Mn(II) oxidation with O_2 constant	K_mn_ox	d^{-1}	2
Mn(IV) reduction with Sulfide constant	K_mn_rd	d^{-1}	22
Mn(III) oxidation with O2 constant	K_mn_ox2	d^{-1}	18
Mn(IV) reduction with sulfide constant	K_mn_rd2	d^{-1}	2
Fe oxidation with O2 constant	K_fe_ox	d^{-1}	4
Fe oxidation with Mn(IV) constant	K_fe_mnox	d^{-1}	1
Fe oxidation with NO3 constant	K_fe_nox	d^{-1}	5
Fe(III) reduction by sulfide	K_fe_rd	d^{-1}	0.05
Phytoplankton			
Maximum specific growth rate	K_{NF}	d^{-1}	1.86
Specific respiration rate	K_FN	d^{-1}	0.05
Incident light	I_0	Wm^{-2}	80
Optimal light	I_{opt}	Wm^{-2}	25
Extinction coefficient	K	m^{-1}	0.07
Half-saturation constant for uptake of PO_4	K_{PO4}	μM	0.01
Strength of ammonium inhibition of nitrate uptake constant	K_{psi}		1.46
Half saturation constant for uptake of NH_4	K_{NH4}	μM	0.02
Half saturation constant for uptake of NO_3+NO_2	K_{NO3}	μM	0.03

Table 4.2: (continued)

Specific rate of mortality	K_{FP}	d^{-1}	0.05
Specific rate of excretion	K_{FD}	d^{-1}	0.05
Zooplankton			
Specific respiration rate	K_{ZN}	d^{-1}	0.1
Maximum specific rate of grazing of Zoo on Phy	K_{FZ}	d^{-1}	0.5
Half-saturation constant for the grazing of Zoo on Phy for Phy/Zoo ratio	K_F		1
Maximum specific rate of grazing of Zoo on POP	K_{PZ}	d^{-1}	0.6
Half-saturation constant for the grazing of Zoo on POP in dependence to ratio POP/Zoo	K_{PP}		200
Maximum specific rate of grazing of Zoo on Bae	K_{BaeZ}	d^{-1}	0.6
Half-saturation constant for the grazing of Zoo on Bae for Bae/Zoo ratio	K_{Bae}		1.5
Maximum specific rate of grazing of Zoo on Bhe	K_{BheZ}	d^{-1}	1.02
Half-saturation constant for the grazing of Zoo on Bhe for Bhe/Zoo ratio	K_{Bhe}		1.1
Maximum specific rate of grazing of Zoo on Baa	K_{BaaZ}	d^{-1}	0.78
Half-saturation constant for the grazing of Zoo on Baa for Baa/Zoo ratio	K_{Baa}		1.5
Maximum specific rate of grazing of Zoo on Bha	K_{BhaZ}	d^{-1}	0.6
Half-saturation constant for the grazing of Zoo on Bha for Bha/Zoo ratio	K_{Bha}		1
Maximum specific rate of mortality of Zoo	K_{ZP}	d^{-1}	0.001 for:$H_2S \leq 20\mu M$ 0.9 for:$H_2S > 20\mu M$
Food absorbency for zooplankton	U_z		0.7
Ratio between dissolved and particulate excretes of zooplankton	H_z		0.6
Aerobic heterotrophic bacteria			
Maximum specific growth rate of Bhe	K_{Bhe}^{max}	μM^{-1}	2
Half-saturation constant for the dependence of maximum specific growth rate of Bhe on POM and DOM content	K_{Bhe}^{N}	μM	0.5
Maximum specific rate of mortality of Bhe	K_{Bhe}^{Mort}	d^{-1}	0.03 for:$O_2 > 1\mu M$ 0.99 for:$O_2 \leq 1\mu M$
Aerobic autotrophic bacteria			
Maximum specific growth rate of Bae	K_{Bae}^{max}	μM^{-1}	1
Half-saturation constant for the dependence of maximum specific growth rate of Bae on NH_4	K_{Bae}^{N}	μM	0.05
Half-saturation constants for the dependence of maximum specific growth rate of Bae on PO_4	K_{Bae}^{P}	μM	0.3
Maximum specific rate of mortality of Bae	K_{Bae}^{Mort}	d^{-1}	0.01 for:$O_2 > 1\mu M$ 0.99 for:$O_2 \leq 1\mu M$
Anaerobic heterotrophic bacteria			
Maximum specific growth rate of Bha	K_{Bha}^{max}	μM^{-1}	2
Half-saturation constant for the dependence of maximum specific growth rate of Bha on POM and DOM	K_{Bha}^{N}	μM	6
Maximum specific rate of mortality of Bha	K_{Bha}^{Mort}	d^{-1}	0.01
Anaerobic autotrophic bacteria			
Maximum specific growth rate of Baa	K_{Baa}^{max}	μM^{-1}	6.5
Half-saturation constants for the dependence of maximum specific growth rate of Baa on NH_4	K_{Baa}^{N}	μM	3
Half-saturation constants for the dependence of maximum specific growth rate of Baa on PO_4	K_{Baa}^{P}	μM	3
Maximum specific rate of mortality of Baa	K_{Baa}^{Mort}	d^{-1}	0.001 for:$H_2S > 16\mu M$ 0.99 for:$H_2S \leq 16\mu M$
Sinking			
Rate of sinking of Phy	W_{Phy}	$m\,d^{-1}$	0.5
Rate of sinking of Zoo	W_{Zoo}	$m\,d^{-1}$	1.0
Rate of sinking of (Bhe,Bae,Bha,Baa)	W_{Bact}	$m\,d^{-1}$	0.5
Rate of sinking of (POP, PON)	W_D	$m\,d^{-1}$	6.0

Table 4.2: (continued)

Rate of accelerated sinking of particles with settled Mn hydroxides	W_{Me}^{max}	$m\,d^{-1}$	18

Table 4.3: Rates of biogeochemical production/consumption of the model compartments R_i.

Phosphate (PO_4)	$R_{PO4} = Sp(GrowthPhy(K_{FN} - 1.) - Chemos - ChemosA + K_{ZN}Zoo) + +PhosPOP + PhosDOP + Coprecip$
Dissolved Organic Phosphorus (DOP)	$R_{DOP} = Sp(ExcrPhy + Grazing(1. - Uz)Hz + +0.7MortBact - Hetero - HeteroA - DON/(DON + PON) * *(Hetero + HeteroA)) + AutolisP - PhosDOP$
Particulate Organic Phosphorus (POP)	$R_{POP} = Sp(MortPhy + MortZoo + 0.3MortBact + +Grazing(1. - Uz)(1. - Hz) - GrazPOP - PON/(DON + PON) * *(Hetero + HeteroA)) - AutolisP - PhosPOP$
Particulate Organic Nitrogen (PON)	$R_{PON} = Sn(MortPhy + MortZoo + 0.3MortBact + +Grazing(1. - Uz)(1. - Hz) - GrazPOP - PON/(DON + PON) * *(Hetero + HeteroA)) - AutolisN - AmmonPON$
Dissolved Organic Phosphorus (DON)	$R_{DON} = Sn(ExcrPhy + Grazing(1. - Uz)Hz + 0.7MortBact - -(Hetero + HeteroA)) + AutolisN - AmmonDON$
Ammonia (NH4)	$R_{NH4} = Sn * (GrowthPhy(KFN - 1.)(LimNH4/LimN)x - -Chemos - ChemosA + KZN * Zoo) + AmmonPON + +AmmonDON - Nitrif1 + Nfixation$
Nitrite (NO2)	$R_{NO2} = Sn * (GrowthPhy * (KFN - 1.) * (LimNO3/LimN) * *(NO2/(NO2 + NO3))) + Nitrif1 - Nitrif2 + Denitr1 - Denitr2 - sulfido2$
Nitrate (NO3)	$R_{NO3} = Sn * (GrowthPhy * (KFN - 1.) * (LimNO3/LimN) * *(NO3/(NO2 + NO3))) + Nitrif2 - Denitr1 - 1.25sulfido - ox - fe\_nox$
Oxygen (O2)	$R_{O2} = OkPSpGrowthPhy + 2.SnGrowthPhy(NO3/(NO2 + NO3)) (LimNO3/LimN) + 0.5SnGrowthPhy(NO2/(NO2 + NO3)) * *(LimNO3/LimN) - Destr\_OM - OkPSp(GrowthPhyKFN + KZNZoo) - -1.5Nitrif1 - 0.5Nitrif2 - 0.5hs\_ox - s0\_ox - 2s23\_ox - mn\_ox - fe\_ox$
Hydrogen sulfide (H2S)	$R_{H2S} = -hs_ox + s23_rd - 0.5fe_rd - mn_rd - -sulfido - sulfido2 + 0.5Disprop$
Elemental sulphur (S0)	$R_{S0} = hs_ox - s0_ox + 1.mn_rd - Disprop$
Thiosulfate (S2O3)	$R_{S2O3} = s0_ox - s23_ox + s4_rd - s23_rd + 0.5Disprop$
Sulfate (SO4)	$R_{SO4} = s23_ox - s4_rd + sulfido + sulfido2$
Bivalent manganese (Mn(II))	$R_{Mn2} = mn_rd2 - mn_ox + 0.5 * fe_mnox$
Quadrivalent manganese (Mn(IV))	$R_{Mn4} = mn_ox2 - mn_rd - 0.5 * fe_mnox$
Trivalent manganese (Mn(III))	$R_{Mn3} = mn_ox - mn_ox2 + mn_rdmn_rd2$
Bivalent iron (Fe(II))	$R_{Fe2} = fe_rd - fe_ox - fe_mnox - 5. * fe_nox$
Trivalent iron (Fe(III))	$R_{Fe3} = fe_ox + fe_mnox + 5. * fe_nox - fe_rd$
Phytoplankton (Phy)	$R_{phy} = GrowthPhy(1 - K_{FN}) - MortPhy - ExcrPhy - GrasPhy$
Zooplankton (Zoo)	$R_{Zoo} = Grazing * Uz - MortZoo - K_{ZN} * Zoo$
Aerobic heterotrophic bacteria (Bhe)	$R_{Bhe} = C_{Bhe} - Mort_{Bhe} - Graz_{Bhe}$
Aerobic autotrophic bacteria (Bae)	$R_{Bae} = C_{Bae} - Mort_{Bae} - Graz_{Bae}$
Anaerobic heterotrophic bacteria (Bha)	$R_{Bha} = C_{Bha} - Mort_{Bha} - Graz_{Bha}$
Anaerobic autotrophic bacteria (Baa)	$R_{Baa} = C_{Baa} - Mort_{Baa} - Graz_{Baa}$

Table 4.3: (continued)

Where Sn=0.016, Sp=0.001 are ratios between N and P content and the wet weight, OkP=106 is the O:P ratio.

Table 4.4: Parameterization of the biogeochemical processes $Rates_{BG}$.

Name of process/reaction	Parameterizations
Autolysis	$Autolis\_P = K_{PD} POP$
	$Autolis\_N = K_{PD} PON$
Mineralization at oxic conditions	$DcDM\_O2 = exp(Ktox * T) * K_{ND4} * DON * Fox$
$(CH_2O)_{106}(NH_3)_{16}H_3PO_4 + 106O_2 =$	$DcPM\_O2 = exp(Ktox * T) * K_{NP4} * PON * Fox$
$106CO_2 + 16NH_3 + h_3PO_4 + 106H_2O$	$Fox = \begin{cases} = 0 & for\, O_2 > O_2dn \\ = \frac{O_2 - O_2ox}{O_2 - O_2ox + Kox} & for\, O_2 \leq O_2ox \end{cases}$
Denitrificatin	$Denitr1\_PM = K_{N32} * Fdnox * FdnNO3 * PON$
$(CH_2O)_{106}(NH_3)_{16}H_3PO_4 + 84.8HNO_3 =$	$Denitr2\_PM = K_{N24} * Fdnox * FdnNO2 * PON$
$106CO_2 + 42.2N_2 + 148.4H_2O + 16NH_3 + H_3PO_4$	$Denitr1\_DM = K_{N32} * Fdnox * FdnNO3 * DON$
$\frac{1}{2}CH_2O + NO_3^- \rightarrow NO_2^- + \frac{1}{2}H_2O + \frac{1}{2}CO_2$	$Denitr2\_DM = K_{N24} * Fdnox * FdnNO2 * DON$
$\frac{3}{4}CH_2O + H^+ + NO_2^- \rightarrow \frac{1}{2}N_2 + \frac{5}{4}H_2O + \frac{3}{4}CO_2$	$Fdnox = \begin{cases} = 0 & for\, O_2 > O_2dn \\ = 1 - \frac{O_2}{O_2dn(O_2dn + 1 - O_2)} & for\, O_2 \leq O_2ox \end{cases}$
	$FdnNO3 = \begin{cases} = 0 & for\, NO_3 \leq NO_3mi \\ = 1 - \frac{NO_3 - NO_3mi}{NO_3 - NO_3mi + 1} & for\, NO_3 > NO_3mi \end{cases}$
	$FdnNO2 = \begin{cases} = 0 & for\, NO_2 \leq NO_2mi \\ = 1 - \frac{NO_2 - NO_2mi}{NO_2mi + 1} & for\, NO_2 > NO_2mi \end{cases}$
	$DcP_NO_3 = Denitr1\_PM + Denitr2\_PM$
	$DcDM\_NO_3 = Denitr1\_DM + Denitr2\_DM$
Sulfatereduction	$s4\_rd\_PM = K\_s4\_rd * Fsox * Fsnx * SO_4 * PON$
$(CH_2O)_{106}(NH_3)_{16}H_3PO_4 + 53SO_4^{2-} =$	$s4\_rd\_DM = K\_s4\_rd * Fsox * Fsnx * SO_4 * DON$
$106CO_2 + 106H_2O + 16NH_3 + H_3PO_4 + 53S^{2-}$	$s23\_rd\_PM = K\_s23\_rd * Fsox * Fsnx * PON * S_2O_3$
	$s23\_rd\_DM = K\_s23\_rd * Fsox * Fsnx * DON * S_2O_3$
	$Fsox = \begin{cases} = 0 & for\, O_2 > O_2sr \\ = 1 & for\, O_2 \leq O_2sr \end{cases}$
	$Fsnx = \begin{cases} = 0 & for\, (NO_3 + NO_2) > Nosr \\ = 1 & for\, (NO_3 + NO_2) \leq Nosr \end{cases}$
	$DcPM\_SO_4 = s23\_rd\_PM + s4\_rd\_PM$
	$DcDM\_SO_4 = s23\_rd\_DM + s4\_rd\_DM$
Ammonification and phosphatification	$AmmonPON = DcPM\_O_2 + DcPM\_NO_3 + DcPM\_SO_4$
	$AmmonDON = DcDM\_O_2 + DcDM\_NO_3 + DcDM\_SO_4$
	$PhosPOP = AmmonPON/16$
	$PhosDOP = AmmonDON/16$
Nitrification	$Nitrif1 = K_{N42} * NH_4 * O_2/(O_2 + O_2nf)$
$NH_4^+ + 1.5O_2 \rightarrow NO_2^- + 2H^+ + H_2O$	$Nitrif2 = K_{N23} * NO_2 * O_2/(O_2 + O_2nf)$
$NO_2^- + 0.5O_2 \rightarrow NO_3^-$	

Table 4.4: (continued)

Nitrogen fixation	$Nfixation = K_{Nfix}^{max} \frac{1}{1+\left(\frac{NO_3+NO_2+NH_4}{16PO_4}\right)^4} \frac{PO_4}{PO_4+0.3} * K_{NF} * f_i(i) * f_i(T) * Phy * Sn$
Anammox $NO_2 + NH_4 \rightarrow N_2 + 2H_2O$	$Anammox = NO_2 * NH_4 * K_{anammox}$
Oxidation of reduced S forms with oxygen	
$2H_2S + O_2 \rightarrow 2S^0 + 2H_2O$	$hs\_ox = K_{\_hs\_ox} * H_2S * O_2$
$2S^0 + O_2 + H_2O \rightarrow S_2O_3^{2-} + 2H^+$	$s0\_ox = K_{\_s0\_ox} * S^0 * O_2$
$S_2O_3^{2-} + 2O_2 + OH^- \rightarrow 2SO_4^{2-} + H_2O$	$s23\_ox = K_{\_s23\_ox} * S_2O_3 * O_2$
S^0 disproportionation	
$4S^0 + 4H_2O \rightarrow 2H_2S + S_2O_3^{2-} + 2H^+$	$Disprop = Kdisp * S^0$
Thiodenitrification	$hs\_NO3 = K_T * H_2S * NO_3$
$3H_2S + 4NO_3^- + 6OH^- \rightarrow 3SO_4^{2-} + 2N_2 + 6H_2O$	$hs\_NO2 = K_T * H_2S * NO_2$
Mn oxidation and reduction	
$4Mn^{2+} + O_2 + 4H^+ \rightarrow 4Mn^{3+} + 2H_2O$	$mn\_ox = K_{\_mn\_ox} * O_2 * Mn(II)$
$4Mn^{3+} + O_2 + 6OH^- \rightarrow 4MnO_2 + 6H_2O$	$mn\_ox2 = K_{\_mn\_ox2} * O_2 * Mn(III)$
$2MnO_2 + 7H^+ + HS^- \rightarrow 2Mn^{3+} + 4H_2O$	$mn\_rd = K_{\_mn\_rd} * Mn(IV) * H_2S$
$2Mn^{3+} + HS^- \rightarrow 2Mn^{2+} + S^0 + H^+$	$mn\_rd2 = K_{\_mn\_rd2} * Mn(III) * H_2S$
Fe oxidation and reduction	
$4Fe^{2+} + O_2 + H_2O \rightarrow 4Fe^{3+} + 4OH^-$	$fe\_ox = K_{\_fe\_ox} * Fe(II) * O_2$
$2Fe_2^+ + MnO_2 + 2H_2O \rightarrow FeOOH + Mn^{2+} + 2H^+$	$fe\_mnox = K_{\_fe\_mnox} * Fe(II) * Mn(IV)$
$10Fe^{2+} + 2NO_3^- + 12H^+ \rightarrow 10Fe^{3+} + N_2 + 6H_2O$	$fe\_nox = K_{\_fe\_nox} * Fe(II) * NO_3$
$2FeOOH + H_2S \rightarrow 2Fe^{2+}S^0 + 4OH^-$	$fe\_rd = K_{\_fe\_rd} * Fe(III) * H_2S$
P sorption/desorption and complexation	$Coprecip = (fe\_rd - fe\_ox - fe\_mnox)/2.7$ $-(mn\_ox - mn\_ox2 + mn\_rd - mn\_rd2)/0.66$
Phy growth rate	$GraowthPhy = K_{NF} f_t(T) f_i(i) min\{f_P(PO_4), f_N(NO_3, NO_2, NH_4)\}$ $f_t(T) = 0.2 + 0.22 \frac{(exp(0.21T)-1)}{(1+0.28exp(0.21T))}$ $f_i(i) = f_\varphi(\varphi) \frac{I_0}{I_{opt}} exp(-kh) exp(1 - \frac{I_0}{I_{opt}} exp(-kh))$ $f_P(PO_4) = \frac{PO_4}{K_{PO_4}+PO_4}$ $f_N(NO_3, NO_2.NH_4) = \frac{(NO_3+NO_2)exp(-K_{psi}NH_4)}{K_{NO_3}+NO_3+NO_2} + \frac{NH_4}{K_{NH_4}+NH_4}$
Phy excretion rate	$ExcrPhy = K_{FD} * Phy$
Phy mortality rate	$MortPhy = K_{FP} * Phy$
Grazing of Zoo	$Grazing = GrazPhy + GrazPOP + GrazBact$
Grazing of Zoo on Phy	$GrazPhy = K_{FZ} * Zoo * \frac{Phy/Zoo}{Phy/Zoo+K_F}$
Grazing of Zoo on detritus	$GrazPOP = K_{PZ} * Zoo * \frac{POP/Zoo}{POP/Zoo+K_{PP}/0.001}$
Grazing of Zoo on bacteria	$GrazBact = Graz_{Bhe} + GrazBae + Graz_{Bhat} + Graz_{Baa}$ $Graz_{Bhe} = K_{BhaZ} * Zoo * \frac{Bhe/Zoo}{Bhe/Zoo+K_{Bhe}}$ $Graz_{Bae} = K_{BhaZ} * Zoo * \frac{Bae/Zoo}{Bae/Zoo+K_{Bae}}$ $Graz_{Bha} = K_{BhaZ} * Zoo * \frac{Bha/Zoo}{Bha/Zoo+K_{Bha}}$

Table 4.4: (continued)

	$Graz_{Baa} = K_{BhaZ} * Zoo * \frac{Baa/Zoo}{Baa/Zoo+K_{Baa}}$
Mortality of Zoo	$MortZoo = K_{ZP} * Zoo * Zoo$
Growth rate of Bhe	$C_{Bhe} = K_{Bhe}^{max} * (DcPM\_O_2 + DcDM\_O_2) f_{Bhe}(DON + PON) Bhe$ $f_{Bhe}(DON + PON) = \frac{PON+DON}{PON+DON+K_{Bhe}^{N}}$
Rate of mortality oh Bhe	$Mort_{Bhe} = K_{Bhe}^{Mort} Bha^2$
Growth rate of Bae	$C_{Bae} = K_{Bae}^{max} * (Nitrif\_1 + Nitrif\_2 + S^0\_ox + S_2O_3\_ox + mn\_ox + fe\_ox) f_{Bae}^{NP}(NH_4, PO_4) Bae$ $f_{Bae}^{NP}(NH_4, PO_4) = min\left\{\frac{NH_4}{NH_4+K_{Bae}^{N}}, \frac{PO_4}{PO_4+K_{Bae}^{P}}\right\}$
Rate of mortality of Bae	$Mort_{Bae} = K_{Bae}^{Mort} Bae^2$
Growth rate of Bha	$C_{Bha} = K_{Bha}^{max} * (DcPM\_NO_3 + DcDM\_NO_3 + DcPM\_SO_4 + DcDM\_SO_4) f_{Bha}^{NP}(DON + PON) Bha$ $f_{Bha}(DON + PON) = \frac{PON+DON}{PON+DON+K_{Bha}^{N}}$
Rate of mortality of Bha	$Mort_{Bha} = K_{Bha}^{Mort} Bha^2$
Growth rate of Baa	$C_{Baa} = K_{Baa}^{max} * (mn\_rd + fe\_rd + hs\_ox + hs\_NO3 + hs\_NO2 + anammox) f_{Baa}^{NP}(NH_4, PO_4) Baa$ $f_{Baa}^{NP}(NH_4, PO_4) = min\left\{\frac{NH_4}{NH_4+K_{Baa}^{N}}, \frac{PO_4}{PO_4+K_{Baa}^{P}}\right\}$
Rate of mortality of Baa	$Mort_{Baa} = K_{Baa}^{Mort} Baa^2$

4.5 The application of ERGOM with a function to correct the oxygen consumption processes in oxygen-deficient conditions

Results of modelling by Yakushev et al. (2007) (see section 4) have given the chance to parametrize, more correctly, the consumption of oxygen in oxygen-deficient conditions on oxidation of reduced forms of sulfur and metals (Mn, Fe) coming from the anaerobic zone without adding in ecological models cycles of such elements in an explicit form. Such parametrization was performed by the author and published in the co-authorship in Yakushev et al. (2008). This parametrization has been of the form:

$$Ox_{cons}MnSFe = f(C_{O_2}) * (O_2resp + O_2Nitr + O_2Mineral) \tag{4.14}$$

where, $Ox_{cons}MnSFe$ - loss of oxygen on oxidation of reduced forms; O_2resp, O_2Nitr, $O_2Mineral$ - loss of oxygen on respiration, nitrification and OM mineralization, respectively.

$$f(C_{O_2}) = 0.5\left(1 + \tanh\left(\frac{\gamma_1 - C_{O_2}}{\gamma_2}\right)\right) \tag{4.15}$$

$\gamma_1 = 30\ [\mu M\, O_2\, m^{-3}]$ is a constant which defines the oxygen concentration where loss of oxygen doubles, $\gamma_2 = 0.03\ [\mu M\, O_2\, m^{-3}]$ is a constant which determines the rate of oxygen consumption. $f(C_{O_2})$ ranges from 0 to 1.

To estimate the significance of oxygen consumption on oxidation of reduced forms of sulfur and metals the 1D study with the model ERGOM was performed. The parametrization (eq. 4.14) was included in the ERGOM model. For this study, the model setup for years 1978 - 1993 from Kuznetsov et al. (2008) was used. Here, the results of two simulations, one with simulation from Kuznetsov et al. (2008) ("base" simulation) and one simulation with parametrization (eq. 4.14) included, are presented.

Result

Physical scenarios for both simulations were the same and identical to the simulations in Kuznetsov et al. (2008).

Observed and modeled oxygen zero levels are shown in Figure 4.10. The simulated oxygen depleted slower after the inflow event in year 1978 than in the observations. However, after 5 years of modeling the simulated oxygen zero level was higher than in the observations. That can be explained by the impact of inflow events, which was not parametrized in the model. Taking into account the small inflows in 1982 and 1983, the oxygen zero level is reproduced within the range of the observations. Along with the oxygen zero level, the nitrate zero level decreased

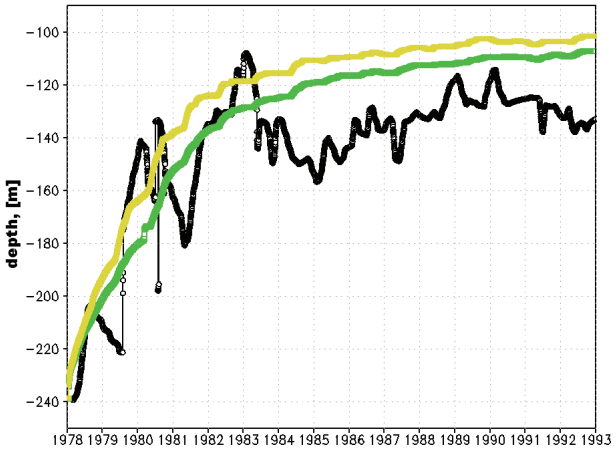

Figure 4.10: Oxygen zero level. Black - observation, green - "base" simulation, yellow - simulation with additional consumption of oxygen on oxidation reduced forms of sulfur and metals.

slower after the inflow and the nitrate zero level was higher after 5 years of simulations (see Figure 4.11).

The parametrization of the oxygen loss effect influenced the rate of oxygen depletion. The oxygen zero level in the simulation with additional consumption of oxygen rises faster than in the "base" simulation (see Fig. 4.10). The oxygen zero level difference between the simulation with additional consumption of oxygen and the "base" simulation is shown in Fig. 4.12. The strong effect of the additional consumption of oxygen can be seen in the first years of the simulations. The difference between the two simulations reached 20 meters. However, after the first 3 years of the simulations the effect of additional oxygen consumption was reduced. After the first 10 years the difference was fixed at 6 meters.

Discussion and conclusion

The parametrization of additional oxygen consumption due to the oxidation of reduced forms of sulfur, Mn and Fe increased the rate of oxygen depletion and raised the oxygen zero level. Thus, the effect played the biggest role during the first years of the stagnation period.

Changing the depth of the oxygen zero level can significantly change the anoxic area of the whole basin, that can affect the flux conditions at the bottom - water column boundary.

However, small and moderate lateral intrusions which affect the observed oxygen dynamics are not included in the model. Varying river runoff, transports from the coastal areas to the open sea, inflow events and different upwelling intensities were not taken into account.

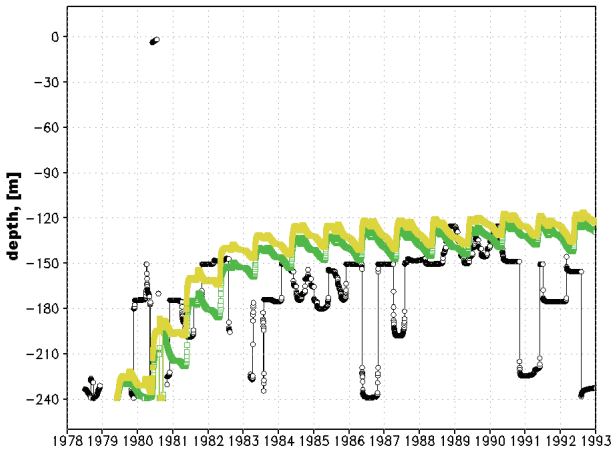

Figure 4.11: Nitrate zero level. Black - observation, green - "base" simulation, yellow - simulation with additional consumption of oxygen on oxidation reduced forms of sulfur and metals.

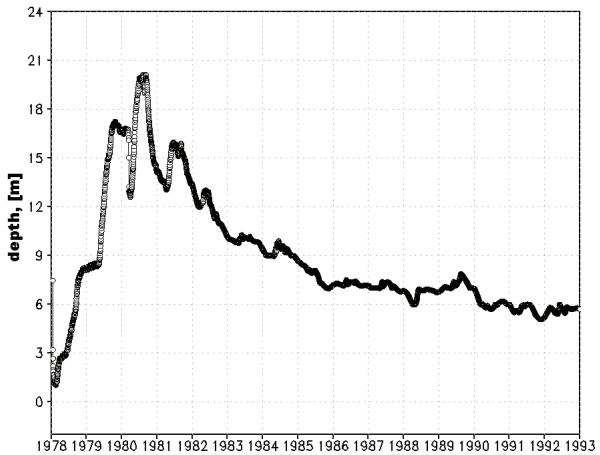

Figure 4.12: Oxygen zero level difference between the two simulations.

These processes are known to be important for interannual variations. Such processes can be considered with 3D models.

Results of this study can be used for more detailed 3D studies of the importance of the oxygen consumption due to oxidation of reduced forms of sulfur, Mn and Fe.

Chapter 5

Processes regulating the pCO2 in the Baltic Sea surface waters, a model study

This chapter to be submitted to Journal of Marine Systems :

Kuznetsov, I., Neumann, T., Schneider, B., Yakushev, E. 2008. Processes regulating the pCO2 in the Baltic Sea surface waters, a model study.

Statement on my contribution to this publication :

The model modification, model setup and analysis of the results were done by me. The manuscript was written by myself. T. Neumann, B. Schneider and E. Yakushev contributed in editing the writing, expertise and scientific advice.

Abstract

Simulation of the seasonal changes of the CO_2 partial pressure is presented here. Verification of modeling results with data from observations was performed. That will allow the improvement of the ability of the model to estimate nitrogen fixation in the Central Baltic and to study its impact on the ecological state of the Baltic Sea. The model used in this study is the public domain water column model GOTM (General Ocean Turbulence Model, see www.gotm.net) coupled with a modificated Baltic Sea ecosystem model ERGOM (The Baltic Sea Research Institutes Ecosystem Model). To estimate the nitrogen fixation rates in the Gotland Sea we elaborated a modification of the ERGOM model, where we included an additional phytoplankton group able to fix nitrogen during March-June. Furthermore, we extended the model with a simple CO_2 cycle. Variable C:N:P ratios controlled by phosphate concentrations in ambient water are used for cyanobacteria, detritus and sediment detritus. After inclusion of an additional

phytoplankton group, we got improved reproduction of the dynamics of sea surface phosphate and pCO_2. Resulting nitrogen fixation rates for the year 2005 were 259 $mmol\ m^{-2}\ year^{-1}$ and 278 $mmol\ m^{-2}\ year^{-1}$ for the simulation with the additional phytoplankton group and the "base" simulation, respectively.

5.1 Introduction

The area of our investigation is the Gotland Sea - one of the Baltic Seas sub-basins (see Fig. 5.1). The Baltic Sea is a small sea on a global scale, but at the same time one of the largest brackish water area in the world. With an average depth of 53 metres it contains $21,547\ km^3$ of water, rivers bring about 2% of its volume yearly (HELCOM, 2003). The narrow and shallow Danish straits (Kattegat region, see Fig. 5.1) connect the Baltic Sea with the North Sea and limit the water exchange of the Baltic Sea with the world's oceans. Due to the strongly limited water exchange with the North Sea, the residence time of the Baltic waters lasts up to 30 years. Surface salinity varies from 20 PSU in the Kattegat to 1-2 in the Bothnian Bay. The vertical structure of the Gotland Sea is characterized by a permanent salinity stratification, the halocline, that limits the vertical exchange of water.

Though the Baltic Sea is one of the most investigated seas, not all biogeochemical processes are clearly investigated. And frequently results of different researches draw a controversial picture. One of the most important processes in the ecosystem of the Baltic Sea is nitrogen-fixation which plays a significant role in the balance of the marine nutrient budget. The Baltic Sea is one of the few brackish water areas in the world where nitrogen-fixing cyanobacteria, some of which are toxic, are an important component of the phytoplankton (Howarth et al., 1988).

Estimates of N_2 fixation rates were obtained by different methods. Model studies of N_2 fixation rates were performed by Savchuk and Wulff (1999) and Neumann et al. (2002). Different measurement-based methods, founded on nitrogen,phosphate and CO_2 budgets (Larsson et al. (2001), Rahm et al. (2000), Schneider et al. (2003), Schneider et al. (2009)), N^{15} isotope tracer techniques (Wasmund et al. (2001)) and ocean color satellite data (Kahru et al. (2007)) were used to evaluate nitrogen fixation rates. These different estimates give N_2 fixation rates varying from 10 to 318 $mmol\ m^{-2}\ year^{-1}$.

Mathematical modelling of marine ecosystems is one of the effective ways to improve our understanding of the features of biogeochemical processes and estimation of marine ecological states. An important step in such modeling work is the verification of ecosystem models. The

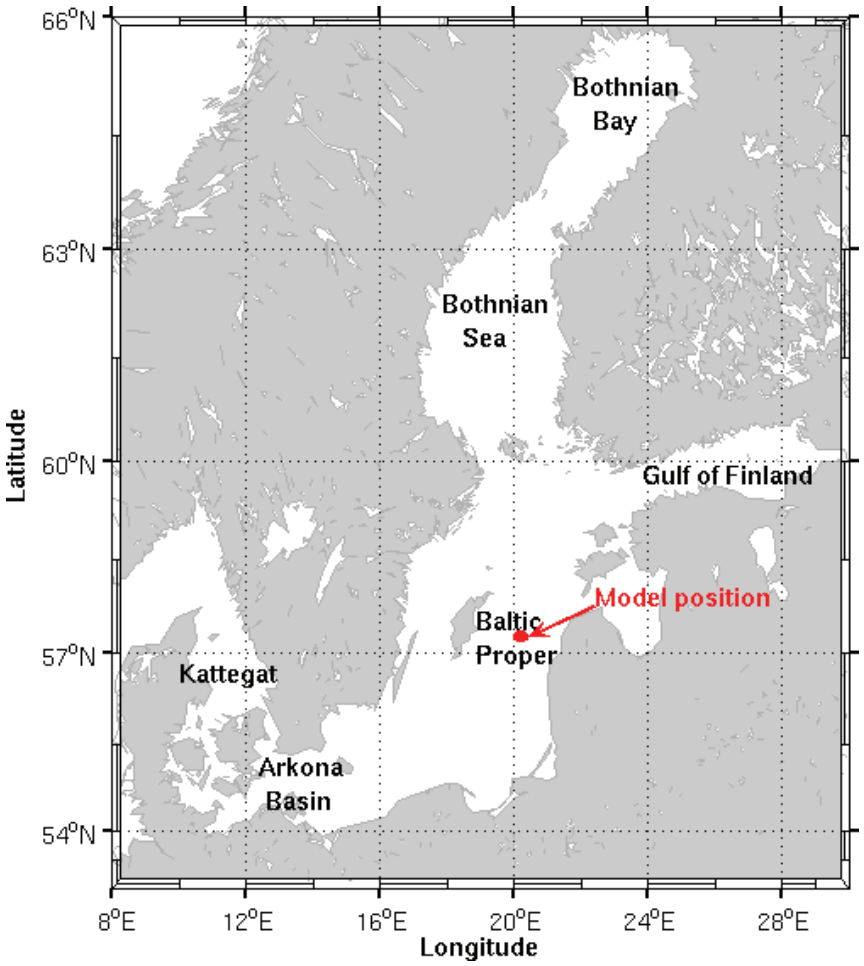

Figure 5.1: Map of the Baltic Sea with indicated regions. Red point is the deepest place in the Baltic Proper, where the described model is applied.

carbon cycle unites most parts of the biogeochemical processes in a marine ecosystem, but at the same time carbon is not the limiting factor for such processes as primary production. Most ecological models which exist and develope are not calibrated on CO_2. Extending a biogeochemical model with a carbon cycle can contribute to the verification of these models. Unique data of CO_2 partial pressure (pCO_2) obtained in the Baltic Sea from the Helsinki-Lubeck ferries received by Schneider et al. (2006) and Schneider et al. (2009) gives a possibility to verify models.

An attempt to simulate the seasonal changes of the CO_2 partial pressure (pCO_2) has been undertaken by Leinweber (2002). However, possible underestimation of N_2-fixation and fixed C:P ratios make it impossible to simulate the observed pCO_2 values. The quantity of the pCO_2 data was insufficient to make model verification possible.

The goal of this study was to simulate seasonal changes of the carbon dioxide flux and to verify modeling results with the data of observations. That will allow us to improve the ability of the model to estimate the nitrogen fixation rates in the Central Baltic and to study its impact on the development of the ecological state of the Baltic Sea.

5.2 Methodology

The model used in this work is the public domain water column model GOTM (General Ocean Turbulence Model, see www.gotm.net, Burchard et al. (2006)) coupled with a modified Baltic Sea ecosystem model ERGOM (Neumann et al. (2002)). The physical basis for this model approach is the model GOTM originally published by Burchard et al. (1999) and regularly extended since then (see Umlauf et al. (2005)). GOTM is based on the Reynolds-averaged Navier-Stokes equations in a rotating reference frame, as well as on Reynolds-averaged versions of the transport equations of temperature and salinity. In GOTM, specific emphasis has been put on the implementation of two-equation statistical turbulence closure models with algebraic second-moment closures; for an overview, see Burchard (2002), Umlauf and Burchard (2003) and Umlauf and Burchard (2005).

The biogeochemical model described in this study is based on the modified Baltic Sea ecosystem model ERGOM (Neumann et al. (2002)). The biogeochemical model ERGOM is coupled to the physical model as an Eulerian-type model in which all state variables, dissolved elements (O_2,NH_4,PO_4,...) and particles (zooplankton, phytoplankton,...), are expressed as concentrations. A detailed description of the model coupling of GOMT with ERGOM can be found in Burchard et al. (2006). The biogeochemical model consists of 18 state variables. The

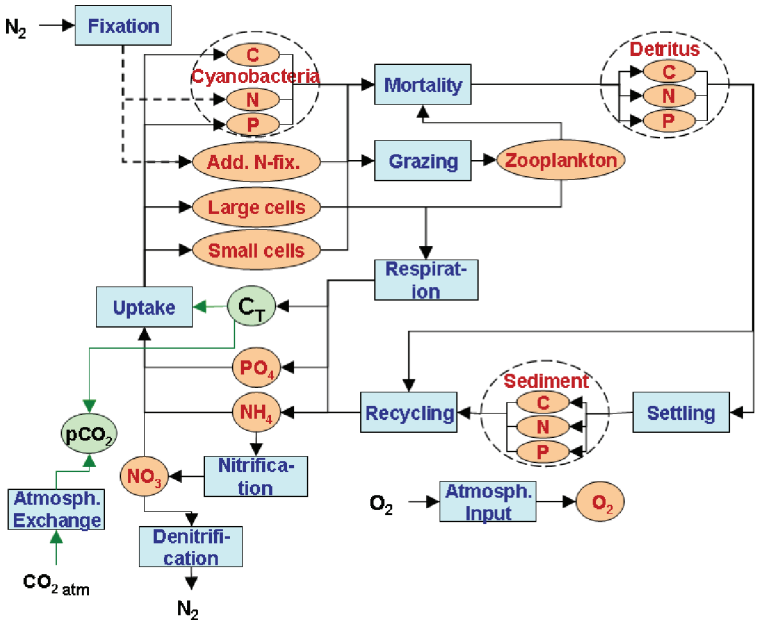

Figure 5.2: Structure of the biogeochemical model with C, N and P in cyanobacteria, large cells, small cells, additional nitrogen fixation phytoplankton group (Add.N-Fix.), zooplankton, C,N and P in detritus, C, N and P in sediment detritus, ammonium (NH_4), nitrate (NO_3), phosphorus (PO_4), carbon (C_T) and oxygen (O_2). The concentrations are in $mmol\ C\ m^{-3}$, $mmol\ C\ m^{-2}$, $mmol\ N\ m^{-3}$, $mmol\ N\ m^{-2}$, $mmol\ P\ m^{-3}$, $mmol\ P\ m^{-2}$ and $mmol\ O_2\ m^{-3}$. Orange and green ovals are models state variables. Blue rectangles are models processes.

basic structure of the model is explained in Fig. 5.2.

The nutrient state variables are dissolved ammonium, nitrate, phosphate and total CO_2. Primary production is provided by four functional phytoplankton groups: diatoms, flagellates and two groups of cyanobacteria. Diatoms represent larger cells that grow fast in nutrient-rich conditions. Flagellates represent smaller cells with an advantage at lower nutrient concentrations during summer conditions. The cyanobacteria are able to fix and utilize atmospheric nitrogen and, therefore, the model assumes that phosphate is the only limiting nutrient for cyanobacteria. Owing to their ability to fix nitrogen, cyanobacteria are a nitrogen source for the ecosystem. A dynamically developing bulk zooplankton variable provides grazing pressure on the phytoplankton. Dead particles are accumulated in a detritus state variable. The detritus is mineralized into dissolved ammonium, phosphate and total CO_2 during the sedimentation process. A certain amount of the detritus reaches the bottom, where it accumulates in the sedimentary detritus. Detritus is buried in the sediment or mineralized. The development of oxygen in the model is coupled to the biogeochemical processes via stoichiometric ratios (see

Table 5.7). The oxygen concentration controls processes such as denitrification and nitrification. All variables of the model are presented in Table 5.1. Equations of the model can be found in the Appendix. The ecosystem model ERGOM has been successfully applied for several studies in the Baltic Sea (Neumann et al., 2002; Fennel and Neumann, 1996; Janssen et al., 2004; Schernewski and Neumann, 2005; Neumann and Schernewski, 2005), however validation of the model did not include validation on pCO_2 data.

The model was extended with a simple carbon cycle, specifically to deal with the pCO_2 at the sea surface. In the model the additional variable C_T, total CO_2 inorganic carbon, was added (see eq. 5.34). Equations for C_T are similar to the equations of other nutrients (phosphate, nitrate,...). The exchange process at the air-sea border, the CO_2 flux, is calculating according to:

$$C_T^{flux} = k * k_0 * \left(pCO_2 - pCO_2^{atm}\right) \tag{5.1}$$

where k - is the gas transfer velocity, k_0 - CO_2 solubility constant, pCO_2 - the surface water CO_2 partial pressure, pCO_2^{atm} - the atmospheric CO_2 partial pressure. pCO_2^{atm} is taken as a function of day of the year, sea surface temperature and sea surface salinity (Bernd Schneider, pers. comm. (2007)). pCO_2^{atm} ranges from 365 μatm to 392 μatm during the year. The CO_2 solubility constant, k_0, is calculated according to Wanninkhof (1992). To calculate pCO_2 at the sea surface we use the value-iteration method based on the equations from Dickson and Goyet (1994). Such calculations involved the use of thermodynamic equilibrium constants after Dickson and Millero (1987). The two CO_2 system parameters used to calculate pCO_2 are total CO_2 (C_T) and total alkalinity (TA). C_T is received from the model (see eq. 5.34) and TA is assume as constant. The mean TA for the eastern Gotland Sea (1580 $\mu molkg^{-1}$) determined by Schneider and Kuss (2004), was used.

The computations of pCO_2 were examined with the computer programme CO2SYS developed by Lewis and Wallace (1998). Gas transfer velocity (k) is calculated according to Liss and Merlivat (1986).

It was observed that the elemental composition of cyanobacteria can change drastically over the growth season. The C:P and N:P ratios of peak population may exceed the Redfield values fourfold, while C:N ratio is near Redfield (Larsson et al. (2001)). The increase of the C:P ratio in cyanobacteria (up to 420) can exert an influence on the carbon cycle. To take proper account of changes in elemental composition of cyanobacteria, the model was improved with variable C:N:P ratio for cyanobacteria, detritus and sediment detritus. C, N and P components in cyanobacteria, detritus and sediment detritus were treated as independent variables. The

derived equations are similar to the equations in the "basic" model (see eq. 5.18 .. 5.20, 5.25 .. 5.30). Empirical model parameters for such processes as mineralization of detritus and sediment detritus, sedimentation of detritus and cyanobacteria as well as mortality of cyanobacteria, have been taken to be the same as in the standard version of the model.

An exception is the uptake of the nutrients N and C by cyanobacteria. In the cyanobacteria equations the growth term (nitrogen fixation term) was modified. The functions $f_C(PO_4)$ and $f_N(PO_4)$ (see eq. 5.21, 5.22) were added to increase C:P and N:P ratios in cyanobacteria. These functions control the uptake dynamics and realize increased C:P and N:P ratios in the case of a low PO_4 concentration. The functions were taken in such a way that modeled C:P and N:P ratios in cyanobacteria match data from Larsson et al. (2001). Such an approach was tested before by Kuznetsov et al. (2008).

Based on two independent approaches; on continuous records of the pCO_2 and on data for the concentrations of total nitrogen and total phosphorus, Schneider et al. (2009) provided evidence for "cold fixation" during spring in the central Baltic Sea. To take this process into account, an additional phytoplankton group similar to the cyanobacteria group (second cyanobacteria group) was added to the model. This group is able to fix and utilize atmospheric nitrogen (see eq. 5.23). The growth rate of the new phytoplankton compared to the old cyanobacteria group is not limited by a temperature. The additional nitrogen fixation phytoplankton group (Phy_{fix}) was included in the Redfield ratio. Phy_{fix}, in contrast to cyanobacteria, reach their maximum abundance in late spring while the phosphorous concentration is still high, thus, including a dynamic C:N:P ratio for this phytoplankton group, depending on phosphorous concentration as with cyanobacteria, is not reasonable.

The surface fluxes of nutrients have been calibrated in such a way that a compromise was found between too low winter nutrient concentrations and too high spring and summer chlorophyll concentrations in the surface mixed layer. By doing so, the effect of lateral nutrient transport is parametrized (Burchard et al., 2006). The constant surface fluxes as in Burchard et al. (2006) were relaxed and new time depended fluxes were implemented:

$$c_i^{flux} = \theta(day - 330, \delta_{day}, c_i^{flux}{}_{min}, c_i^{flux}{}_{max}) + \theta(100 - day, \delta_{day}, c_i^{flux}{}_{min}, c_i^{flux}{}_{max}) \quad (5.2)$$

with $\vec{c}^{flux} = (NH_4^{flux}, NO_3^{flux}, PO_4^{flux})$ denoting the surface fluxes of nutrients. $day[day]$ represents day of the year, $c_i^{flux}{}_{min}$ is the response for the minimum (summer) half of flux values and $c_i^{flux}{}_{max}$ is the response for the maximum (winter) values of fluxes (see Table 5.2).

$\delta_{day} = 15[day]$ is a constant which defines the half of time during which changes of fluxes from $c_i^{flux}{}_{min}$ to $c_i^{flux}{}_{max}$ happen. θ is a smoothed hyperbolic tangent transition with prescribed width (see eq. 5.4). Thus, the effect of winter lateral nutrient transport and atmospheric nutrients deposition were taken into account.

This one-dimensional model was applied to the Central Eastern Gotland Sea at 240 m water depth (20E, 57.3N) (see Fig. 5.1). Initial conditions for the first time step for variables: NO_3, NH_4, PO_4 C_T, O_2, temperature and salinity were derived from the measurements by interpolations of the observed data. For other variables constant vertical distributions were taken. Meteorological forcing was available from the ECMWF forecast data set (Persson and Grazzini, 2005). Salinity concentrations are nudged to observations with a time scale of $\tau_R = 2$ days. Model results and observations will be compared for the years 2002 - 2005. The water column has been divided into 240 vertical layers with a resolution of $1/, m$. The time step for the simulations was $t = 60/, min$.

5.3 Results and discussion

In this section we present and discuss the results of two simulations, one with additional nitrogen fixation phytoplankton group and one without early N-fixation ("base" model), and compare the findings with observations from Schneider et al. (2003) and Schneider et al. (2009). We assumed zero additional phytoplankton growth rate $r_4^{max} = 0$ (see eq. 5.14) in simulation of "base" model, thus additional phytoplankton was not involved in biochemical processes. The time period of both simulations was January 2002 - January 2006.

A spin up period of three years was applied to adjust the model to initial conditions. The last year of simulations (January 2005 - January 2006) was used for result comparisons. Initial conditions for both simulations were the same, the spin up period for each simulation was calculated separately. Thus, concentrations of some parameters can slightly differ between the simulations at the beginning of the year 2005.

Along with the initial conditions the surface fluxes of nitrate, ammonia and phosphate were the same, except for maximum values of phosphate fluxes during the winter (see Table 5.2). The changes in phosphate fluxes were made with the purpose of having similar winter phosphate concentrations to avoid differences in the spring bloom. The difference in phosphate winter fluxes was about 15%.

After the long stagnation period in the Baltic Proper since 1993, a series of inflow events were observed in the period between 2003 and 2005 (Matthäus, 2006; Nausch et al., 2003).

Lateral intrusions, which affect the observed nutrient dynamics, are not included in the model. Varying river runoff, transports from coastal areas to open sea, inflow events and different upwelling intensities were not taken into account. These processes are known to be important for interannual variations (Burchard et al., 2006). However, the model reproduces the observed annual cycles of surface nutrients concentrations well. Thus, we will mostly compare results from the sea surface layer.

As the given work is focused on biogeochemical model, we will concern the physical part of results only superficially. In view of the fact that used physical model resulted in other articles and model algorithms description is a matter of a separate manuscript (Burchard et al. (1999),Burchard et al. (2006) and Umlauf et al. (2005)), the physical description of the model is not provided here and could exceed the boundaries of this paper drastically.

For both simulations the physical scenarios were nearly the same. The difference between physical scenarios was owing to feedback from the biogeochemistry to the water column physics. In Fig. 5.3(a) the sea surface temperature for the year 2005 is shown. Sea surface temperature played a significant role in our biogeochemical model, as the temperature was the limiting factor of flagellate and cyanobacteria growth rates. Also, sea surface temperature determines the exchange processes on the air-sea boundary. Taking into account that comparisons of point measurements of a patchy distribution are subject to observational undersampling, the model reproduces the observed data reasonably well. However, the winter temperature is slightly underestimated and that influenced the pCO_2 at the sea surface.

Observed and modeled sea surface CO_2 partial pressures for the year 2005 are shown in Fig. 5.3(e). The differences in observed and modeled pCO_2 values during the January - February period can be explained by differences in temperature due to tha fact that in this period pCO_2 is mostly defined by exchange processes at the air-sea boundary. The slight decrease of pCO_2 during February - March is connected with a slight temperature decrease. The March - April time period is characterized by a spring bloom (see Fig. 5.3). Due to C_T loss by production, a strong decrease of pCO_2 in observations and model results is observed. Time of the beginning and duration of the spring bloom is well reproduced by both simulations.

The absence of differences in pCO_2 between the simulations is explained by the fact that the spring bloom is mostly dependent on winter concentrations of nitrogen. For both simulations the nitrogen dynamics in the upper layers were nearly the same (see Fig. 5.3(b)). The increase of modeled sea surface nutrient concentrations during the winter months (January - middle March) (see Fig. 5.3(b)-(c)) occurred due to vertical mixing and lateral fluxes. Winter lateral

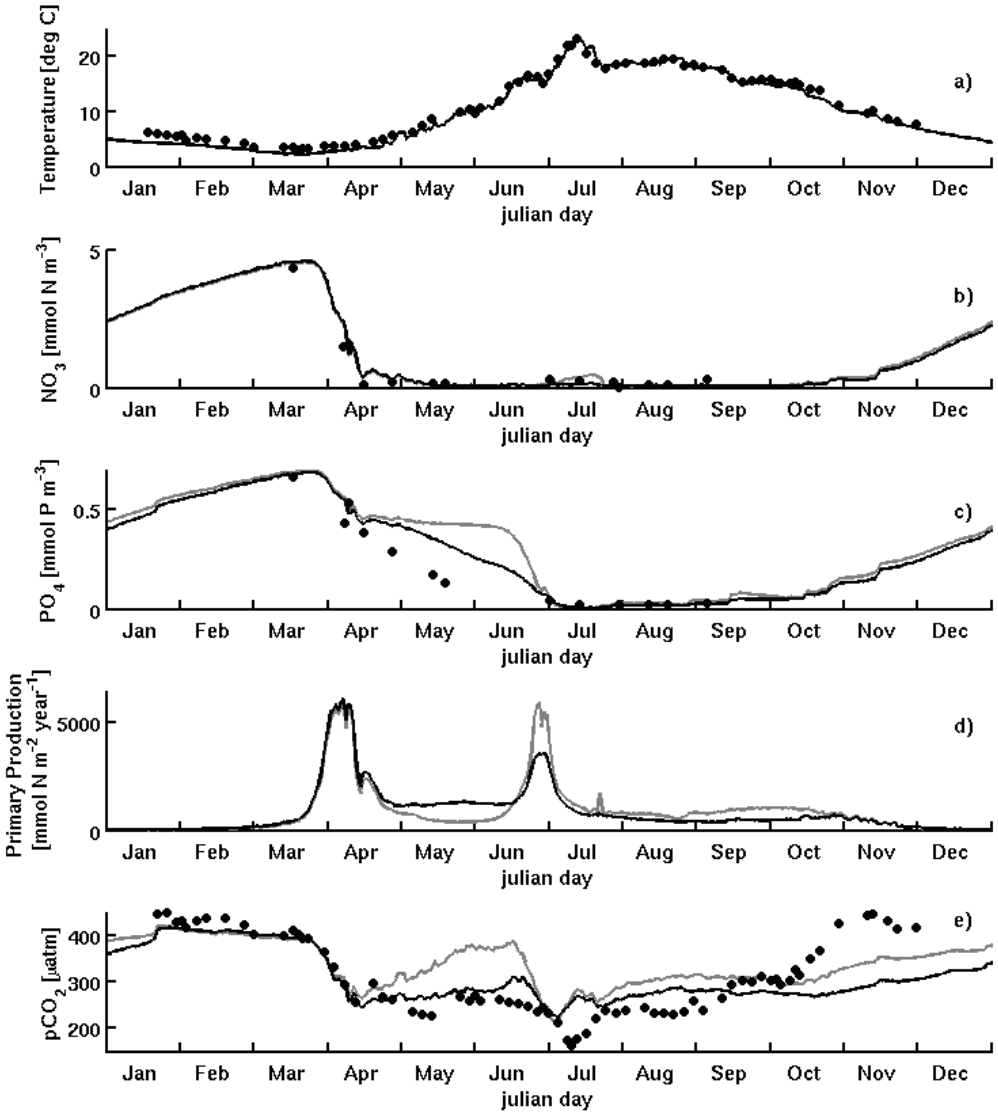

Figure 5.3: Observations extracted from Schneider et al. (2009) (black circles) and model results for two simulations, black lines - simulation with additional N-fixation phytoplankton, grey lines - "base" model for the year 2005. (a): temperature near the sea surface, (b): dissolved inorganic nitrogen near the sea surface, (c): dissolved inorganic phosphate near the sea surface, (d): day averaged primary production, (e): CO_2 partial presure (pCO_2) near the sea surface.

fluxes were parametrized in the model as the increase of nutrient fluxes at the upper boundary during winter (see eq. 5.2)). The decrease of nutrients in both model and observations was detected during the spring bloom. Observed consumption of nitrate and phosphate in spring time is well reproduced by the model.

After the spring bloom had generally ended, the phosphate consumption was still present in the observations (see Fig. 5.3(c), April - May), while at the same time observed nitrate concentrations were negligible. The modeled nitrate in both simulations was fully depleted, just as in the observations. However, modeled phosphate concentrations differed from observations and varied markedly among the two simulations. In the simulation with the additional nitrogen fixation phytoplankton group, consumption of phosphate still present, due to nitrogen fixation. However, the phosphate consumption rate in the model was smaller than in the observations. On the contrary, in the "base" model, phosphate concentrations were approximately constant during this period. Primary production was not able to decrease the phosphate concentration since, in the absence of nitrogen fixation, it was limited by nitrate.

Differences in primary production between the simulations during April - June are seen in Fig. 5.3(d). Summer primary production in the simulation with additional nitrogen fixation was higher compared to the "base" simulation. During this period pCO_2 at the sea surface in the base simulation started to increase (see Fig. 5.3(e)). The increase of pCO_2 was not compensated by primary production and was related to the temperature increase. At the same time, in the simulation with additional nitrogen fixation, pCO_2 values stayed at the same level during April - June as after the spring bloom, and were comparable with the observations.

The summer cyanobacteria bloom can be clearly defined from observations by the decrease of pCO_2 values in June - July. The model reflected the begin time of the cyanobacteria bloom well in both simulations (see pCO_2 decrease in jun Fig. 5.3(e)). Howere, the duration of the modeled cyanobacteria bloom was shorter than was observed. At the same time modeled pCO_2 did not reach the observed pCO_2 minimum in the simulation with additional nitrogen fixation. In the base simulation the summer cyanobacteria bloom was stronger, so the phosphate concentration at the beginning of the bloom was higher. During the summer cyanobacteria bloom the dissolved inorganic phosphate was fully used up by the cyanobacteria in both simulations.

Further system evolution occurred with nutrient limitation until November, when nutrients concentrations increased owing to vertical mixing and lateral fluxes. The pCO_2 values in the simulation with additional nitrogen fixation were slightly overestimated compared to the observed data, due to modeled pCO_2 not reaching the observed pCO_2 minimum during the

summer bloom. The strong increase of observed pCO_2 values in October-November, which can be connected to lateral fluxes, was not reproduced by the model. However, further modeled pCO_2 values reached the observed level of pCO_2 in winter.

The comparison of modeled nitrogen fixation rates with rates received by Schneider et al. (2009) is obtained for the year 2005, and presented in Table 5.3. The modeled rates in Table 5.3 were calculated between the dates indicated in Schneider et al. (2009). Though the primary production peaks can differ from modeled to observation, we can qualitatively compare modeled results with the results from Schneider et al. (2009). Results from the simulation with the additional nitrogen fixation phytoplankton group were in good agreement with the results obtained by Schneider et al. (2009). The total modeled nitrogen fixation rates were larger then those obtained by Schneider et al. (2009). This is due to the fact that in the model nitrogen fixation occurs not only in the period of April-July, but also in the period of August-October.

The total nitrogen fixation rate in the "base" simulation was comparable with the total rates from Schneider et al. (2003) and with the results of simulation with additional nitrogen fixation. However, the "base" simulation rates vary significantly in time, compared to Schneider et al. (2009). The absence of nitrogen fixation during April-May is noticeably reflected on the phosphate dynamics and pCO_2 values (see Fig. 5.3(b,c)). The summer cyanobacteria bloom in the "base" simulation had a 1.7 times higher nitrogen fixation rate compared to Schneider et al. (2009).

5.4 Conclusion

For correct calculation of pCO_2 it is necessary to extend the model with an additional phytoplankton group similar to the cyanobacteria group that is able to fix and utilize atmospheric nitrogen and that would reach its highest abundance in late spring. After the inclusion of this additional phytoplankton group, we got a better reproduction of the dynamics of the sea surface phosphate concentration and pCO_2. Compared to the "base" simulation, in the simulation with the additional phytoplankton group consumption of phosphate was observed during the summer period. At the same time, in the simulation with additional nitrogen fixation, pCO_2 values were comparable to observations, while in the "base" simulation an increase of pCO_2 was observed.

Resulting nitrogen fixation rates for the year 2005 were 259 $mmol\ m^{-2}\ year^{-1}$ and 278 $mmol\ m^{-2}\ year^{-1}$ for the simulation with the additional phytoplankton group and the "base" simulation respectively. Modeled N_2 fixation rates were larger than the rates of 173 $mmol\ m^{-2}\ year^{-1}$

obtained by Schneider et al. (2009) for the year 2005. Modeled pCO_2 have not reached the observed pCO_2 minimum during the summer cyanobacteria bloom and have overestimated the observed pCO_2 during the May-June period.

To estimate the nitrogen fixation rates in the Gotland Sea we elaborated a modification of the ERGOM model, where we included an additional phytoplankton group able to fix nitrogen during March-June period. We extended the model with a simple carbon cycle to have the possibility to verify the model with observed sea surface pCO_2. The modification of the ERGOM model used in the present model will be available on the web.

Acknowledgments

The German part of the Baltic Monitoring Program (COMBINE) in the Baltic Sea is conducted by IOW on behalf of the Bundesamt für Seeschifffahrt and Hydrographie (BSH), financed by the Bundesministerium für Verkehr, Bau- und Wohnungswesen (BMCBW). Funding for this work was received from the DFG-grant: NE G17/3-1.

Table 5.1: State variables of the model.

Variable	Meaning	Dimension
O_2	Dissolved Oxygen	mmol O m^{-3}
	N	
NH_4	Ammonia	mmol N m^{-3}
NO_3	Nitrate	mmol N m^{-3}
Det_N	Nitrogen in detritus	mmol N m^{-3}
Sed_N	Nitrogen in sediments	mmol N m^{-2}
	P	
PO_4	Phosphate	mmol P m^{-3}
Det_P	Phosphate in detritus	mmol P m^{-3}
Sed_P	Phosphate in sediments	mmol P m^{-2}
	C	
C_T	Total CO_2	mmol C m^{-3}
Det_C	Carbon in detritus	mmol C m^{-3}
Sed_C	Carbon in sediments	mmol C m^{-2}
	Biological parameters	
Dia	Diatoms	mmol N m^{-3}
Fla	Flagellates	mmol N m^{-3}
Cya_C	Carbon in cyanobacteria	mmol C m^{-3}
Cya_N	Nitrogen in cyanobacteria	mmol N m^{-3}
Cya_P	Phosphate in cyanobacteria	mmol P m^{-3}
Phy_{fix}	Additional Nit. fix. phytoplantkon	mmol N m^{-3}
Zoo	Zooplankton	mmol N m^{-3}

Table 5.2: The surface fluxes of nutrients.

c_i^{flux}	$c_i^{flux}{}_{min}$	$c_i^{flux}{}_{max}$	Dimension
NH_4^{flux}	0.05	0.4	$[mmol\ N\ m^2\ d^{-1}]$
NO_3^{flux}	0.1	0.7	$[mmol\ N\ m^2\ d^{-1}]$
PO_4^{flux}	0.01	$0.14^{(a)}$ $0.12^{(b)}$	$[mmol\ P\ m^2\ d^{-1}]$

(a) - for the simulation with additional nit. fix. phytoplantkon

(b) - for the basic simulation

Table 5.3: Comparison of nitrogen fixation rates. All values are in $[mmol\ m^{-2}\ year^{-1}]$ units.

Time period (julian day)	Schneider et al. (2009)	Simulation with spring N-fixation	"base" simulation
April-May	74	71.8	3.3
June-July	99	143.7	174
Total	173	215.5(259)*	177.3(278)*

* - In brackets nitrogen fixation rates calclulated for whole year (January 2005 - January 2006) are showed.

5.5 Appendix. - Biogeochemical model equations and parameters.

The model described here in detail consists of 18 state variables see Table 5.1. The general structure of a biogeochemical model expressed as ensemble averaged concentrations is given by the following set of equations:

$$\begin{aligned} &\partial_t c_i + \partial_z(m_i c_i - K_V \partial_z c_i) = R_{c_i}, \\ &i = 1, ..., 18, \end{aligned} \tag{5.3}$$

with $\vec{c} = (c_1, \ldots, c_{18})^T$ denoting the concentrations of the state variables. Furthermore, m_i represents the autonomous motion of the ecosystem component m_i (e.g. sinking or active swimming), and K_V represents the eddy diffusivity (Burchard et al. (2006)). The source and sink terms of the ecosystem component c_i are summarized in R_{c_i}.

The biogeochemical model described in this study is based on the Baltic Sea ecosystem model ERGOM (Neumann et al. (2002)). The present model simulates the C, N and P components of cyanobacteria, detritus (dead organic material within the water column) and sediment detritus separately. Stoichiometries of all phytoplankton groups (except cyanobacteria) and zooplankton are fixed, and are in the Redfield ratio (C:N:P=106:16:1). The basic structure of the model is explained in Fig. 2.

Two different limiting functions proposed by Burchard et al. (2006) are used. Heavyside switches as in Neumann et al. (2002) are changed to a smoothed hyperbolic tangent transition with prescribed width x_w:

$$\theta\left(x, x_w, y_{min}, y_{max}\right) = y_{min} + (y_{max} - y_{min})\frac{1}{2}\left(1 - tanh\left(\frac{x}{x_w}\right)\right) \tag{5.4}$$

Also, as a limiting function a modified Michaelis-Menten formula with squared arguments argued by Fennel and Neumann (1996) is used:

$$Y\left(x_w, x\right) = \frac{x^2}{x_w^2 + x^2} \tag{5.5}$$

As well as in Burchard et al. (2006) limits constructed on Eqs. (5.4) and (5.5) for chemical reactions which depend on the availability of oxygen and nitrate are used:

$$
\begin{aligned}
l_+^+ &= \theta(O_2, O_2^t, 0, 1) Y(NO_3^t, NO_3) \\
l_+^- &= \theta(-O_2, O_2^t, 0, 1) Y(NO_3^t, NO_3) \\
l_-^- &= \theta(-O_2, O_2^t, 0, 1)(1 - Y(NO_3^t, NO_3)) \\
L_+^+ &= \frac{l_+^+}{l_+^+ + l_+^- + l_-^-} \\
L_+^- &= \frac{l_+^-}{l_+^+ + l_+^- + l_-^-} \\
L_-^- &= \frac{l_-^-}{l_+^+ + l_+^- + l_-^-}
\end{aligned} \tag{5.6}
$$

For the phytoplankton we assume that the light limitation function (PPI), as well as some other rates, are the same for all phytoplankton groups:

$$
PPI = \frac{I_{par}}{I_{opt}} exp\left(1 - \frac{I_{par}}{I_{opt}}\right) \tag{5.7}
$$

where I_{opt}, the optimum irradiance for algal photosynthesis, is:

$$
I_{opt} = max\left(\frac{I_0}{4}, I_{min}\right) \tag{5.8}
$$

I_0, is the albedo-corrected surface radiation. The photosynthetically available radiation, I_{PAR}, follows from

$$
I_{PAR}(z) = I_0(1 - a) exp\left(\frac{z}{\eta_2}\right) B(z) \tag{5.9}
$$

where $B(z)$ denote the absorption of the blue-green part of the light spectrum by phytoplankton and detritus:

$$
B(z) = exp\left(-k_c \int_z^0 \left(P_{sum}(\xi) + Det_N(\xi)\right) d\xi\right) \tag{5.10}
$$

The variables in Eqs. 5.9 and 5.10 are the absorption length scales for the blue-green part of the light spectrum η_2, the weighting parameter, a, and the attenuation constant for self shading, k_c. The coordinate z is taken to point upwards with the origin $z = 0$ at the mean sea surface elevation. $P_{sum} = Dia + Fla + Cya_N + Phy_{fix}$ is the sum of the concentrations of all phytoplankton groups in nitrogen units.

Because the diatom (Dia) bloom is in early spring, when the temperature is low, the growth rate for diatoms is independent of temperature:

$$
R_1 = r_1^{max} min\left[Y\left(\alpha_1, NH_4 + NO_3\right), Y\left(s_{NP}\alpha_1, PO_4\right), PPI\right] \tag{5.11}
$$

Flagellates (Fla) in contrast to diatoms reach their highest abundances in summer and benefit from moderate temperatures (Neumann et al. (2002)):

$$R_2 = r_2^{max}\left(1 + Y\left(T_f, T\right)\right) min\left[Y\left(\alpha_2, NH_4 + NO_3\right), Y\left(s_{NP}\alpha_2, PO_4\right), PPI\right] \tag{5.12}$$

As well as for flagellates, the cyanobacteria growth rate depends on temperature, but, compared to flagellates and diatoms, cyanobacteria are not limited by nitrate:

$$R_3 = r_3^{max}\frac{1}{1 + exp(\beta_{bg}(T_{bg} - T))} min\left[Y\left(s_{NP}\alpha_3, PO_4\right), PPI\right] \tag{5.13}$$

The expression for the cyanobacteria growth rate was motivated by observations [see Wasmund (1997)]. The growth rate for the additional phytoplankton group was parametrized in the same way as for cyanobacteria, except that the temperature dependence was dismissed. Also we had to increase the half saturation constant.

$$R_4 = r_4^{max} min\left[Y\left(s_{NP}\alpha_4, PO_4\right), PPI\right] \tag{5.14}$$

Compared to the original ERGOM model by Neumann et al. (2002), we had to change the maximum growth rates, half saturation and temperature control constants. This is due to the fact that ERGOM was developed by Neumann et al. (2002) in a three dimensional version for the whole Baltic Sea in such way that all phytoplankton constants were applied to all regions of the Baltic Sea. The present one dimensional model was applied only to one region of Baltic Sea, the Gotland Sea.

The grazing by zooplankton depends on the temperature and has a lower efficiency for the ingestion of cyanobacteria [see, e.g., Muller-Navarra et al. (2000)],

$$G_n = g_n^{max}\left(1 + \frac{T^2}{T_{opt}^2} exp\left(1 - \frac{2T}{T_{opt}}\right)\right)\left(1 - exp\left(I_{Ivlev} P_{sum}^2\right)\right) \tag{5.15}$$

where g_n^{max} are maximum grazing rates, T_{opt} is a optimum temperature, and I_{Ivlev} is a modified Ivlev constant (Neumann et al., 2002).

The phytoplankton group - diatoms evolve according to:

$$\frac{d}{dt}Dia = R_1 Dia - l_{PA} Dia - l_{PD} Dia - G_1 \frac{Dia}{P_{sum}} Zoo \tag{5.16}$$

The flagellates' equation is:

$$\frac{d}{dt}Fla = R_2 Fla - l_{PA} Fla - l_{PD} Fla - G_2 \frac{Fla}{P_{sum}} Zoo \tag{5.17}$$

The diatoms and flagellates are in the Redfield ratio. In contrast to this, cyanobacteria can be in other ratios than the Redfield ratio. For cyanobacteria we have three state variables for

each compound C, N and P:

$$\frac{d}{dt}Cya_C = f_C(PO_4)R_3Cya_C - l_{PA}Cya_C - l_{PD}Cya_C - G_3\frac{Cya_C}{P_{sum}}Zoo \tag{5.18}$$

$$\frac{d}{dt}Cya_N = f_N(PO_4)R_3Cya_N - l_{PA}Cya_N - l_{PD}Cya_N - G_3\frac{Cya_N}{P_{sum}}Zoo \tag{5.19}$$

$$\frac{d}{dt}Cya_P = R_3Cya_P - l_{PA}Cya_P - l_{PD}Cya_P - G_3\frac{Cya_P}{P_{sum}}Zoo \tag{5.20}$$

The modified model includes a dynamic C:N:P = (106-400):(16-60):1 ratio in cyanobacteria with the relation:

$$f_C(PO_4) = 106 + 147\left(1 + tanh\left(\frac{\gamma_{P0} - PO_4}{\gamma_{P1}}\right)\right) \tag{5.21}$$

$$f_N(PO_4) = 16 + 22\left(1 + tanh\left(\frac{\gamma_{P0} - PO_4}{\gamma_{P1}}\right)\right) \tag{5.22}$$

$\gamma_{P0} = 0.1$ [mmol P m^{-3}] is a constant which defines the phosphorus concentration, where the changes in the cyanobacteria C:P and N:P ratios double, $\gamma_{P1} = 0.03$ [mmol P m^{-3}] is a constant which determines the rate of changes of C:P and N:P ratios. $f_C(PO_4)$ ranges from 106 to 400 and $f_N(PO_4)$ ranges from 16 to 60.

The additional nitrogen fixation phytoplankton group (Phy_{fix}) was included in the Redfield ratio. Phy_{fix}, in contrast to cyanobacteria, reach their maximum abundances in late spring while the phosphorous concentration is still high, thus including a dynamic C:N:P ratio for this phytoplankton group, depending on phosphorous concentration as for the cyanobacteria, is not reasonable.

$$\frac{d}{dt}Phy_{fix} = R_4Phy_{fix} - l_{PA}Phy_{fix} - l_{DP}Phy_{fix} - G_4\frac{Phy_{fix}}{P_{sum}}Zoo \tag{5.23}$$

The model zooplankton evolved according to:

$$\frac{d}{dt}Z = \frac{G_1Dia + G_2Fla + G_3Cya_N + G_4Phy_{fix}}{P_{sum}}Z - l_{ZA}Z^2 - l_{ZD}Z^2 \tag{5.24}$$

where l_{ZA} and l_{ZD} are constant rates for the mortality and excretion of zooplankton respectively. Ratios between the terms $-G_3\frac{Cya_C}{P_{sum}}Zoo : -G_3\frac{Cya_N}{P_{sum}}Zoo : -G_3\frac{Cya_P}{P_{sum}}Zoo$ in eq. 5.18..5.20 can be outside the Redfield ratio. However, the model zooplankton remain in the Redfield ratio, but grazing on phytoplankton is a non-Redfield ratio. To solve these problems with the additional sink for C and N we assume additional source terms in the detritus equations, and thus the system is completed as follows: $+G_3\frac{Cya_C - 106Cya_P}{P_{sum}}Zoo$ in the equation for Det_C (see eq. 5.25) and $+G_3\frac{Cya_N - 16Cya_P}{P_{sum}}Zoo$ in the equation for Det_N (see eq. 5.25). This means that

parts of the N and C components are transferred to the detritus immediately. The detritus variable as in Neumann et al. (2002) was divided in three state variables for each compound C, N and P. The detritus equations then are:

$$\frac{d}{dt}Det_C = l_{PD}\left(s_{NC}\left(Dia + Fla + Phy_{fix}\right) + Cya_C\right) + s_{NC}l_{ZD}Zoo^2 + G_3\frac{Cya_C - 106Cya_P}{P_{sum}}Zoo - L_{DA}Det_C - l_{DS}\frac{Det_C}{H_{bottom}}\delta_{k,k_{bottom}} \quad (5.25)$$

$$\frac{d}{dt}Det_N = l_{PD}\left(Dia + Fla + Phy_{fix} + Cya_N\right) + l_{ZD}Zoo^2 + G_3\frac{Cya_N - 16Cya_P}{P_{sum}}Zoo - L_{DA}Det_N - l_{DS}\frac{Det_N}{H_{bottom}}\delta_{k,k_{bottom}} \quad (5.26)$$

$$\frac{d}{dt}Det_p = l_{PD}\left(s_{NP}\left(Dia + Fla + Phy_{fix}\right) + Cya_P\right) + s_{NP}l_{ZD}Zoo^2 - L_{DA}Det_P - l_{DS}\frac{Det_P}{H_{bottom}}\delta_{k,k_{bottom}} \quad (5.27)$$

where $L_{DA} = l_{DA}(1 + \beta_{DA}Y(T_{DA}, T))$ is the temperature on which mineralization of detritus depends, l_{DS} is the sedimentation rate, the thickness of the box next to the bottom H_{bottom}, $\delta_{k,k_{bottom}}$ is the Kronecker delta, indicating that this term exists only in the bottom layer of the model with index $k = k_{bottom}$. As well as detritus, the sediment detritus is described by three state variables for each compound C, N and P:

$$\frac{d}{dt}Sed_C = l_{DS}Det_C\delta_{k,k_{bottom}} - L_{SA}Sed_C \quad (5.28)$$

$$\frac{d}{dt}Sed_N = l_{DS}Det_N\delta_{k,k_{bottom}} - L_{SA}Sed_N \quad (5.29)$$

$$\frac{d}{dt}Sed_P = l_{DS}Det_P\delta_{k,k_{bottom}} - L_{SA}Sed_P \quad (5.30)$$

where $L_{SA} = l_{SA}exp(\beta_{SA}T)\theta(O_2, O_2^t, 0.2, 2)$ is the sediment mineralization rate under oxic and anoxic conditions. The state equations governed the nitrate, ammonium, phosphate and total

carbon dynamics:

$$\frac{d}{dt}NH_4 = -\frac{NH_4}{NH_4+NO_3}\left(R_1 Dia + R_2 Fla\right) + l_{PA}P_{sum} + l_{ZA}Z^2 + L_{DA}Det_N + \frac{NH_4^{flux}}{H_{surf}}\delta_{k,k_{surf}} - L_{AN}NH_4 + \theta(O_2, O_2^t, 0.5, 1)L_{SA}\frac{Sed_N}{H_{bottom}}\delta_{k,k_{bottom}} \quad (5.31)$$

$$\frac{d}{dt}NO_3 = -\frac{NO_3}{NH_4+NO_3}\left(R_1 Dia + R_2 Fla\right) + L_{AN}NO_3 + \frac{NO_3^{flux}}{H_{surf}}\delta_{k,k_{surf}} - s_{ND}\left(L_{DA}Det_C + L_{SA}\frac{Sed_C}{H_{bottom}}\delta_{k,k_{bottom}}\right)L_+^- \quad (5.32)$$

$$\frac{d}{dt}PO_4 = s_{NP}\left[-R_1 Dia - R_2 Fla - R_4 Phy_{fix} + l_{PA}\left(Dia + Fla + Phy_{fix}\right) + l_{ZA}Z^2\right] - R_4 Cya_P + l_{PA}Cya_P + \frac{PO_4^{flux}}{H_{surf}}\delta_{k,k_{surf}} + L_{DA}Det_P + L_{SA}\left(1 - p_1\theta(O_2, O_2^t, 0, 1)Y(p_2, O_2)\right)\frac{Sed_P}{H_{bottom}}\delta_{k,k_{bottom}} \quad (5.33)$$

$$\frac{d}{dt}C_T = s_{NC}\left[-R_1 Dia - R_2 Fla - R_4 Phy_{fix} + l_{PA}\left(Dia + Fla + Phy_{fix}\right) + l_{ZA}Z^2\right] - R_4 Cya_C + l_{PA}Cya_C + \frac{C_T^{flux}}{H_{surf}}\delta_{k,k_{surf}} + L_{DA}Det_C + L_{SA}\frac{Sed_C}{H_{bottom}}\delta_{k,k_{bottom}} \quad (5.34)$$

The nutrient uptake of diatoms and flagellates involves a prefence for ammonium by means of the ratios $\frac{A}{A+N}$ and $\frac{N}{A+N}$. Nutrient fluxes on the upper boundary were added as source terms in the nutrient equations with the Kronecker delta $\delta_{k,k_{surf}}$. $L_{AN} = l_{AN}\theta(O_2, O_2^t, 0, 1)\frac{O_2}{O_{AN}+O_2}exp(\beta_{AN}T)$ is the nitrification rate which is controlled by oxygen and temperature (Stigebrandt and Wulff, 1987). The last term in the eq. 5.32 is the response to denitrification. The oxygen dynamics are described as:

$$\frac{d}{dt}O_2 = \frac{s_{NC}NH_4 + s_{NO}NO_3}{NH_4+NO_3}\left(R_1 Dia + R_2 Fla\right) + R_3 Cya_C + s_{NC}R_4 Phy_{fix} - l_{PA}\left(s_{NC}\left(Dia + Fla + Phy_{fix}\right) + Cya_C\right) + s_{NC}l_{ZA}Z^2 - s_{ON}L_{AN}NH_3 - \left(L_+^+ + L_-^-\right)\left(L_{DA}Det_C + L_{SA}\frac{Sed_C}{H_{bottom}}\delta_{k,k_{bottom}}\right) - \theta(O_2, O_2^t, 0, 0.5)L_{SA}\frac{Sed_N}{H_{bottom}}\delta_{k,k_{bottom}} + \frac{O_2^{flux}}{H_{surf}}\delta_{k,k_{surf}} \quad (5.35)$$

Table 5.4: Phytoplankton rates.

Parameters	Dia	Fla	Cya_X	Phy_{fix}
Growth rate	$r_1^{max} = 1.35\, d^{-1}$	$r_2^{max} = 0.6\, d^{-1}$	$r_3^{max} = 0.85\, d^{-1}$	$r_4^{max} = 1.3\, d^{-1}$
Half Saturaion	$\alpha_1 = 1.35$	$\alpha_2 = 0.2$	$\alpha_3 = 0.75$	$\alpha_4 = 12$
Sinking speed	$m_1 = -50\, cm\, d^{-1}$	$m_2 = 0\, cm\, d^{-1}$	$m_3 = 10\, cm\, d^{-1}$	$m_4 = 0\, cm\, d^{-1}$
Respiration	$l_{PA} = 0.01\, d^{-1}$	$l_{PA} = 0.01\, d^{-1}$	$l_{PA} = 0.01\, d^{-1}$	$l_{PA} = 0.01\, d^{-1}$
Mortality	$l_{PD} = 0.05\, d^{-1}$	$l_{PD} = 0.05\, d^{-1}$	$l_{PD} = 0.05\, d^{-1}$	$l_{PD} = 0.05\, d^{-1}$
Temperature	-	$T_f = 10\, ^oC$	$T_{bg} = 13\, ^oC$	-
control			$\beta_{bg} = 0.1\, ^oC^{-1}$	

Oxygen is consumed through respiration, nitrification and mineralization. The sources for oxygen are the primary production and fluxes at the upper boundary. The surface flux is prescribed by

$$O_2^{flux} = p_{vel}\,(O_{sat} - O_2) \tag{5.36}$$

where

$$O_{sat} = a_0\,(a_1 + a_2 T) \tag{5.37}$$

with $a_0 = 31.25$ mmol m^{-3}, $a_1 = 14.603$, and $a_2 = 0.4025\ T^{-1}$ (Neumann et al. (2002)).

Table 5.5: Biogeochemical process rates.

Parameter	Notation and Value
Nitrification	
Nitrification constant	$l_{AN} = 0.1\, d^{-1}$
Oxygen parameter	$O_{AN} = 0.01$
Temperature control	$\beta_{AN} = 0.11\, ^oC^{-1}$
Mineralization	
Detritus mineralization constant	$l_{DA} = 0.003\, d^{-1}$
Temperature control	$T_{DA} = 13\, ^oC, \beta_{DA} = 20$
Sediment miniralization constant	$l_{SA} = 0.001\, d^{-1}$
Temperature control	$\beta_{SA} = 0.15\, ^oC^{-1}$
Release of phosphate	$p_1 = 0.15, p_2 = 0.1$
Oxygen tolerance	$O_2^t = 60 mmol\, O_2\, m^{-3}$
Nitrate tolerance	$NO_3^t = 0.1 mmol\, N\, m^{-3}$

Table 5.6: Zooplankton rates.

Parameter	Notation	Value
Grazing on Dia	g_1^{max}	$1\, d^{-1}$
Grazing on Fla	g_2^{max}	$1\, d^{-1}$
Grazing on Cya_X	g_3^{max}	$0.7\, d^{-1}$
Grazing on Phy_{fix}	g_4^{max}	$0.7\, d^{-1}$
Exudation	l_{ZA}	$0.06\, mmol\, N\, d^{-1}\, m^{-3}$
Mortality	l_{ZD}	$0.13\, mmol\, N\, d^{-1}\, m^{-3}$
IvLev constant	I_{IvLev}	0.24
Optimum temperature	T_{opt}	$20\, ^oC$

Table 5.7: Further parameters.

Minimum irradiance	$I_{min} = 25\,Wm^{-2}$
Detritus sinking	$m_{det} = 3md^{-1}$
Sedimentation rate	$l_{DS} = 3.5md^{-1}$
Piston velocity	$p_{vel} = 5md^{-1}$
Redfield ratio (P/N)	$s_{NP} = 1/16$
Redfield ratio (C/N)	$s_{NC} = 6.625$
oxygen production related to N	$s_{NO} = 8.625$
nitrification	$s_{ON} = 2$
reduced nitrate/oxidized detritus	$s_{ND} = 0.8$

Chapter 6

Model study on the ecosystem impact of a variable C:N:P ratio for cyanobacteria in the Baltic Sea, 3D study

This chapter to be submitted to Ecological Modelling :

Kuznetsov, I. and T. Neumann, 2008. Model study on the ecosystem impact of a variable C:N:P ratio for cyanobacteria in the Baltic Sea, 3D study. Ecological Modelling.

Statement on my contribution to this publication :

The model modification, model setup and analysis of the results were done by me. The manuscript was written by myself. T. Neumann contributed in editing the writing, expertise and scientific advice.

6.1 Introduction and Methodology

This study is a prolongation of the study that was described in Kuznetsov et al. (2008). In Kuznetsov et al. (2008) the 1D coupled physical-biogeochemical model GOTM-ERGOM was used. Howevere, 1D simulation can not reproduce inflow events which played significant role in the Baltic Sea. Also, the effect of lateral nutrient transport was parametrized by variable surface nutrient fluxes. Such approach gives a possibility to estimate the changes in consumption of O_2 in the deep layers of the Baltic Proper. Howevere, for investigations of changes in the elemental composition of cyanobacteria on the Baltic Seas ecological state it is necessary to use 3D model simulation. With 3D simulation it is possible to estimate such changes for the whole Baltic Sea, since such processes as lateral fluxes, surface fluxes, river loads of nutrients and inflow events are taken into account. Especially, the effect of inflow events can be studied, that was not possible with 1D simulation. The goal of this study was to estimate the effect of changes in

the elemental composition of cyanobacteria on the development of the Baltic Sea's ecological state, with the aid of a numerical 3D model.

The model used in this study is a coupled physical-biogeochemical model described by Neumann (2000); Neumann et al. (2002); Neumann and Schernewski (2008). The physical part of the model is the circulation model MOM 3.1. The biogeochemical part of the model described in this study is the Baltic Sea ecosystem model ERGOM (Neumann et al., 2002; Neumann and Schernewski, 2008) with some modification.

The circulation model is an application of the Modular Ocean Model (MOM 3.1) for the Baltic Sea and includes an explicit free surface, an open boundary condition to the North Sea, and riverine fresh water input. The model grid is horizontally and vertically stretched. High horizontal resolution (3 nautical miles) was applied in the southwestern Baltic Sea and the whole Baltic proper. Towards the north and east, the grid size gradually increases up to 9 nautical miles. Vertically the model is resolved into 77 layers. The layer thickness of the upper 100 m is 3 m and below this a constant thickness of 6 m is applied. Fig. 2.1 shows the model topography (Neumann and Schernewski, 2008).

The biogeochemical model used here is partly described in Appendix of chapter 5. Difference is only that in this study the variables CO_2 and pCO_2 were not considered, since, these variables do not play any role in processes connected with all other variables and the investigation of the carbon cycle was not in the goals of this work. Moreover, including these variables in 3D simulations is not possible due to the fact that the assumption from Kuznetsov et al. (2008) for constant alkalinity probably does not work. Further modifications by Neumann and Schernewski (2008) were applied, that allowed phosphate in the sediment layer to bind ironoxide under oxic conditions. These complexes form particles which sink out and accumulate in the sediment layer. Erosion events can re-suspend phosphate-rich particles and currents transport them towards the deposition areas. Under anoxic conditions, iron-oxide becomes reduced and phosphate is liberated and available as dissolved phosphate. Depending on the sediment thickness, a part of the particulate iron-phosphate-complexes is assumed to be diagenetically consolidated and, hence, buried in the sediments. This is the final sink for phosphate in the model. And furthermore, it has taken into account the effect of bioturbation. In an oxygenated environment, benthic animals populate the sediment. Their activity reduces the cohesive forces in the sediment and injects sedimentary material into the water column and, hence, contributes to re-suspension (Neumann and Schernewski, 2008).

Thus, the differences between the model described in Neumann and Schernewski (2008)

and model used in this study are:

- The equations for cyanobacteria, detritus and sediment detritus of the basic model have been replaced each with three equations for the description of its C, N and P components.
- In the cyanobacteria equations the growth term (nitrogen fixation term) was modified. The functions $f_C(PO_4)$ and $f_N(PO_4)$ (see Kuznetsov et al. (2008) eq. (1) or chapter 5 eqs. (A.19) - (A.20)) were added to increase C:P and N:P ratios in cyanobacteria.
- Additional sink terms in the detritus equations were assumed: $+G_3 \frac{Cya_C - 106 Cya_P}{P_{sum}} Zoo$ in the equation for Det_C and $+G_3 \frac{Cya_N - 16 Cya_P}{P_{sum}} Zoo$ in the equation for Det_N (chapter 3 eqs. (A.23) - (A.25)).

Initial conditions for all variables were derived from previous simulation made by Neumann and Schernewski (2008). Initial conditions for new declared variables were derived by using the Redfield ratio. Model results and observations will be compared for the years 1984 – 1999, the period of the longest stagnation in the Central Baltic and subsequent series of inflows. All simulation results are based on monthly means.

6.2 Results

In this section we discuss the results of two simulations, one with Redfield C:N:P ratio and one simulation with variable C:N:P ratio. Also, we compare the simulations results with observations from the Baltic Monitoring Program of the Leibnitz Institute of Baltic Sea Research Warnemuede (IOW) at a stations 113 - in Arkona basin, 213 - in Bornholm basin, 271 - in Gotland Basin and 284 - in Landsort deep (see fig. 6.1).

Physical parameters

First, we compare simulated temperature and salinity with observations of the Baltic Monitoring Programme at several stations (see fig. 6.1). For both simulations (variable and Redfield ratio of C:N:P) the physical scenarios were the same. A comparison of the modeled and observed sea surface temperature at these stations is shown in Figure 6.2.

Taking into account that comparisons of point measurements of a patchy distribution are subject to observational undersampling, we find that the model reproduces the observed sea surface temperature data reasonably well. The interannual trends of the minimum and maximum sea surface temperatures are also seen in the model. However, in some instances the

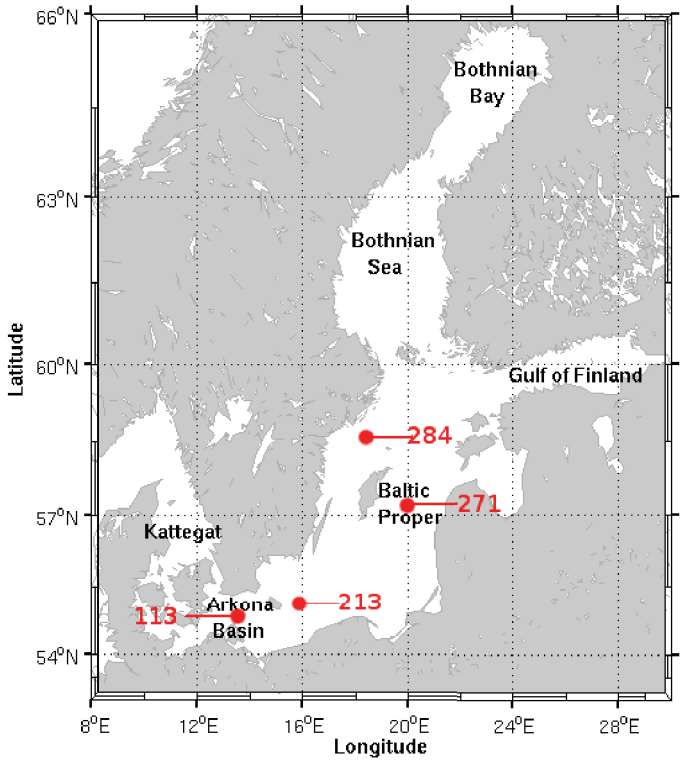

Figure 6.1: Map of the Baltic Sea with indicated sations of the Baltic Monitoring Program of the Baltic Sea Research Institute Warnemuende (IOW).

summer sea surface temperature is slightly overestimated. Bottom temperature is shown in Figure 6.3. Due to low depth on the station 113 (see Figure 6.3(a)) the whole water column is mixed up, and temperature near the bottom as well as near the sea surface has the interannual trends of the minimum and the maximum, which was reproduces by the model. Howevere, in some instances bottom temperature at station 113 does not reach summer maximum and winter minimum temperature. Modeled bottom temperature at stations 213, 271 and 284 (see Figure 6.3(b)-(d)) is overestimated compared to the observed data, still the modeled temperature is reproduces the basic dynamics of the observations. Moreover, the depth on station 284 in the model is less then the observed depth, since the maximum depth of 446 is not resolved become of computational reasons.

While the modeled sea surface temperature is strongly influenced by the surface boundary conditions, the salinity signatures in the model develop in response to the river runoff, the salt exchange at the open boundary to the North Sea, and the internal water mass transformations. Modeled and observed sea surface and bottom salinity is shown on Figures 6.2 and 6.3.

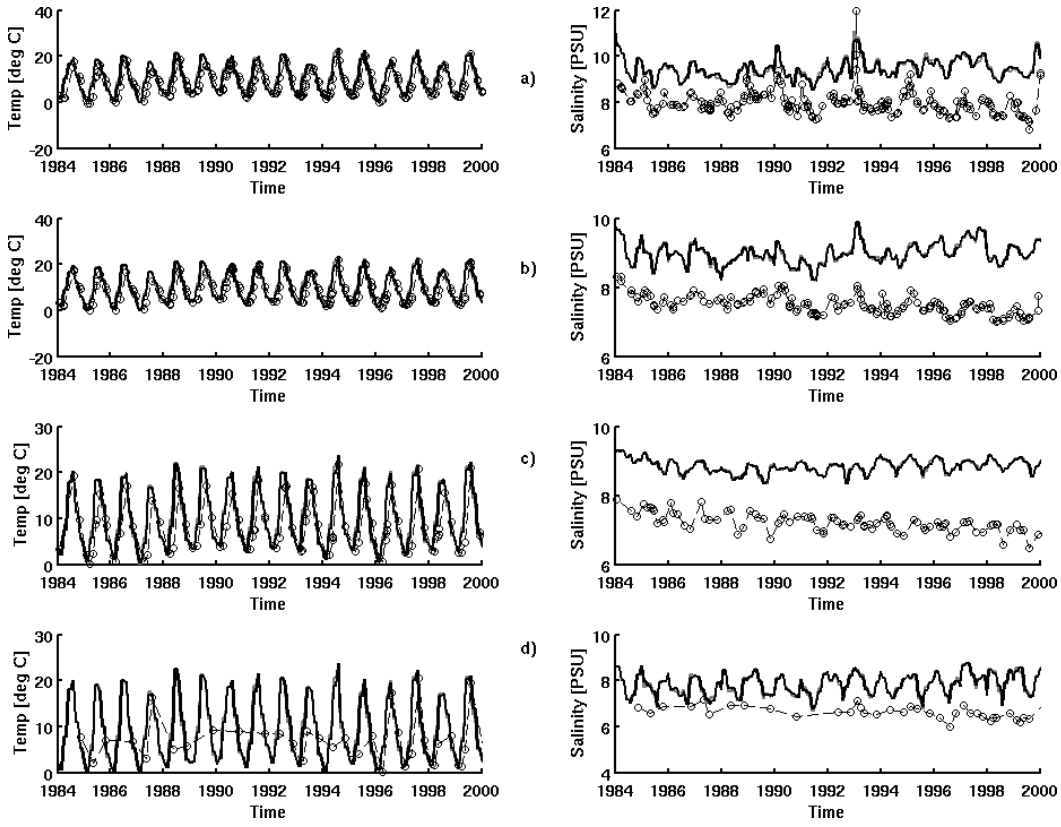

Figure 6.2: Sea surface temperature and salinity. Observed (circles) and modeled (black solid lines) at four stations: (a) - 113, (b) - 213, (c) - 271, (d) - 284. Locations of stations are indicated in Figure 6.1.

Modeled salinity shows an offset of 1 – 2 at all stations, at the same time the difference between sea surface and bottom salinity gives comparable gradients in model results and observations. Most of the observed events are displayed in the model data.

Biogeochemical parameters

The difference between the two simulations is only the different parametrization of N_2-fixation (growth term of cyanobacteria) due to increase C:P and N:P ratios in cyanobacteria. N_2-fixation is one of the sources of nitrogen for the system, the differences in the two simulation are initially caused by changing of N_2-fixation rate. Yearly averaged N_2-fixation rate for two simulations is shown in Figure 6.4. Modeled results vary from 20 to 130 $mmol\ m^{-2}\ year^{-1}$ and it is in the range of the previous estimations of N_2-fixation in the Baltic Sea. These different estimates give N_2 fixation rates varying from 10 to 214 $mmol\ m^{-2}\ year^{-1}$ (Savchuk and Wulff, 1999; Rahm et al., 2000; Larsson et al., 2001; Wasmund et al., 2001; Neumann et al., 2002; Schneider

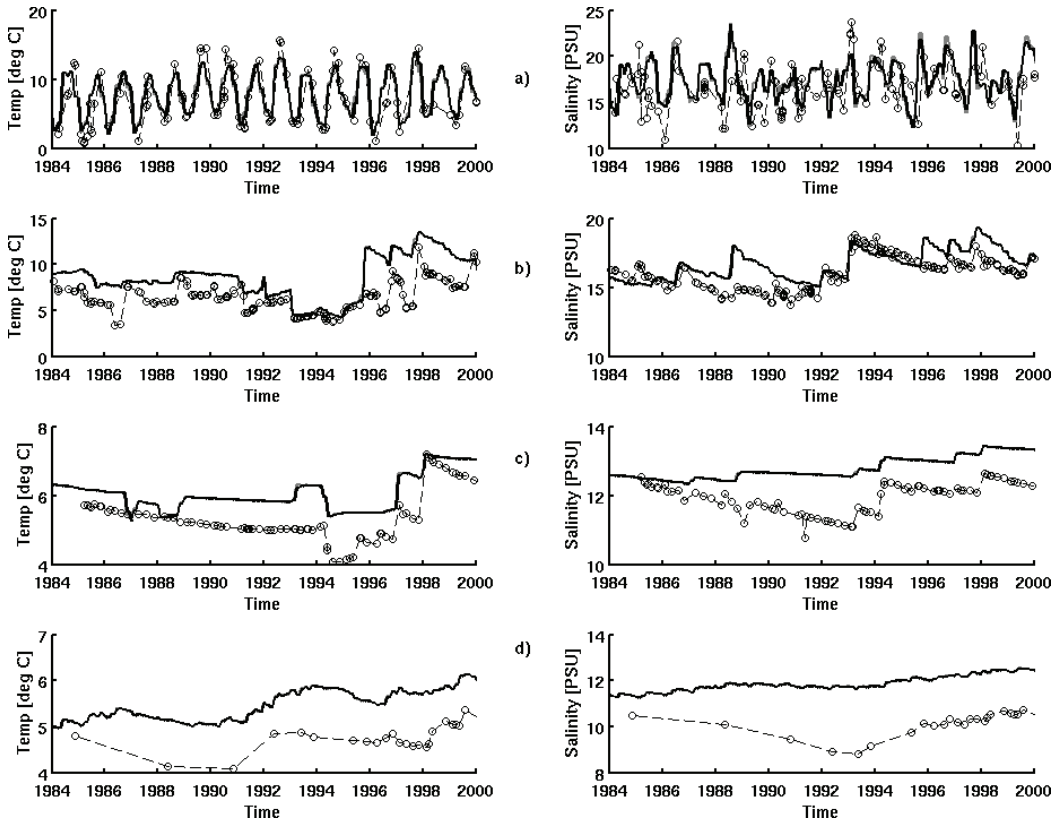

Figure 6.3: Bottom temperature and salinity. Observed (circles) and modeled (black solid lines) at four stations: (a) - 113, (b) - 213, (c) - 271, (d) - 284. Locations of stations are indicated in Figure 6.1.

et al., 2003; Kahru et al., 2007). The nitrogen fixation rate in simulation with variable C:N:P ratio was up to two times more compare to simulation with Redfield C:N:P ratio in some years (1992 year), however in some years nitrogen fixation rates were nearly the same (1987 year).

Modeled and observed sea surface dissolved inorganic phosphate (DIP) and nitrogen (DIN: ammonium and nitrate) are shown on Figure 6.5. Modeled DIP and DIN are follow the annual cycles, however, winter nutrient concentrations were underestimated by the model. Despite the increase of the nitrogen fixation rate the sea surface dissolved inorganic phosphate and nitrogen dynamics have not undergone serious changes.

In Figure 6.6 the bottom DIN and DIP concentrations are shown. Though the model can not reproduce in details the dynamics of DIP and DIN, the main observed events are seen in the model results (annual oscillations at station 113, increase of DIP and DIN during stagnation periods). Exception is the decrease of DIP at station 271 connected with an unexpected inflow event. In contrast to unchanged surface DIN and DIP, bottom DIN is different due to changes

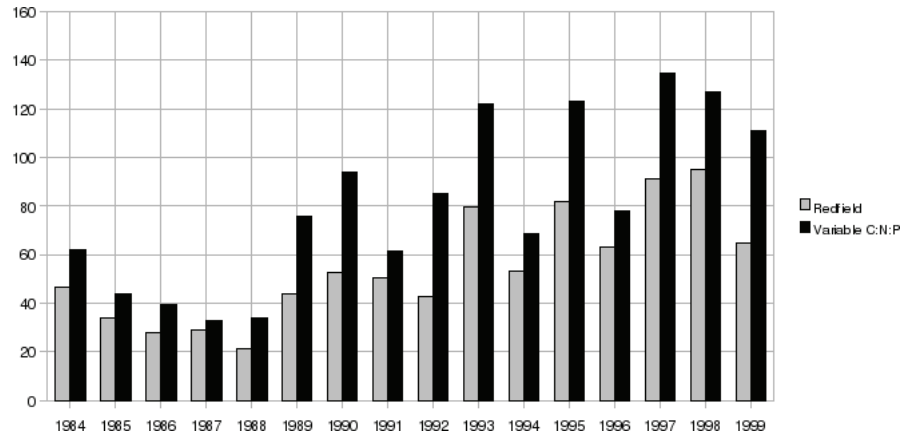

Figure 6.4: Yearly N_2-fixation rate $[mmol\,N\,year^{-1}\,m^{-2}]$, averaged for the whole simulation area. Black - simulation with variable C:N:P ratio, gray - simulation with Redfield ratio.

in N_2-fixation rates. First 6 - 8 years the differences between the two simulations are not visible. Howevere, in the second half of simulations differences between DIN concentrations are observed. The change of DIN concentrations can be explained by different oxygen dynamics near the bottom for both simulations (see fig. 6.7). DIP concentrations for both simulations are nearly the same, with some insignificant exceptions.

Modeled and observed oxygen concentration near the bottom and carbon compound of sediments are shown in Figure 6.7. As well as DIN and DIP, bottom oxygen follows the annual cycle at station 113 (see Figure 6.7(a)). Maximal oxygen concentrations are reached during the winter time and minimal in the summer, when oxygen is demanded for mineralization of organic matter (OM) which sink out after the spring bloom and accumulates in sediments. At the more deep stations 213,271,284 (see Figure 6.7(b)-(d)) the bottom oxygen was not effected by mixing with surface layers, and was mostly controlled by OM in the bottom layers and by inflow events. Bottom oxygen concentrations at stations 213 and 271 (see Figure 6.7(b)-(c)) are in good agreement with observations. An exception is the inflow event in the model in year 1987 at the station 271, which increased oxygen concentration. The difference in modeled and observed oxygen at station 284 (see Figure 6.7(c)) can be explained by different depth in the model and in the observations. Model resolution gives a possibility to make a maximum depth up to 265 meters, and the real depth of the station 284 is 446 meters. Moreover, the observed data is an average for the last 20 meters above the bottom. Howevere, such a deep and isolated station gives a possibility to compare deep oxygen dynamics in two simulations without the effect of strong inflow events.

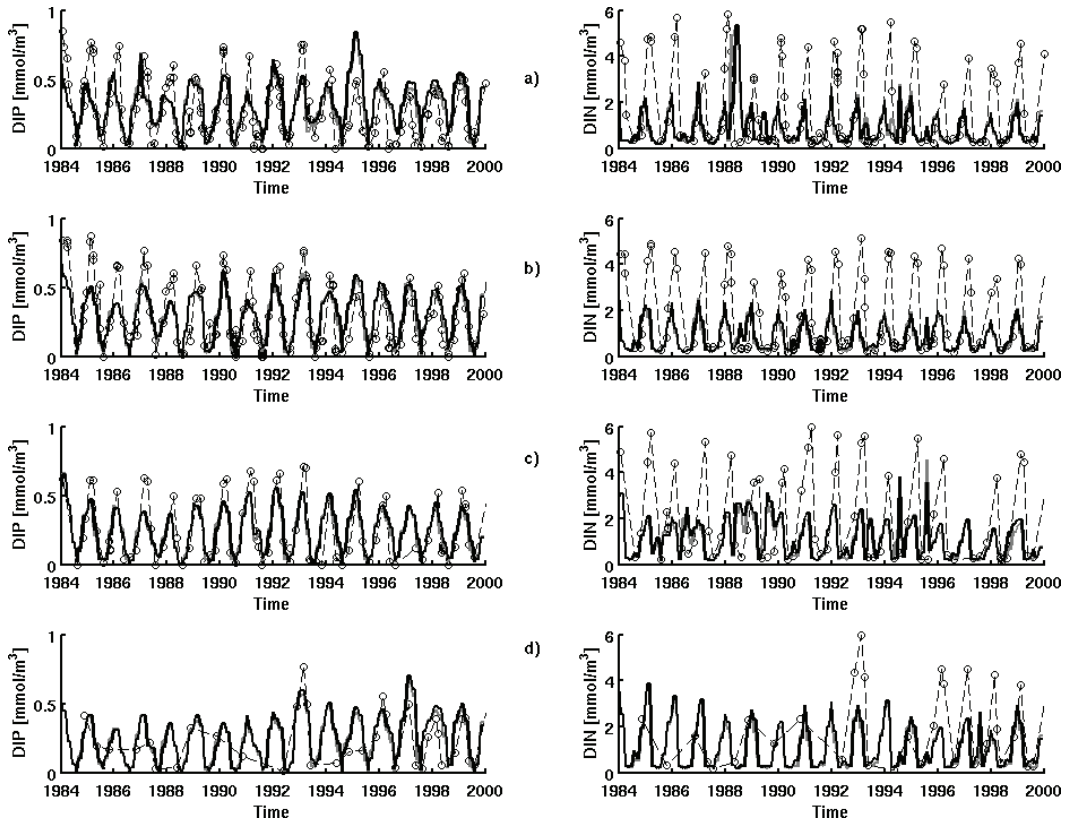

Figure 6.5: Sea surface DIP and DIN. Observed (circles) and modeled (black solid lines - simulation with variable C:N:P ratio, gray solid lines - simulation with Redfield C:N:P ratio) at four stations: (a) - 113, (b) - 213, (c) - 271, (d) - 284. Locations of stations are indicated in Figure 6.1.

Increase of nitrogen fixation rate raise the flux of carbon compound of OM into the deep layers, where this carbon is accumulated in the sediment variable. Increase of carbon in the sediments is clearly seen in model result (see Figure 6.7(b)-(c)). As a result of such increase, the oxygen consumption rates in the simulation with variable C:N:P ratio are increased as compared to the simulation with Redfield C:N:P ratio.

Modeled anoxic area of the Baltic Sea for both simulations are shown on Figure 6.8. The annual oscillations of anoxic area are presented in both simulations. Both simulations have the same dynamics of anoxic area, however, in the simulation with variable C:N:P ratio the anoxic area is larger.

The increase of nitrogen fixation rate and the subsequent increase of OM transport towards the deep layers has led to changes of oxygen consumption rates in these layers. Comparison of oxygen consumption rates near the bottom for two simulations during the modeled stagnation

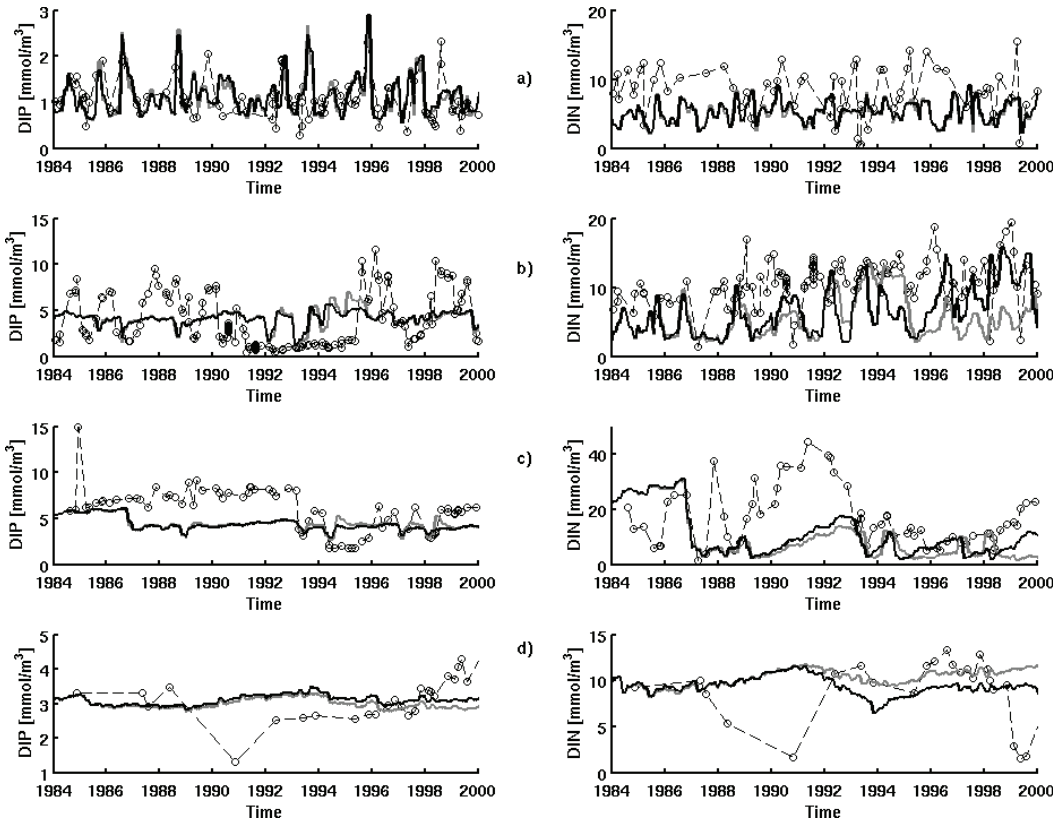

Figure 6.6: Bottom DIP and DIN. Observed (circles) and modeled (black solid lines - simulation with variable C:N:P ratio, gray solid lines - simulation with Redfield C:N:P ratio) at four stations: (a) - 113, (b) - 213, (c) - 271, (d) - 284. Locations of stations are indicated in Figure 6.1.

period (for station 271 during the period from 1987 to 1993 years, and for the station 284 from 1989 to 1994 years) give an increase of this rates for the simulation with variable C:N:P ratio approximately for 15%. Simultaneously, increasing oxygen concentration on comparable values for both simulations occurs after inflows events. Thus, the difference before and after inflows in oxygen concentrations is remains former, there is an accumulative effect.The same accumulative effect is seen in sediments on deep stations.

6.3 Conclusions

To study the influence of non-Redeld stoichiometry on the ecosystem of the Baltic Sea we applied a modication of the ERGOM model, with variable C:N:P ratio in cyanobacteria,detritus and sediment detritus. We used a dependence on PO_4 for the parametrization of seasonal dynamics of the C:N:P ratio in cyanobacteria and modified the parametrization of zooplankton

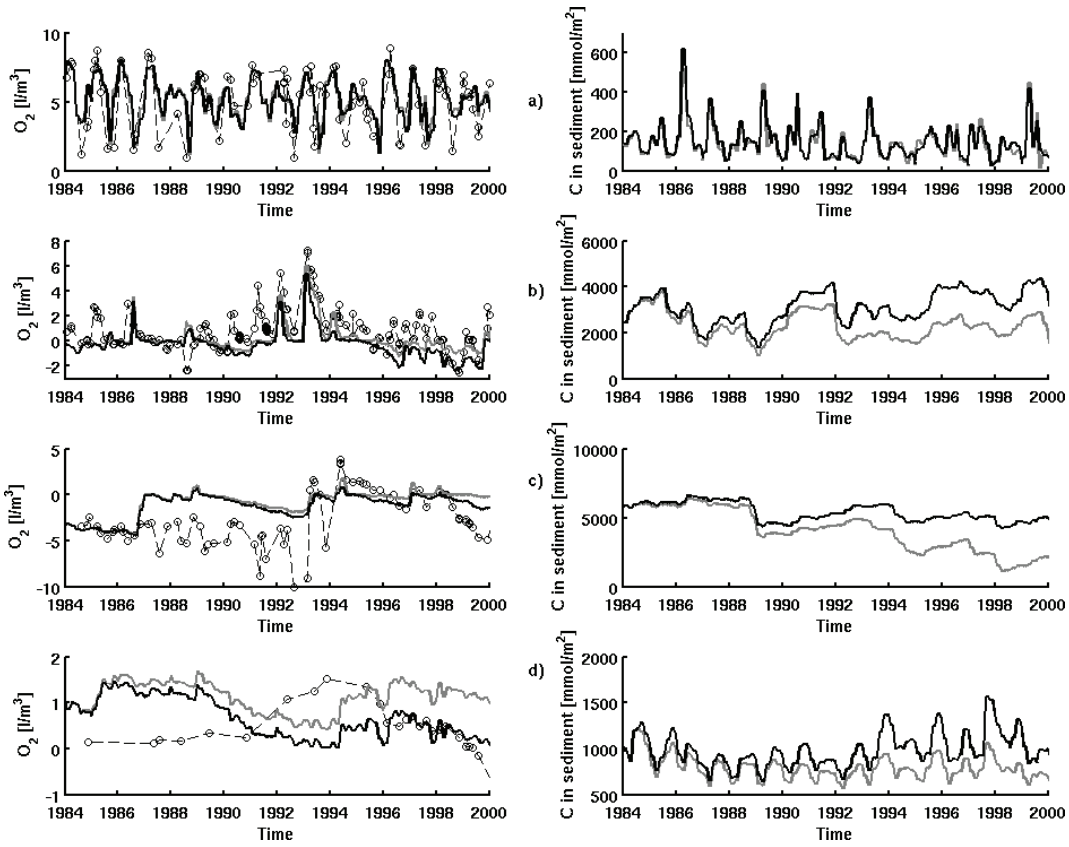

Figure 6.7: Bottom oxygen and carbon compound of sediment. Observed (circles) and modeled (black solid lines - simulation with variable C:N:P ratio, gray solid lines - simulation with Redfield C:N:P ratio) at four stations: (a) - 113, (b) - 213, (c) - 271, (d) - 284. Locations of stations are indicated in Figure 6.1.

grazing in conditions of the variable C:N:P ratio.

After the increase of C:N:P ratios in cyanobacteria, N-fixing rates increased significantly. At the same time no significant changes in the dynamics of the nutrients near the sea surface occurred. Also, dynamics of the nutrients and oxygen near the bottom did not change in shallow waters.

Owing to the increased C:P and N:P ratios in cyanobacteria the OM flux towards the deep layers has increased, too. This affects the concentrations of oxygen and DIN in the bottom layer of the deep regions. Total anoxic ares had increased after 8 years of simulation.

Comparison of oxygen consumption rates near the bottom for two simulations during the modeled stagnation periods gives an increase of these rates for the simulation with variable C:N:P ratio approximately for 15% as compared to the simulation with Redfield ratio. On a short-time perspective of several years the effect is negligible. This 3D study has confirmed

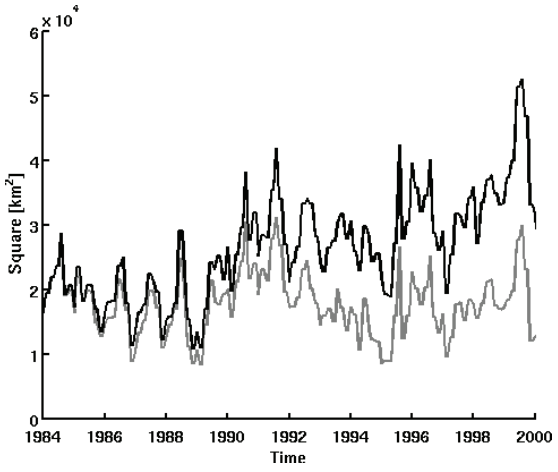

Figure 6.8: Modeled anoxic area of the Baltic Sea [km^2]. Black solid lines - simulation with variable C:N:P ratio, gray solid lines - simulation with Redfield C:N:P ratio.

conclusions made by means of previous one-dimensional study. Such effect can become signicant for prognostic long-term simulations of the Baltic Proper development.

Simulations with variable C:N:P ratio in cyanobacteria has been realized before with 1D (Kuznetsov et al., 2008). Though results of 1D simulations answered on significance of such changes in C:N:P ratios for oxygen dynamic in the deep part of Baltic Proper, it does not give a clearly answer on how this changes can influence on the ecosystem of whole Baltic Sea.

Small and moderate lateral intrusions which affect the observed oxygen dynamics are not included in the 1D model. Varying river runoff, transports from coastal areas to open sea, inow events and different upwelling intensities were not taken into account. These processes are known to be important for interannual variations. Such processes was consider with 3D model.

This 3D simulations gave the possibility to investigate the influence of such changes in different regions of the Baltic Sea. Moreover, with 3D simulations was possible to investigate the differences in the systems during and after the inflow events. Also, 3D simulations clearly show the changes in the anoxic area due to the changes in the OM flux connected with variable C:N:P ratio in cyanobacteria.

Chapter 7

Final conclusions and future outlook

To study the influence of such biogeochemical factors as non-Redfield stoichiometry of cyanobacteria, oxygen consumption due to the oxidation of reduced forms of sulfur, Mn and Fe and N-fixation during the spring on the ecosystem of the Baltic Sea several modifications of the ERGOM model were elaborated. These modified biogeochemical models were coupled to the physical models: 1D model GOTM and 3D model MOM.

During the investigation of these factors the dependence of a variable C:N:P ratio on PO_4 for the parametrization in cyanobacteria was proposed. Further, it was proposed to use an algorithm with the Redfield stoichiometry for zooplankton and non-Redfield stoichiometry for phytoplankton in one biogeochemical model. The parametrization of additional oxygen consumption due to oxidation of reduced forms of sulfur, Mn and Fe was stated. The possible parametrization of spring N-fixation was suggest.

The completed work allows to conclude that:

- After the increase of C:N:P ratios in cyanobacteria, N-fixing rates increase significantly. At the same time no significant changes in the dynamics of the nutrients near the sea surface occurs. Also, dynamics of nutrients and oxygen near the bottom do not change in shallow waters.

  Owing to increased C:P and N:P ratios in cyanobacteria the OM flux towards the deep layers increases, too. This affects the concentrations of oxygen and dissolved inorganic nitrogen in the bottom layer of the deep regions. The total anoxic area increased after 8 years of simulation.

  Oxygen consumption rates near the bottom during the stagnation periods increase in the simulations with variable C:N:P ratio in cyanobacteria approximately for 10 - 15% compare to the simulations with Redfield ratio.

On a short-time perspective of several years the effect of non-Redfield ratio in cyanobacteria is negligible for nutrients and oxygen dynamics. Such effect can become signicant for prognostic long-term simulations of the Baltic Sea development.

- The parametrization of additional oxygen consumption due to oxidation of reduced forms of sulfur, Mn and Fe increase the rate of oxygen depletion and raise the oxygen zero level. Thus effect mostly play a role during the first years of a stagnation period.

- For correct simulation of the sea surface pCO_2 with a 1D model it is necessary to extend the model with an additional phytoplankton group similar to cyanobacteria group that is able to fix and utilize atmospheric nitrogen and that would reach its highest abundance in late spring.

  Resulting nitrogen fixation rates for the year 2005 were 259 $mmol\ m^{-2}\ year^{-1}$ and 278 $mmol\ m^{-2}\ year^{-1}$ for the simulation with additional phytoplankton group and the "base" simulation, respectively. Modeled N_2 fixation rates were larger then rates of 173 $mmol\ m^{-2}\ year^{-1}$ obtained by Schneider et al. (2009) for the year 2005. Modeled pCO_2 have not reached the observed pCO_2 minimum during the summer cyanobacteria bloom and overestimated the observed pCO_2 during the May-June period.

Experiment with variable C:N:P ratio in cyanobacteria has been realized with 1D simulations (see chapter 3) and with 3D simulations (see chapter 6). Though results of 1D simulations have proved the significance of such changes in the C:N:P ratios for oxygen dynamic in the deep part of the Baltic Proper, they did not give a clear answer on how those changes can influence the ecosystem of the whole Baltic Sea.

Small and moderate lateral intrusions which affect the observed oxygen dynamics are not included in the 1D model. Varying river runoff, transports from coastal areas to open sea, inflow events and different upwelling intensities were not taken into account. These processes are known to be important for interannual variations. Such processes are considered with 3D model.

3D realization of the experiment with variable C:N:P ratio in cyanobacteria was performed in Chapter 6. These 3D simulations gave the possibility to investigate the influence of such changes in different regions of the Baltic Sea. Moreover, with 3D simulations it was possible to investigate the differences in the system during and after the inflow events. Also, 3D simulations clearly showed changes in the anoxic area due to changes in OM flux connected with variable C:N:P ratio in cyanobacteria.

The results of this thesis can be used for more detailed 3D studies of the importance of oxygen consumption due to the oxidation of reduced forms of sulfur, Mn and Fe. Changing the redoxcline depth changes the anoxic area in the basin, which affects the flux conditions at the sediment - water interface.

The CO_2 partial pressure (pCO_2) as an additional independent parameter in the ecosystem models gives an opportunity for validation of these models, since carbon is not the limiting factor for such processes as primary production. In chapter 5 the possibility to verify the biogeochemical models with the observed pCO_2 data was shown. However, this study considered only the Central Baltic. The 2 days - frequency seasonal pCO_2 data is available between the southwestern (Lübeck) and the northeastern (Helsinki) of the Baltic Sea for the year 2005 from Schneider et al. (2009). This available data give a unique possibility to verify the 3D model. However, including the carbon cycle in the 3D model as it was done in the chapter 5 is not possible due to the fact that the assumption from Kuznetsov et al. (2008) for constant alkalinity is not valid for 3D studies.

Acknowledgments

It is impossible to name all the people I am grateful to for their contribution to the existence of this work. It does not mean though that those who are not named were forgoten. First I would like to say thanks to my official supervisor Prof. Hans Burchard, who was always ready to answer all my question and to cheer me up. I would also like to especially thank Dr. Thomas Neumann for the continues and stable guidance of my researches. I thank Evgeniy Yakushev for the advisement during my work. I feel obliged to express appreciation to Dr. Bernd Schneider, Prof. Wolfgang Fennel, Dr. Torsten Seifert and Dr. Falk Pollehne of great assistance in carrying out the work and valuable discussion of the results. IOW interdisciplinary Project Group an "Dynamics of the O_2 depletion in the Baltic Sea" provided advice and very fruitful scientific discussions. I also express appreciation to colleagues from the Baltic Sea Research Institute Warnemuende and the Shirshov Institute of Oceanology, RAS. I want to thank my family and friends who always stand behind me. Funding for this work was partly received from the Deutsche Forschungsgemeinschaft grant: "Partikeltransporte und Sauerstoffdynamik im Tiefenwasser der Gotlandsee", NE 617/3-1.

Bibliography

Ayzatulllin, T., Leonov, A., 1975. Kinetics and mechanism of the oxidizing transformation of anoxic sulfur compounds in the sea water. Okeanologiya 15 (6), 1026 –1033. (in Russian).

Ayzatulllin, T., Skopincev, B., 1974. Izucheniye skorosti okisleniya serovodoroda v vode chernogo morya. Okeanologiya 14 (3), 336–380. (in Russian).

Balzer, W., Erlenkeuser, H., Hartmann, M., Müller, P., Pollehne, F., 1987. Diagenesis and exchange processes at the benthic boundary. Seawater - Sediment Interactions in Coastal Waters. Springer-Verlag, Berlin, pp. 111 – 161.

Bauer, S., 2003. Structure and function of nitrifying bacterial communities in the eastern Gotland basin (central Baltic Sea). Ph.D. thesis, Mathematisch-Naturwissenschaftliche Fakultat. Universitat Rostock, Rostock.

Belyaev, V., Sovga, E., Lyubartseva, S., 1997. Modeling the hydrogen sulfide zone of the Black Sea. Ecological Modelling 96, 51–59.

Boudreau, B., 1996. A method-of lines code for carbon and nutrient diagenesis in aquatic sediments. Computers & Geosciences 22 (5), 479–496.

Brettar, I., Rheinheimer, G., 1991. Denitrification in the central baltic: evidence for H_2S-oxidation as motor of denitrification at the oxic-anoxic interface. Marine Ecology Progress Series 77, 157–169.

Bryan, K., 1969. A numerical method for the study of the circulation of the world ocean. Journal of Computational Physics 4, 347–376.

Burchard, H., 2002. Applied turbulence modelling in marine waters. Vol. 100 of Lecture Notes in Earth Sciences. Springer, Berlin, Heidelberg, New York.

Burchard, H., Bolding, K., Kühn, W., Meister, A., Neumann, T., Umlauf, L., 2006. Description

of a flexible and extendable physical–biogeochemical model system for the water column. Journal of Marine Systems 61 (3-4), 180–211.

Burchard, H., Bolding, K., Villarreal, M., 1999. GOTM, a general ocean turbulence model. Theory, implementation and test cases. European Commission (Report EUR 18745), 103.

Canfield, D., Thamdrup, B., Kristensen, E., 2005. Aquatic geomicrobiology. Vol. 48 of Advances in Marine Biology. Elsevier Academic Press, Amsterdam – Tokio.

Cline, J., Richards, F., 1969. Oxygenation of hydrogen sulfide in seawater at constant temperature, salinity and pH. Environ. Sci. Technol 3 (9), 78–89.

Dalsgaard, T., Canfield, D., Peterson, J., Thamdrup, B., Acuna-Gonzales, J., 2003. N production by anamox in the anoxic water column of Golfo Dulce, Costa Rica. Nature 422, 606–608.

Davies, G., 1969. Some aspects of chemistry of Mn(III) in aqueous solutions. Coord. Chem. Review 4, 199–224.

Detmer, A., Giesenhagen, H., Trenkel, V., Auf dem Venne, H., Jochem, F., 1993. Phototrophic and heterotrophic pico- and nanoplankton in anoxic waters of the central Baltic Sea. Marine Ecology Progress Series 99, 197–203.

Dickson, A., Goyet, C., 1994. DOE handbook of methods for the analysis of the various parameters of the carbon dioxide system in sea water, Version 2.0.

Dickson, A., Millero, F. J., 1987. A comparison of the equilibrium constants for the dissociation of carbonic acid in seawater media. Deep-Sea Research 34, 1733–1743.

Enoksson, V., 1986. Nitrification rates in the Baltic Sea: Comparison of tree isotope techniques. Applied and Environmental Microbiology 51, 244–250.

Erdogan, S., Yemenicioglu, S., Tugrul, S., 2003. Oceanography of the Eastern Mediterranean and Black Sea. Tubitak Publishers, Ankara, Ch. Distribution of dissolved and particulate forms of iron and manganese in the Black Sea., pp. 447–451.

Fasham, M., Ducklow, H., McKelvie, S., 1990. A nitrogen-based model of plankton dynamics in the oceanic mixed layer. Journal of Marine Researches 48, 591 – 639.

Fenchel, T., King, G., Blackburn, T., 1998. Bacterial Biogeochemistry: the ecophysiology of mineral cycling. Academic Press, San Diego.

Fennel, W., Neumann, T., 1996. The mesoscale variability of nutrients and plankton as seen in a coupled model. Ger. J. Hydrogr. 48, 49–71.

Fennel, W., Neumann, T., 2003. Variability of copepods as seen in a coupled physicalbiological model of the Baltic Sea. ICES Marine Science Symposia 219, 208 – 219.

Fennel, W., Neumann, T., 2004. Introduction to the modeling of marine ecosystems. Vol. 72. Elsevier Oceanography, Devon, p. 298.

Fonselius, S., 1974. The Black Sea – Geology, Chemistry and Biology. Amer. Ass. of Petrol. Geologists, Tusla, Ch. Phosphorus in the Black Sea., pp. 144–150.

Francke, E., Nehring, D., 1986. The salt water influx in autumn 1982 and in winter 1982/83: the beginning of a renewed change in the marine environment of the Baltic Sea in 1983. In: Symposium on ecological investigations of the Baltic Sea environment. Riga, 1983, pp. 148 – 160.

Gargett, A., 1984. Vertical eddy diffusivity in the ocean interior. Journal of Marine Researches 42, 359–393.

Gregoire, M., Beckers, J., Nihoul, J., Stanev, E., 1997. Sensitivity to Change: Black Sea, Baltic Sea and North Sea. Kluwer, Netherlands, Ch. Coupled hydrodynamic ecosystem model of the Black Sea at basin scale., pp. 487–499.

Gritsenko, V. A., 2001. Benthic gravity currents in the ocean. Soros Educational journal 7 (1), 64–70.

Hannig, M., Lavik, G., Kuypers, M., Wobken, D., Jurgens, K., 2006. Distribution of denitrification and anammox activity in the water column of the central Baltic Sea. In: 9th Int. Estuarine Biogeochemistry Symposium. Estuaries and Enclosed Seas under Changing Environmental Conditions, May 7-11, 2006. IOW, Warnemuende, Germany. p. 49.

HELCOM, 2002. Environment of the Baltic Sea area 1994-1998. Baltic Sea Environment Proceedings 82B, 216.

HELCOM, 2003. The Baltic marine environment 1999 - 2002. Baltic Sea Environment Proceedings 87.

HELCOM, 2006. Development of tools for assessment of eutrophication in the Baltic Sea. Baltic Sea Environment Proceedings 104.

Howarth, R., Marino, R., Lane, J., Cole, J., 1988. Nitrogen fixation in freshwater, estuarine, and marine ecosystems. 1. Biogeochemical controls. Limnology and Oceanography 33, 669–687.

Janssen, F., Neumann, T., Schmidt, M., 2004. Inter-annual variability in cyanobacteria blooms in the Baltic Sea controlled by wintertime hydrographic conditions. Marine Ecology Progress Series 275, 59–68.

Jorgensen, B., Fossing, H., Wirsen, C., Jannasch, H., 1991. Sulfate oxidation in the anoxic Black Sea chemocline. Deep Sea Research (II) 38, 1083–1104.

Kahru, M., Savchuk, O., Elmgren, R., 2007. Satellite measurements of cyanobacterial bloom frequency in the Baltic Sea: interannual and spatial variability. Marine Ecology Progress Series 343, 15–23.

Kautsky, L., Kautsky, N., 2000. Seas at the Millennium: An Environmental Evaluation. Elsevier, Amsterdam, Ch. The Baltic Sea, including Bothnian Sea and Bothnian Bay.

Konovalov, S., Murray, J., Luther, G., Tebo, B., 2006. Processes controlling the Redox budget for oxic/anoxic water column of the Black Sea. Deep Sea Research (II) 53, 1817–1841.

Kostka, J. E., Luther III, G. W., Nealson, K. H., 1995. Chemical and biological reduction of Mn(III)-pyrophosphate complexes: potential importance of dissolved Mn(III) as an environmental oxidant. Geochim. Cosmochim. Acta 59, 885–894.

Kuypers, M., Sliekers, A., Lavik, G., Schmid, M., Jorgensen, B., Kuenen, J., Sinnenghe Damste, J., Strous, M., Jetten, M., 2003. Anaerobic ammonium oxidation by anammox bacteria in the Black Sea. Nature 422, 608–611.

Kuznetsov, I., Neumann, T., Burchard, H., Nov. 2008. Model study on the ecosystem impact of a variable C:N:P ratio for cyanobacteria in the Baltic Proper. Ecological Modelling 219 (1-2), 107–114.

Larsson, U., Hajdu, S., Walve, J., Elgren, R., 2001. Baltic Sea nitrogen fixation estimated from the summer increase in upper mixed layer total nitrogen. Limnology and Oceanography 46 (4), 811–820.

Leinweber, A., 2002. Saisonaler Kohlenstoffkreislauf im Oberflächenwasser der zentralen Ostsee: numerische Prozessstudien zur Simulation des CO_2-Partialdrucks. Ph.D. thesis, Rostock University, (in German).

Leonov, A., Ajzatillin, T., 1987. Mathematical simulation of hydrogen sulphide oxidation in relation to calculation of the dynamics of oxygen-hydrogensulphide coexistence layer and thechnology regime for obataining sulphur from the Black Sea water. Okenologiya 27 (2), 238–244.

Lewis, B., Landing, W., 1991. The biogeochemistry of manganese and iron in the Black Sea. Deep Sea Research (II) 38, 773–803.

Lewis, E., Wallace, D. W. R., 1998. Program Developed for CO_2 System Calculations. ORNL/CDIAC - 105. Tech. rep., Carbon Dioxide Information Analysis Center, Oak Ridge National Laboratory, U.S. Department of Energy, Oak Ridge, Tennessee.

Liss, P., Merlivat, L., 1986. The role of air-sea exchange in geochemical cycling. Vol. 185. NATO ASI Series, Reidel, Ch. Airsea gas exchange rates: introduction and synthesis., pp. 113 – 127.

Lukashev, Y., Yakushev, E., 1999. Dissolved oxygen content measurements on the border of the sulfide zone of the Black Sea. In: PACON-99 Symposium. The Russian Academy of Sciences, Moscow, Russia., p. 167.

Luther, G., Sundby, B., Lewis, B., Brendel, P.J., a. S. N., 1997. Interaction of manganese with the nitrogen cycle: Alternative pathways to dinitrogen. Geochem.et Cosmochem. Acta 61 (9), 4043–4052.

Lyubartseva, S., Lyubartsev, V., 1997. The model of the Black Sea hydrogen sulfide zone ecosystem. In: NATO TU-Black Sea Project. Symp. On Sci. Results. Crimea, Ukraine, Sebastopol, pp. 167–168.

Lyubartseva, S., Lyubartsev, V., 1998. Modeling of the Black Sea anoxis zone processes. In: Ivanov, L., Oguz, T. (Eds.), NATO TU-Black Sea Project. Ecosystem Modeling as a Tool for the Black Sea, Symposium on Scientific Results. Vol. 2. Kluwer Academic Publishers, pp. 385–395.

Markus Meier, H., 2007. Modeling the pathways and ages of inflowing salt- and freshwater in the Baltic Sea. Estuarine, Coastal and Shelf Science 74 (4), 610–627.

Matthäus, W., 2006. The history of investigation of salt water inflows into the Baltic Sea - from the early beginning to recent results. Marine science reports N 65, Baltic Sea Research Institute (IOW), Seestrae 15, D-18119 Rostock-Warnemnde, Germany.

Matthäus, W., Franck, H., 1992. Characteristics of major Baltic inflows - a statistical analysis. Continental Shelf Research 12 (12), 1375 – 1400.

Moore, J., Doney, S., Kleypas, J., Glover, D., Fung, I., 2002. An intermediate complexity marine ecosystem model for the global domain. Deep-Sea Research II 49, 403 – 462.

Morgan, J., Quinby, H., Ducklow, H., 2006. Bacterial abundance and production in the Western Black Sea. Deep Sea Research (II) 53, 1945–1960.

Muller-Navarra, D. C., Brett, M. T., Liston, A. M., Goldman, C. R., 2000. A highly unsaturated fatty acid carbon transfer between primary producers and consumers. Nature (403), 74–76.

Murray, J., Codispoti, L., Friederich, G., 1995. The suboxic zone in the Black Sea. In: Huang, C., OMelia, R., Morgan, J. (Eds.), Aquatic chemistry: interfacial and interspecies processes. American Chemical Society, pp. 157–176.

Murray, J., Lee, B., Bullister, J., Luther III, G., 1999. The suboxic zone of the Black Sea. NATO ASI Series 256, Kluwer Academic Publishers, Dordrecht, Ch. Environmental Degradation of the Black Sea: Challenges and Remedies., pp. 75 – 92.

Naqvi, S., 2006. Oxygen deficiency in the North Indian Ocean. Gayana 70(suplemento), 53–58.

Nausch, G., Matthäus, W., Feistel, R., 2003. Hydrographic and hydrochemical conditions in the Gotland Deep area between 1992 and 2003. Oceanologia 45 (4), 557–569.

Nealson, K., Myers, C., Wimpee, B., 1991. Isolation and identification of manganese reducing bacteria and estimates of microbial Mn(IV)-reducing potential in the Black Sea. Deep-Sea Research (II) 38, 907–920.

Nealson, K., Stahl, D., 1997. Microorganisms and biogeochemical cycles: what can be learn from layered microbial communities ? In: Banfield, J., Nealson, K. (Eds.), Geomicrobiology: Interactions between Microbes and Minerals, Reviews in mineralogy,. Vol. 35. Mineralogical Society of America, Washington D.C., pp. 5 – 34.

Neretin, L., Pohl, C., Jost, G., Leipe, T., Pollehne, F., 2003. Manganese cycling at the oxic/anoxic interface in the Gotland deep, Baltic Sea. Marine Chemistry 82, 125–143.

Neumann, T., Jul. 2000. Towards a 3D-ecosystem model of the Baltic Sea. Journal of Marine Systems 25 (3-4), 405–419.

Neumann, T., Fennel, W., Kremp, C., 2002. Experimental simulations with an ecosystem model of the Baltic Sea: A nutrient load reduction experiment. Global biogeochemical cycles 16 (3), 450.

Neumann, T., Schernewski, G., 2005. An ecological model evaluation of two nutrient abatement strategies for the baltic sea. Journal of Marine Systems 56 (1-2), 195–206.

Neumann, T., Schernewski, G., 2008. Eutrophication in the Baltic Sea and shifts in nitrogen fixation analyzed with a 3D ecosystem model. Journal of Marine Systems 74 (1-2), 592–602.

Oguz, T., Ducklow, H., Shushkina, E., Malonotte-Rizzoli, P., Tugrul, S., Lebedeva, L., 1998. Simulation of upper layer biochemical structure in the Black Sea. In: Ivanov, L., Oguz, T. (Eds.), NATO TU-Black Sea Project. Ecosystem Modeling as a Tool for the Black Sea. Vol. 2. Symp. on Sci. Res., Kluwer Academic Publishers, Norwell, pp. 257–299.

Oguz, T., Murray, J. W., Callahan, A. E., Mar. 2001. Modeling redox cycling across the suboxic-anoxic interface zone in the Black Sea. Deep Sea Research Part I: Oceanographic Research Papers 48 (3), 761–787.

Overmann, J., Manske, A., 2005. Past and Present Water Column Anoxia. NATO Sciences Series, Springer, Dordrecht, Ch. Anoxygenic phototrophic bacteria in the Blcak Sea chemocline., pp. 501–522.

Pacanowski, R. C., Griffies, S. M., Feb 2000. MOM 3.0 Manual.

Pakhomova, S., 2005. Dissolved forms of iron and manganese in marine water, sediments and the water-bottom boundary. Ph.D. thesis, SIO RAS, Moscow, (in Russian).

Persson, A., Grazzini, F., 2005. User guide to ECMWF forecast products. Tech. rep.

Pimenov, N., Neretin, L., 2006. Past and Present Water Column Anoxia. NATO Sciences Series, Springer, Dordrecht, Ch. Composition and activities of microbial communities, involved in carbon, sulfur, nitrogen and manganese cycling in the oxic/anoxic interface of the Black Sea., pp. 501–522.

Pshenin, L., 1963. Symposium on marine microbiology. Charles C Thomas, Publisher, Springfield, Ill.,, Ch. Distribution and ecology of Azotobacter in the Black Sea., pp. 383–391.

Rahm, L., Jonsson, A., Wulff, F., 2000. Nitrogen fixation in the Baltic Proper: an empirical study. Journal of Marine Systems 25 (3-4), 239–248.

Redeld, A., 1934. James Johnson Memorial Volume. University Press of Liverpool, Ch. On the proportions of organic derivations in sea water and their relation to the composition of plankton., pp. 177 – 192.

Reissmann, J., Burchard, H., Feistel, R., Hagen, E., Lass, H., Mohrholz, V., Nausch, G., Umlauf, L., Wieczorek, G., 2007. State-of-the-art review on Baltic mixing and consequences for eutrophication. Progress in Oceanography, accepted for publication.

Richards, F., 1965. Chemical Oceanography. Vol. 1. Academic Press, NY, Ch. Anoxic basins and fjords., pp. 611–645.

Richardson, K., Jorgenson, B., 1996. Eutrophication: definition, history and effects. Vol. 52 of Eutrophication in Coastal Marine Ecosystems, Coastal and Estuarian Studies. AGU, Washington D.C., pp. 1 – 19.

Samodurov, A., Ivanov, L., 1998. Processes of Ventilation of the Black Sea Related to Water Exchange through the Bosphorus. In: Ivanov, L., Oguz, T. (Eds.), NATO TU-Black Sea Project. Ecosystem Modeling as a Tool for the Black Sea, Symposium on Scientific Results,. Kluwer Academic Publishers, Netherland, V. 2/47(2). P.II, pp. 221–236.

Savchuk, O., Wulff, F., 1996. Biogeochemical Transformation of nitrogen and phosphorus in the marine environment. Coupling hydrodynamic and biogeochemical processes in models for the Baltic proper. Systems ecology contributions No 2. Stockholm University, 79.

Savchuk, O., Wulff, F., 1999. Modelling regional and large-scale response of Baltic Sea ecosystems to nutrient load reductions. Hydrobiologia 393, 35–43.

Savenko, A., Baturin, G., 1996. Experimental study of the sorption of phosphorus on manganese dioxide. Geochemistry International 5, 472–474.

Savenko, A. V., 1995. Precipitation of phosphate with iron hydroxide forming by mixing of submarine hydrothermal solutions and the sea water (on the base of experimental data). Geochemistry International 9, 1383–1389.

Schernewski, G., Neumann, T., 2005. The trophic state of the Baltic Sea a century ago: a model simulation study. Journal of Marine Systems 53 (1-4), 109–124.

Schneider, B., Kaitala, S., Maunula, P., 2006. Identification and quantification of plankton bloom events in the Baltic Sea by continuous pCO_2 and chlorophyll a measurements on a cargo ship. Journal of Marine Systems 59, 238–248.

Schneider, B., Kaitala, S., Raateoja, M., Sadkowiak, B., 2009. A nitrogen fixation estimate for the Baltic Sea based on continuos pCO_2 measurements on a cargo ship and total nitrogen data. Continental Shelf Research.

Schneider, B., Kuss, J., Oct. 2004. Past and present productivity of the Baltic Sea as inferred from pCO_2 data. Continental Shelf Research 24 (15), 1611–1622.

Schneider, B., Nausch, G., Kubsch, H., I., P., 2002. Accumulation of total CO_2 during stagnation in the Baltic deep water and its relationship to nutrient and oxygen concentrations. Marine Chemistry 77, 227 – 291.

Schneider, B., Nausch, G., Nagel, K., Wasmund, N., 2003. The surface water CO_2 budget for the Baltic Proper: a new way to determine nitrogen fixation. Journal of Marine Systems 42 (1-2), 53–64.

Shaffer, G., 1986. Phosphorus pumps and shuttles in the Black Sea. Letters to Nature, Nature 321, 515–517.

Skopincev, B., 1964. Raschet obrazovaniya i okisleniya organicheskogo veshestva v morskih vodah. Oceanologic researches, 96 106 (in russian).

Sorokin, Y., 2002. The Black Sea. Ecology and Oceanography. Backhuys Publishers, Leiden.

Sorokin, Y., Sorokin, D., Avdeev, V., 1991. Izmenchivost Ekosystemy Chernogo Morya (Estesstvennye i Antropogennyye Faktory). Nauka, Moscow, Ch. Aktivnost mikroflory i okislitelnye protsessy sernogo tsykla v tolshche vody Chernogo morya (Microbial activity and sulfur cycle oxidation processes in the Black Sea water column)., pp. 173–188 (in Russian).

Stal, L., Walsby, A., 2000. Photosynthesis and nitrogen fixation in a cyanobacterial bloom in the Baltic Sea. European Journal of Phycology 35, 97–108.

Stigebrandt, A., Wulff, F., 1987. A model for the dynamics of nutrients and oxygen in the Baltic Proper. Journal of Marine Research 45, 729–759.

Stokozov, N. A., 2004. Long-lived radionuclides 137Cs and 90Sr in the Black Sea after the Chernobyl NPP accident and their use as a tracers of water exchange processes. Ph.D. thesis, MHI, Sebastopol (in Russian).

Tebo, B., 1991. Manganese (II) oxidation in the suboxic zone of the Black Sea. Deep Sea Research (II), Topical Studies in Oceanography 38, 883–906.

Touratier, F., Field, J., Moloney, C., 2001. A stoichiometric model relating growth substrate quality (C:N:P ratios) to N:P ratios in the products of heterotrophic release and excretion. Ecological Modelling 139, 265 – 291.

Trouwborst, R., Brian, G., Tebo, B., Glazer, B., Luther III, G., 2006. Soluble Mn(III) in Suboxic Zones. Science 313(5795), 1955–1957.

Umlauf, L., Burchard, H., 2003. A generic length-scale equation for geophysical turbulence models. Journal of Marine Research 61, 235–265(31).

Umlauf, L., Burchard, H., 2005. Second-order turbulence closure models for geophysical boundary layers. A review of recent work. Continental Shelf Research 25, 795–827.

Umlauf, L., Burchard, H., Bolding, K., 2005. General Ocean Turbulence Model. Scientific documentation. v3.2. Marine Science Reports 63, 274.

Umlauf, L., Burchard, H., Bolding, K., 2007. GOTM. Sourcecode and Test Case Documentation. Version 4.0.

UNESCO, 1986. Progress on oceanographic tables and standards 1983-1986 : work and recommendations of the UNESCO/SCOR/ICES/IAPSO Joint Panel. Unesco Technical papers in marine science, ndeg. 50,.

Uppala, S. M., KÅllberg, P. W., Simmons, A. J., Andrae, U., Bechtold, V. D. C., Fiorino, M., Gibson, J. K., Haseler, J., Hernandez, A., Kelly, G. A., Li, X., Onogi, K., Saarinen, S., Sokka, N., Allan, R. P., Andersson, E., Arpe, K., Balmaseda, M. A., Beljaars, A. C. M., Berg, L. V. D., Bidlot, J., Bormann, N., Caires, S., Chevallier, F., Dethof, A., Dragosavac, M., Fisher, M., Fuentes, M., Hagemann, S., Hlm, E., Hoskins, B. J., Isaksen, L., Janssen, P. A. E. M., Jenne, R., Mcnally, A. P., Mahfouf, J.-F., Morcrette, J.-J., Rayner, N. A., Saunders, R. W., Simon, P., Sterl, A., Trenberth, K. E., Untch, A., Vasiljevic, D., Viterbo, P., Woollen, J., 2005. The ERA-40 re-analysis. Quarterly Journal of the Royal Meteorological Society 131 (612), 2961–3012.

Volkov, I., Rozanov, A., Demidova, T., 1992. Zimnee sostoyanie ekosystemy otkrytoi chasti Chernogo Morya. Shirshov Institute of Oceanology RAS, Moscow, Ch. Vosstanovlenniye soedineniya sery i rastvorennogo margantsa v vode Chyornogo mora (Reduced inorganic sulfur species and dissolved manganese in the water of the Black Sea)., pp. 38–50 (in Russian).

Wanninkhof, R., 1992. Relationship between wind speed and gas exchange over the ocean. Journal of Geophysical Research 97(C5), 7373–7382.

Ward, B., Kilpatrick, K., 1991. Black Sea Oceanography. Kluwer Academic Publishers, Norwell, Mass., Ch. Nitrogen transformations in the oxic layer of permanent anoxic basins: The Black Sea and the Cariaco Trench., pp. 111–124.

Wasmund, N., 1997. Occurrence of cyanobacterial blooms in the Baltic Sea in relation to environmental conditions. Int. Rev. Gesamten Hydrobiol. 82, 169–184.

Wasmund, N., Nausch, G., Schneider, B., Nagel, K., Voss, M., 2005. Comparison of nitrogen fixation rates determined with different methods: a study in the Baltic Proper. Marine Ecology Progress Series 297, 23–31.

Wasmund, N., Voss, M., Lochte, K., 2001. Evidence of nitrogen fixation by non-heterocystous cyanobacteria in the Baltic Sea and re-calculation of a budget of nitrogen fixation. Marine Ecology Progress Series 214 (14), 1–14.

Webb, S., Dick, G., Bargar, J., Tebo, B., 2005. Evidence for the presence of Mn(III) intermediates in the bacterial oxidation of Mn(II). PNAS, 102.

Westrich, J., Berner, R., 1984. The role of sedimentary organic matter in bacterial sulfate reduction the G model tested. Limnology and Oceanography 29, 236–249.

Yakushev, E., 1992. Numerical modeling of transformation of nitrogen compounds in the redox zone of the Black Sea. Oceanology 32 (2), 173–177.

Yakushev, E., 1999. An approach to modeling anoxic conditions in the Black Sea. In: Besiktepe, S., Unluata, U., Bologa, A. (Eds.), Environmental degradation of the Black Sea: Challenges and Remedies. Kluwer Academic Publishers, Dordrecht, pp. 93–108.

Yakushev, E., Debolskaya, E., 2000. Particulate manganese as a main factor of oxidation of hydrogen sulfide in redox zone of the Black Sea. In: Proc. Konstantin Fedorov Memorial Symposium. Oceanic Fronts and Related Phenomena 18 - 22 May, 1998. Pushkin, Saint-Petersburg, Russia.. IOC Workshop Report No.159. Kluwer Academic Publishers,, pp. 592–597.

Yakushev, E., Kuznetsov, I., Podymov, O., Chasovnikov, V., 2008. Estimating dissolved oxygen balance in water column of the Black Sea (mathematical modeling). Science of Kuban (Nauka Kubani, ISSN 1562-9856) (2), 66 – 71. (in russian).

Yakushev, E., Neretin, L., 1997. One-Dimensional Modeling of Nitrogen and Sulfur Cycles in the Aphotic Zones of the Black and Arabian Seas. Global Biogeochemical Cycles 11, 401 – 414.

Yakushev, E., Pollehne, F., Jost, G., Kuznetsov, I., Schneider, B., Umlauf, L., 2006. Redox-Layer Model (ROLM): a tool for analysis of the water column oxci/anoxic interface processes. Meereswissenschaftliche Berichte, Marine Scince Report. vol. 68, Instutut fur Ostseeforschung Warnemuende.

Yakushev, E., Pollehne, F., Jost, G., Kuznetsov, I., Schneider, B., Umlauf, L., Dec. 2007. Analysis of the water column oxic/anoxic interface in the Black and Baltic seas with a numerical model. Marine Chemistry 107 (3), 388–410.

Yilmaz, A., Coban-Yildiz, Y., Telli-Karakoc, F., Bologa, A., 2006. Surface and mid-water sources of organic carbon by photo- and chemoautotrophic production in the Black Sea. Deep Sea Research Part II 53, 1988 – 2004.

Zhurbas, V., Oh, I. S., Paka, V. T., 2002. Generation of cyclonic eddies in the Eastern Gotland Basin of the Baltic Sea following dense water inflows: Numerical experiments. Journal of Marine Systems 46(6), 805–814.

Zopfi, J., Ferdelman, T., Jorgensen, B., Teske, A., Thamdrup, B., 2001. Influence of water column dynamics on sulfide oxidation and other major biogeochemical processes in the chemocline of Mariager Fjord (Denmark). Marine Chemistry 74, 29–51.

Erklärung

Hiermit versichere ich, dass ich die vorliegende Arbeit selbstständig angefertigt und ohne fremde Hilfe verfasst habe, keine ausser den von mir angegebenen Hilfsmitteln und Quellen dazu verwendet habe und die den benutzten Werken inhaltlich und wörtlich entnommenen Stellen als solche kenntlich gemacht habe.

Rostock, den

Curriculum Vitae

PERSONAL

Name: Ivan Kuznetsov

Gender: Male

Date and place of birth: March 31, 1981, Moscow, Russia

Marital Status: Married, one child

Citizenship: Russia

RESEARCH INTERESTS

main field

Biogeochemical Cycles, Marine Physics, Mathematical Modeling, Hydrodynamics, Anoxia in Aquatic Environment

other fields

Marine field studies, oxic/anoxic interfaces, Carbonate System

current research interest

Simulation of oxygen dynamics in the Baltic Sea based on mathematical modeling.

EDUCATION

1998 - 2004

Moscow State University, Physical Department, Physics of sea and mainland waters faculty. Master of Science in Physics under supervision of Dr. B.I. Samolyubov. Diploma thesis: Three-dimensional current structure of stratified artificial lake

2004 - 2005

PhD. Student, P.P.Shirshov Institute of Oceanology of the Russian Academy of Sciences (SIO RAS), Moscow, Russia, Thesis: Mathematical modeling of Black Sea hydrochemical structure forming

2005 - 2009

PhD. - Student (Physical Oceanography), The Physical Oceanography and Instrumentation Department of the Baltic Sea Research Institute Warnemunde (IOW) at the University of Rostock, Thesis: Simulation of oxygen dynamics in the Baltic Sea deep water